

CATALYTIC ROUTES FROM LIGNIN TO USEFUL PRODUCTS

A Dissertation
Presented to
The Academic Faculty

by

Weiyin Xu

In Partial Fulfillment
of the Requirements for the Degree
Doctor of Philosophy in the
School of Chemical & Biomolecular Engineering

Georgia Institute of Technology
August 2013

Copyright © 2013 by Weiyin Xu

CATALYTIC ROUTES FROM LIGNIN TO USEFUL PRODUCTS

Approved by:

Dr. Christopher W. Jones, Advisor
School of Chemical & Biomolecular
Engineering
Georgia Institute of Technology

Dr. Pradeep K. Agrawal, Advisor
School of Chemical & Biomolecular
Engineering
Georgia Institute of Technology

Dr. Dennis W. Hess
School of Chemical & Biomolecular
Engineering
Georgia Institute of Technology

Dr. Charles L. Liotta
School of Chemistry & Biochemistry
Georgia Institute of Technology

Dr. David M. Collard
School of Chemistry & Biochemistry
Georgia Institute of Technology

Dr. Stephen J. Miller
Chevron Fellow
Chevron Energy Technology Company

Date Approved: June 21, 2013

ACKNOWLEDGEMENTS

I would like to thank my advisors, Dr. Christopher Jones and Dr. Pradeep Agrawal, for all their guidance throughout my graduate school years. Their instruction and advice have been instrumental to this thesis work. I would also like to thank Dr. Steven Miller whose insightful questions and thoughtful comments have helped shape some of the research directions. Thanks also to my other committee members, Dr. Dennis Hess, Dr. Charles Liotta and Dr. David Collard for their thought provoking questions and time.

Next, I would like to thank all of the Jones group members I have had the opportunity to interact with. It has been a great joy working with a group of friendly, hardworking and science-loving people. In particular, I would like to thank the people who made up the Chevron subgroup, Do-Young Hong, Teresita Marzioletti and Mariefel Valenzuela Olarte, who were always willing to share their knowledge and inspired me with their work ethic. I would also like to thank Praveen Bollini, Nick Brunelli, Stephanie Didas and Miles Sakwa-Novak for all the fun conversations that provided a good distraction from everyday research and thought provoking discussions about science. Next, I would like to thank Megan Lydon for her great company and providing support through shared experiences.

I would like to thank my mom, dad and sister, who although have no clue about the research I am doing now, were instrumental to providing all the nurturing and guidance in my development and have always being ever so supportive even from afar. Last but not least, I would like to thank my fiancée, Yang-Sheng Wong, who has put up with me through the ups and downs of graduate school, been a pillar of support and continues to inspire me to do better.

CONTENTS

ACKNOWLEDGEMENTS	iii
LIST OF TABLES	vi
LIST OF FIGURES	ix
LIST OF SCHEMES	xiii
LIST OF SYMBOLS AND ABBREVIATIONS	xiv
SUMMARY	xvi
CHAPTER 1: Introduction	1
1.1 Motivation	1
1.2 Depolymerization and Hydrodeoxygenation of Lignin	3
1.3 Zeolite Catalyzed Alkylation of Phenol	9
1.4 Objectives, Hypotheses, and Specific Aims	13
1.5 References	16
CHAPTER 2: Depolymerization and Hydrodeoxygenation of Switchgrass Lignin	21
2.1 Introduction	21
2.2 Experimental Methods	24
2.2.1 Reaction Procedure	24
2.2.2 GC-FID/MS Analysis	25
2.2.3 Elemental Analysis	26

2.2.4	Gel Permeation Chromatography	26
2.2.5	Simulated Distillation using Thermogravimetric analysis	27
2.2.6	^1H and ^{13}C NMR	27
2.3	Results and Discussion	28
2.3.1	Effects of Formic Acid and Catalyst	33
2.3.2	Effects of Reaction Time	37
2.3.3	Effects of Reactor Corrosion	45
2.3.4	Model Compound Studies with Phenol	47
2.3.5	Model Compound Studies with 2-Phenylethyl Phenyl Ether	48
2.3.6	Model Compound Studies with Guaiacol	49
2.4	Conclusions	50
2.5	References	52
CHAPTER 3: Zeolite Topology Effects in the Alkylation of Phenol with Propylene		55
3.1	Introduction	55
3.2	Experimental Methods	57
3.2.1	Materials	57
3.2.2	Materials Characterization	59
3.2.3	Catalytic Testing	61
3.3	Results and Discussion	63

3.3.1	Characterization of Zeolites	63
3.3.2	Alkylation Reaction Pathway	67
3.3.3	Effects of Zeolite Pore Topology	69
3.4	Conclusions	76
3.5	References	77
CHAPTER 4: Zeolite Acid Strength Effects in the Alkylation of Phenol with Propylene		81
4.1	Introduction	81
4.2	Experimental Methods	83
4.2.1	Zeolite Synthesis	83
4.2.2	Catalyst Characterization	84
4.2.3	Reaction Procedure	85
4.3	Results and Discussion	86
4.3.1	Characterization of Synthesized Zeolites	86
4.3.2	Catalytic Performance of Synthesized Zeolites	96
4.4	Conclusions	100
4.5	References	100
CHAPTER 5: Conclusions and Future Work		103

LIST OF TABLES

Table 2.1	Experimental reaction conditions for the depolymerization and hydrodeoxygenation of switchgrass lignin. All reactions were conducted at 350°C and with autogeneous pressure in a batch microreactor.	29
Table 2.2	Chemical assignments for major peaks in ¹³ C NMR spectra of switchgrass lignin feedstock	31
Table 2.3	Chemical assignments for main peaks in ¹³ C NMR spectra of liquid products from switchgrass lignin depolymerization and hydrodeoxygenation reaction under reaction condition D-4	33
Table 2.4	Molecular weight averages of switchgrass lignin and bulk liquid products of switchgrass lignin from different reaction conditions (poly(styrene) weight equivalents)	44
Table 3.1	Summary of zeolites used in this study	58
Table 3.2	Investigating the effects of intraparticle diffusion limitations on alkylation reaction. Reaction conditions: T = 350°C, Pressure = 1 atm, Catalyst = HY, Catalyst loading = 20mg, Phenol concentration = 0.9mol%, Phenol to propylene molar ratio = 1	59
Table 3.3	Micropore volume and external surface area characterization of zeolites	64
Table 3.4	Characterization of zeolite acid sites via ²⁷ Al MAS NMR, isopropylamine temperature programmed desorption and pyridine FT-IR	64
Table 3.5	Assessing the reaction pathway via conversion of reactants, products and possible intermediate species. Reaction conditions: T = 350°C, Pressure = 1 atm, Catalyst = HY, Catalyst loading = 20mg, Aromatic reactant concentration = 0.8 –0.9 mol%	67
Table 3.6	Product selectivities of different zeolites at a similar initial phenol conversion of 5%. Reaction conditions: T = 350°C, Pressure = 1 atm,	

	WHSV = 0.8 - 16.1 h ⁻¹ , Phenol concentration = 1.4 mol%, Phenol to propylene ratio = 1.4	71
Table 3.7	Investigating the effects of surface acid sites on catalytic activity. Characteristics of catalysts before and after TEOS treatment. Reaction conditions: T = 350°C, Pressure = 1 atm, Catalyst loading normalized by aluminum content, phenol concentration = 1.4 mol%, Phenol to propylene ratio = 1.4	75
Table 4.1	Characterization of zeolites - silicon to metal ratio, micropore volume, Brønsted to Lewis acid ratio at 350°C and Brønsted acid site concentration	89
Table 4.2	Li/Zn and Si/Al ratios in ZnBEA zeolites	91
Table 4.3	Comparison of deactivation rates and selectivity of 2-IPP to selectivity of 4-IPP at X ₀ ≈ 4%	97
Table 4.4	Comparison of deactivation rates and selectivity of 2-IPP to selectivity of 4-IPP at X ₀ ≈ 2%	98

LIST OF FIGURES

Figure 1.1	Historical and projected figures of U.S domestic crude oil production by source and year in million barrels per day	2
Figure 1.2	Proposed route of converting lignin to fuel and chemicals via (1) depolymerization followed by (2) alkylation	3
Figure 1.3	Monomeric building blocks of lignin	4
Figure 1.4	Example of lignin synthesis in plants through enzymatic oxidation of p-hydroxyphenyl unit followed by its random polymerization	4
Figure 1.5	Proposed lignin structure with characteristic lignin bonds highlighted	5
Figure 1.6	Van Krevelan diagram comparing the H/C and O/C molar ratios of different biomass and fossil materials	6
Figure 1.7	H/C and O/C molar ratios of products produced from lignin derived phenol after alkylation and hydrogenation	7
Figure 1.8	Hydrogenation of 4-propylphenol and 2-propylphenol over 0.5 wt.% Pt/HY ($\text{SiO}_2/\text{Al}_2\text{O}_3 = 12$) catalyst. Experiments conducted by Do-Young Hong. Reaction conditions: $T = 200\text{ }^\circ\text{C}$; $P_{\text{H}_2} = 40\text{ bar}$; Catalyst loading, 100 mg; WHSV, 5 h^{-1}	8
Figure 1.9	Brønsted acid structure in zeolites, resonance hybrid of (a) bridging hydroxyl and (b) terminal silanol with Al lewis acid-base interaction	10
Figure 2.1	Schematic drawing of batch reactor	24
Figure 2.2	Example of a GC-MS spectrum of extracted liquid products obtained from reaction condition D-4 (Identified and quantified products: (1) phenol, (2) p-cresol, (3), guaiacol, (4) p-methylguaiacol, (5) p-ethylguaiacol, (6) p-propylguaiacol, (7) homovanillyl alcohol)	29

Figure 2.3	Quantitative ^{13}C NMR of the (a) switchgrass lignin feedstock and (b) liquid products from switchgrass lignin depolymerization and hydrodeoxygenation under reaction condition D-4	31
Figure 2.4	Change in H/C and O/C molar ratio of bulk liquid products obtained from switchgrass lignin depolymerization and hydrodeoxygenation with varying conditions – A-4, B-4, C-4 and D-4 (●), and A-20, B-20, C-20 and D-20 (▲)	33
Figure 2.5	Thermogravimetric analysis of switchgrass lignin feedstock and bulk liquid products obtained from switchgrass lignin with varying presence of Pt/C and formic acid (conditions A-20, B-20, C-20 and D-20)	35
Figure 2.6	Mass loss distribution of bulk liquid products obtained from switchgrass lignin with varying presence of Pt/C and formic acid (conditions A-20, B-20, C-20 and D-20) between 135°C and 800°C of thermogravimetric analysis	35
Figure 2.7	Molecular weight distribution of bulk liquid products from switchgrass lignin obtained with reaction conditions A-20, B-20, C-20, and D-20	37
Figure 2.8	Change in individual yields of identified products with increasing reaction time. Identified products are p-cresol (-), phenol (), guaiacol (◆), 4-methylguaiacol (■), 4-propylguaiacol (×), 4-ethylguaiacol (▲), and homovanillyl alcohol (•).	38
Figure 2.9	Change in H/C (▲) and O/C (■) molar ratios of bulk liquid products obtained from switchgrass lignin depolymerization and hydrodeoxygenation with increasing reaction time	40
Figure 2.10	Thermogravimetric analysis of switchgrass lignin feedstock and bulk liquid products obtained from switchgrass lignin under reaction conditions D-1, D-4, D-8 and D-20	41
Figure 2.11	Mass loss distribution of bulk liquid products obtained from switchgrass lignin with Pt/C and formic acid at different reaction times (conditions D-1, D-4, D-8 and D-20) between 135°C and 800°C of thermogravimetric analysis	42

Figure 2.12	Molecular weight distribution of bulk liquid products from switchgrass lignin obtained with reaction conditions D-1, D-4, D-8 and D-20	43
Figure 2.13	Comparing lignin oil properties on Van Krevelan diagram	51
Figure 3.1	Relationship between Brønsted to Lewis acid site ratio calculated via pyridine FT-IR and ^{27}Al NMR.	65
Figure 3.2	^{27}Al NMR spectra of fully hydrated zeolites in proton form	66
Figure 3.3	Predominant reaction pathways established by feeding the various reactants and products to the reactor. Solid lines indicate observed products with conversions of more than 2% and dotted lines indicate hypothetical but unobserved pathways	68
Figure 3.4	Example of reactivity data obtained with increasing time on stream - conversion of phenol (○), 2-isopropylphenol selectivity (■), 4-isopropylphenol selectivity (●) and di-isopropylphenols selectivity (▲). Catalyst = HBEA, T = 350°C, Pressure = 1 atm, WHSV = 8.0 h ⁻¹ , Phenol concentration = 1.4 mol%, Phenol to propylene ratio = 1.4	70
Figure 3.5	Relationship between 2-IPP and 4-IPP molar ratios and the average dimension of the largest zeolite pore. These runs were all conducted with approximately the same conversions (see Table 3.6).	73
Figure 3.6	Relationship between selectivity of di-isopropylphenols and the average dimension of the largest zeolite pore. These runs were all conducted with approximately the same conversions and data can be found in Table 3.6.	73
Figure 3.7	X-ray diffraction (XRD) and nitrogen physisorption characterization of Al-SBA-15 (Si/Al = 26.6)	74
Figure 4.1	X-ray diffraction (XRD) patterns of synthesized zeolites	87
Figure 4.2	XRD pattern of ZnBEA89 as made, ZnBEA89 after ion-exchange (NH ₄ BEA89) and ZnBEA89 after ion-exchange and deammoniation (HZnBEA89). Peaks due to impurities that disappear after ion-	

	exchange step and the deammoniation step are indicated with ▲ and ■ respectively.	87
Figure 4.3	SEM images of synthesized zeolites	88
Figure 4.4	²⁹ Si NMR, ²⁷ Al NMR and ⁷¹ Ga NMR spectra of synthesized zeolites	92
Figure 4.5	FT-IR spectra hydroxyl region of activated zeolites	94
Figure 4.6	Change in number of Brønsted acid sites with increasing pyridine desorption temperature. Percentage of Brønsted acid sites remaining is relative to the number of Brønsted acid sites at 250°C.	95
Figure 4.7	Schematic of dominant reactions occurring in the gas phase alkylation of phenol with propylene at T =350°C and P=1atm	98
Figure 4.8	Differences in adsorption of phenol on (a) stronger acid site and (b) weaker acid site	99
Figure 5.1	Historical and projected figures of U.S domestic crude oil production by source and year in million barrels per day	103

LIST OF SCHEMES

- Scheme 2.1 Proposed reaction to alkylate phenol to p-ethylphenol in the presence of formic acid, ethanol and a Pt/C catalyst at 350°C 47
- Scheme 2.2 Proposed reaction for the cleavage of the β -O-4 linkage of 2-phenylethyl phenyl ether to form phenol, styrene, 2-phenylethyl alcohol, benzene and ethylbenzene in the presence of formic acid, ethanol and a Pt/C catalyst at 350°C 48
- Scheme 2.3 Proposed hydrodeoxygenation reactions of guaiacol in an ethanol solvent with formic acid and Pt/C at 350°C 49

LIST OF SYMBOLS AND ABBREVIATIONS

2-IPP	2-isopropylphenol
4-IPP	4-isopropylphenol
BdB-FHH	Frenkell–Halsey–Hill-modified Broekhoff–de Boer
DMSO	dimethyl sulfoxide
EFAL	extraframework aluminum
FID	flame ionization detector
$F_{\text{phenol feed}}$	molar flowrate of phenol feed
F_{products}	molar flowrate of products formed
FT	fourier transform
GC	gas chromatography
GPC	gel permeation chromatography
G-unit	guaiacyl unit
HPLC	high-performance liquid chromatography
H-unit	p-hydroxyphenyl unit
ICP	inductively coupled plasma
IPPE	isopropyl phenyl ether
IR	infrared
LC	liquid chromatography
LtL	lignin to liquid
MALDI TOF	matrix-assisted laser desorption/ ionisation-time of flight mass spectrometry
MAS	magic angle spinning
M_n	number average molecular weight
MS	mass spectrometry

M_w	weight average molecular weight
N_{2-IPP}	moles of 2-isopropylphenol
N_{4-IPP}	moles of 4-isopropylphenol
NMR	nuclear magnetic resonance
NOE	nuclear overhauser effect
OES	optical emission spectrometry
PPE	2-phenylethyl phenyl ether
ppm	parts per million
Γ_D	normalized deactivation rate
S-unit	syringyl unit
TCD	thermal conductivity detector
TEAOH	tetraethylammonium hydroxide
TEOS	tetraethyl orthosilicate
TGA	thermogravimetric analysis
THF	tetrahydrofuran
TOF	turnover frequency
TPD	temperature programmed desorption
$V_{\text{micropore}}$	micropore volume
WHSV	weight hourly space velocity
X	conversion
XRD	X-ray diffraction

SUMMARY

The objective of this work was to study catalytic routes for the valorization of lignin obtained from biomass. First, the efficacy of formic acid and Pt/C catalyst for the depolymerization and hydrodeoxygenation of lignin was studied. The goal of the study was to produce lignin to liquid oils with properties similar to that of crude oil. The study showed that the combination of formic acid and Pt/C promotes the production of higher fractions of lower molecular weight compounds in the liquid products. After 4 h of reaction, all of the switchgrass lignin is solubilized and one fifth of the biomass was converted into seven prominent phenolic species that were identified and quantified. Reaction time proved to be an important variable in affecting changes in product distributions and bulk liquid product properties such as H/C and O/C molar ratios. After 20 hours, the lignin is significantly depolymerized to form liquid products with a 76 % reduction in the weighted average molecular, a 50 % reduction in O/C and 10 % increase in H/C molar ratios compared to the switchgrass lignin. However, it was also clear that the lignin to liquid oils will require further processing to obtain similar properties as crude oil. Subsequently, the upgrading of phenol, a model compound for monomers in the oils obtained from lignin was investigated.

Second, the use of zeolites to catalyze the alkylation of phenol with propylene to form 2-isopropylphenol, a compound that could be a good feed for a subsequent hydrogenation step, was investigated. Specifically, various zeolite pore topologies and acidic properties were studied to determine how the specific properties would influence the selectivity for 2-isopropylphenol.

The reaction pathway of the alkylation reaction was elucidated by feeding in model compounds and it was determined that main reactions are the alkylation of phenol to form 2-isopropylphenol and 4-isopropylphenol. Other reactions such as O-alkylation and isomerization were minimal at the tested reaction conditions, though 2-isopropylphenol was found to be likely to de-alkylate. Of the zeolite topologies studied (FAU, BEA, MOR, MFI, TUN, MEL, MWW, MTT, CHA), maximum 2-isopropylphenol selectivity is obtained when the reactions are not restricted in the zeolite pores and the conversion occurs predominantly on the external surface. For intrazeolitic reactions, BEA zeolite maximizes the 2-isopropylphenol selectivity by balancing diffusion and steric limitations with secondary reactions producing di-alkylated products.

To further improve the selectivity for 2-isopropylphenol, the effects of varying BEA acid site strength on 2-isopropylphenol was studied. Isomorphously substituted BEA were synthesized and their acid strength and selectivity for 2-isopropylphenol was compared to that of AlBEA. Based on pyridine temperature programmed desorption, the acid strength was found to vary with $\text{AlBEA} \approx \text{GaBEA} > \text{ZnBEA}$. The 2-isopropylphenol selectivity was found to increase with weaker acid sites such as those found in ZnBEA. However, the activity of ZnBEA was also an order of magnitude lower than that of AlBEA and GaBEA. Consequently, GaBEA is recommended for the production of 2-isopropylphenol as it showed slightly better selectivity for 2-isopropylphenol than AlBEA with similar activity.

CHAPTER 1

Introduction

1.1 Motivation

Currently, crude oil is an important source of chemicals and energy for our everyday lives. It not only provides the gas we need for ground and air transportation, it also provides the aliphatic and aromatic molecules that are the building blocks for our fine chemicals, plastics, adhesives, etc. Although fossil fuels are very useful, they are also not renewable and their use can negatively impact our environment as its use is accompanied with the release of greenhouse gases into the atmosphere, a leading cause of global warming. Additionally, our supply of crude oil is not inexhaustible. The average domestic crude oil production in the United States had been on a decline from the 1990s to 2008 (Figure 1.1). However, in 2009, advances in technologies such as hydraulic fracturing increased the accessibility of tight oil and created a temporary increase in crude oil production [1]. In spite of this sudden deviation, the projected long term production of crude oil is still expected to decline since it is a finite resource. Thus, even though crude oil is very useful, we have to find more environmentally friendly alternatives and decrease our reliance on it due to its limited supply.

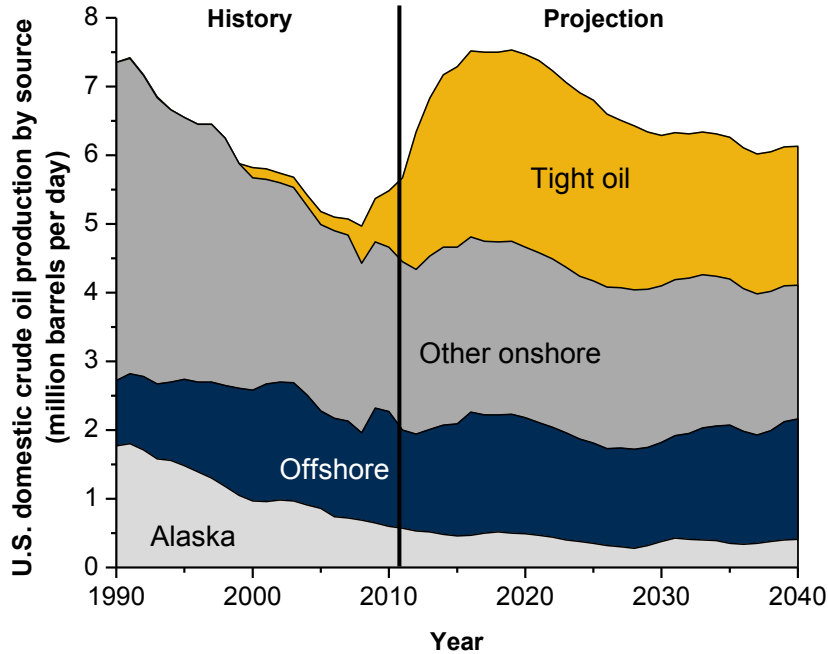


Figure 1.1 Historical and projected figures of U.S domestic crude oil production by source and year in million barrels per day [1]

Currently, the US has adopted the use of ethanol as a means to supplement fossil fuels. With the production of cellulosic ethanol, the U.S Department of Energy estimates that 225 million tons of lignin, a byproduct, will be available annually [2]. Thus, it is important that this byproduct is not wasted, but rather converted into more valuable products such as fuels and petrochemicals. The valorization of lignin requires multiple steps and cannot be done in a one-step process. A possible conversion route is to depolymerize lignin into phenolic monomers that can then be alkylated to give it either enhanced fuel characteristics or allow it to be a feed for the production of other chemicals (Figure 1.2). Consequently, the purpose of this thesis is to investigate heterogeneously catalyzed reactions that can be used to convert lignin into fuels or intermediate chemicals via the aforementioned route.

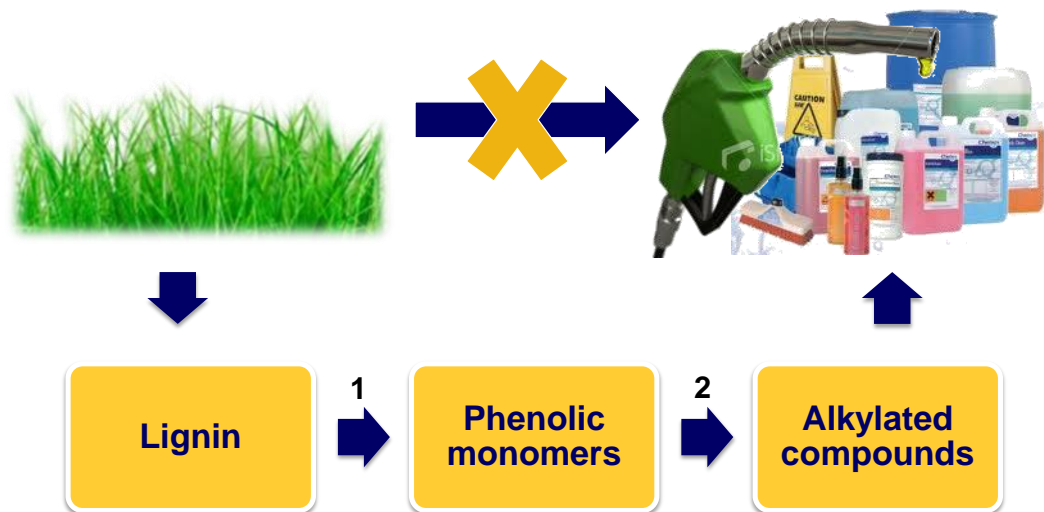


Figure 1.2 Proposed route of converting lignin to fuel and chemicals via (1) depolymerization followed by (2) alkylation

1.2 Depolymerization and Hydrodeoxygenation of Lignin

All biomass material contains three main components – cellulose, hemicellulose and lignin. At present, corn cellulose is utilized for the production of cellulosic ethanol. However, this is not sustainable since use of corn as an energy crop competes with its use as a food crop, and using only the cellulosic component results in wasting the hemicellulosic and lignin components which could potentially be converted into more useful products. More recently, Switchgrass and Miscanthus have been identified as next-generation ethanol feedstocks as they are perennial grasses that have a high productivity per unit area [3]. Consequently, it is important to study methods to convert Switchgrass lignin into useful products.

Lignin is a poly-aromatic structure that is made of three different monomeric units – p-hydroxyphenyl (H), guaiacyl (G) and syringyl (S) units, shown in Figure 1.3, derived

from p-coumaryl alcohol, coniferyl alcohol and sinapyl alcohol respectively. The final lignin structure is synthesized in plants through the enzymatic oxidation and random radical polymerization reactions of these monomeric units as shown in Figure 1.4 [4].

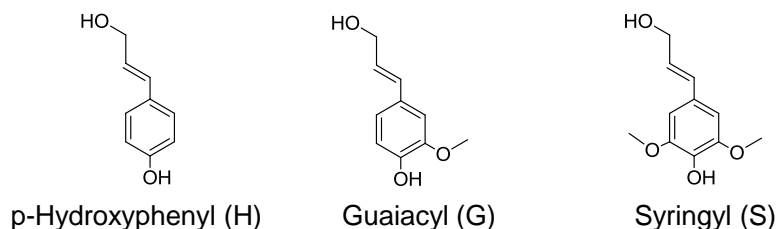


Figure 1.3 Monomeric building blocks of lignin

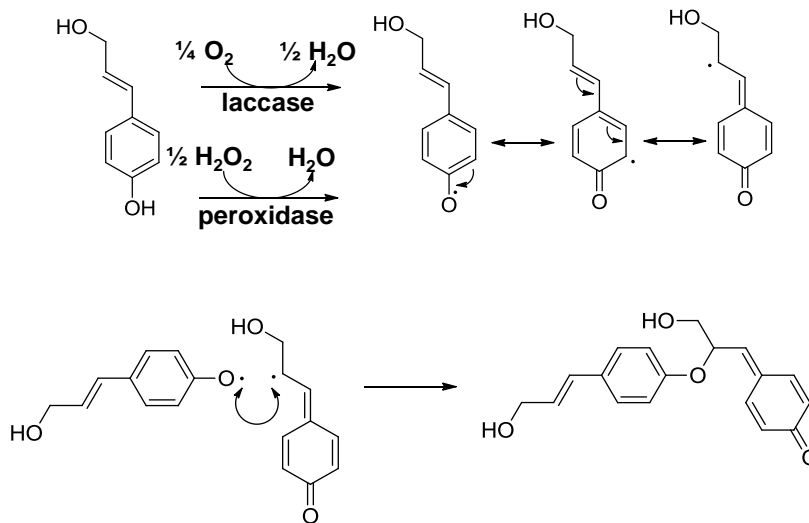


Figure 1.4 Example of lignin synthesis in plants through enzymatic oxidation of p-hydroxyphenyl unit followed by its random polymerization

Lignin is particularly resistant to chemical degradation as its primary functions are to provide structural support and protection against pathogens in plants. The formation of lignin allows it to achieve these characteristics through a range of bond

strengths and chemical reactivities from various combinations of aryl-ether-aryl and aryl-aryl bonds, a variety of methoxy, phenolic, carbonyl and hydroxyl functional groups (Figure 1.5). Subsequently, a wide variety of chemical treatments have been attempted to effectively break down the complex lignin into useful biofuels.

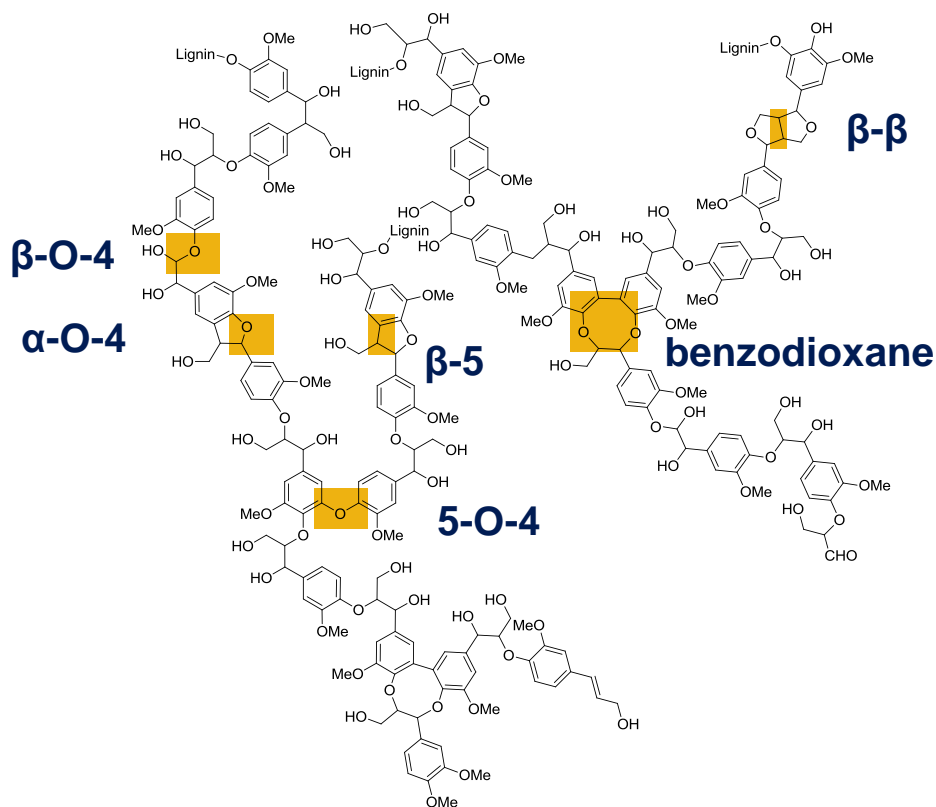


Figure 1.5 Proposed lignin structure with characteristic lignin bonds highlighted [5]

Switchgrass contains approximately 17%-26% lignin [6] which can be isolated in a variety of ways such as kraft pulping, sulfite pulping, soda pulping, acid organosolv processes, alcohol organosolv processes and pyrolysis [7]. Depending on the severity of the method, these processes can result in either the extraction of lignin with most of the lignin structure intact or the various degrees of degradation of lignin into smaller fragments in the process. Once the lignin has been extracted, further reactions are often

required to break the lignin down into more useful, smaller liquid fragments and improve its qualities so that it can be used as a fuel.

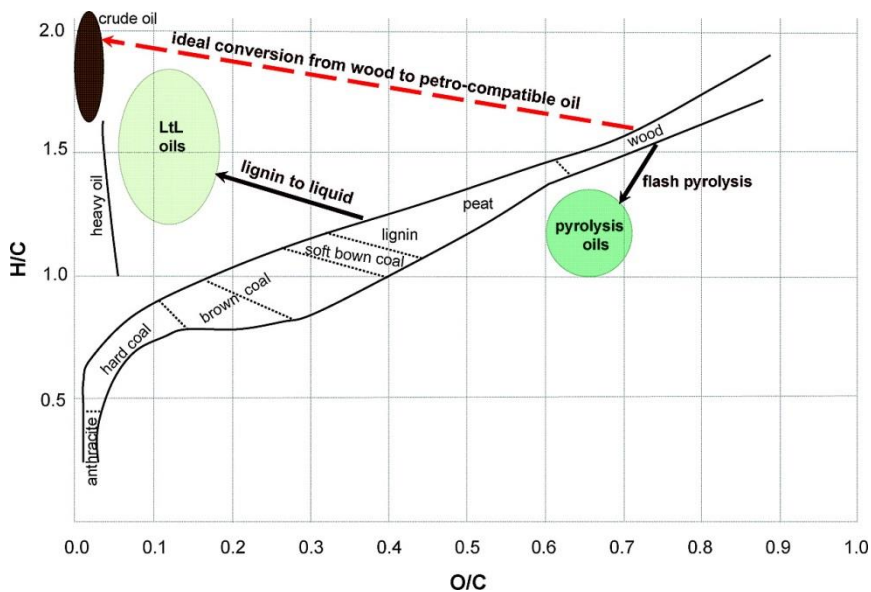


Figure 1.6 Van Krevelan diagram comparing the H/C and O/C molar ratios of different biomass and fossil materials [8]

An overview of the success in converting lignin to liquid oils is shown in the Van Krevelan diagram in Figure 1.6 where the H/C and O/C molar ratios of various starting biomass materials and products are compared to that of crude oil. H/C and O/C molar ratios can be a good general indicator of the overall volatility, viscosity and heating value of the liquid products. Typically, a higher H/C molar ratio will mean higher heating values and compounds with lower O/C molar ratios tend to be less volatile and less viscous.

Current technologies of converting lignin to liquid oils (LtL oils) have made good advances in achieving lower O/C molar ratios and higher H/C molar ratios in the process of converting lignin via hydrogenation, hydrodeoxygenation and various thermochemical

methods. Several papers have published extensive reviews on current research on these methods [7, 9–11]. However, it is clear that even with these advances, the current methods are not enough to fully convert lignin to oils that have the same H/C and O/C molar ratios as crude oil. Consequently, further processing steps such as alkylation and hydrogenation can be applied to obtain the required H/C and O/C molar ratios. In Figure 1.7, an example of the changes in H/C and O/C molar ratios of phenol, a model compound for chemicals found in lignin to liquid oil after 20 hours of reaction, after alkylation and hydrogenation steps is shown.

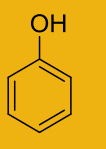
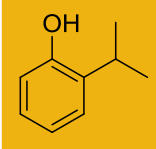
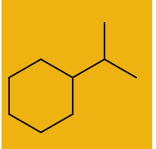
	LtL oil T = 20h			
H/C	1.3	1.0	1.3	2.0
O/C	0.2	0.2	0.1	0

Figure 1.7 H/C and O/C molar ratios of products produced from lignin derived phenol after alkylation and hydrogenation

Previous work in the group involving hydrogenation of phenolic compounds with a Pt/HY catalyst demonstrated that amongst various substituted phenols tested, a phenolic feed with a 3 carbon side chain in the ortho position showed no signs of catalyst deactivation and maintained a high selectivity to the targeted substituted cyclohexane product after 10 hours of reaction (Figure 1.8). Thus, in the phenol alkylation with propylene reactions, the production of *o*-isopropylphenol aka 2-isopropylphenol was optimized as it is potentially a good feed for the subsequent hydrogenation reaction.

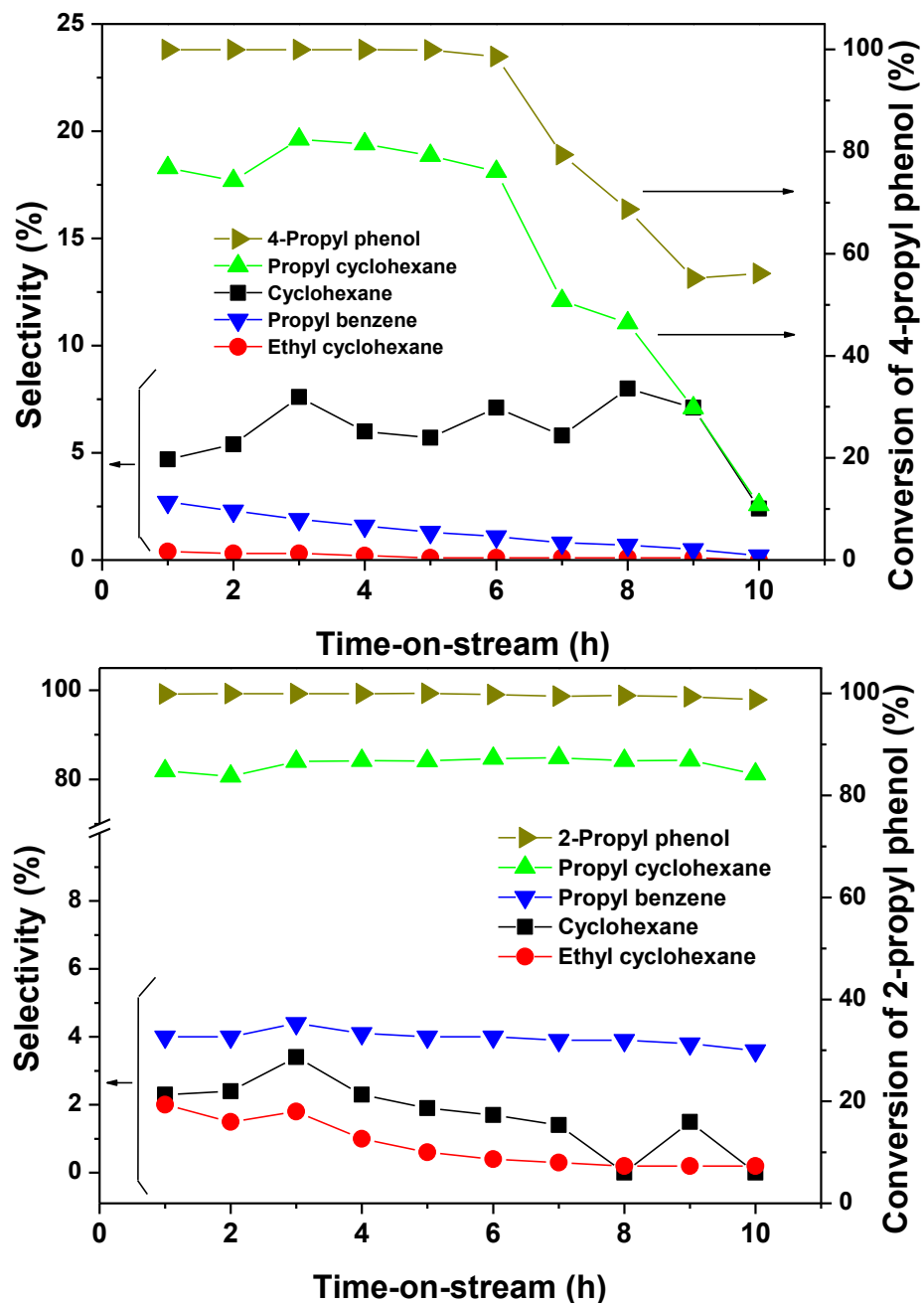


Figure 1.8 Hydrogenation of 4-propylphenol and 2-propylphenol over 0.5 wt.% Pt/HY ($\text{SiO}_2/\text{Al}_2\text{O}_3 = 12$) catalyst. Experiments conducted by Do-Young Hong. Reaction conditions: $T = 200\text{ }^\circ\text{C}$; $P_{\text{H}_2} = 40\text{ bar}$; Catalyst loading, 100 mg; WHSV, 5 h^{-1}

1.3 Zeolite Catalyzed Alkylation of Phenol

Friedel-Crafts alkylation was first discovered in 1877 by Charles Friedel and James Mason Crafts from a reaction that produced amylbenzene using benzene and amyl chloride in the presence of aluminum chloride [12]. Since then, alkylation has become an important reaction employed in industry to synthesize a wide variety of compounds. In particular, ethylbenzene and cumene, which are important intermediates in the industrial production of styrene, phenol and acetone, are synthesized by the alkylation of aromatics [13]. Traditionally, industrial alkylation processes employ AlCl_3 promoted by ethyl chloride or HCl [14]. Such liquid catalysts promote high reactant conversions, but several disadvantages are associated with their use. First, large quantities of acid needed for catalysis, often in stoichiometric amounts, generate a large amount of waste. Second, these catalysts are also highly toxic and corrosive, thus requiring special handling, transportation and storage considerations. Third, the homogeneity of such liquid catalysts creates downstream issues where the acids need to be neutralized and separated from the liquid products. Fourth, there is little product selectivity as product distributions are typically governed by the orientation and reactivity of the reactants, yielding thermodynamic product distributions. Consequently, there has been a move towards solid acid catalysts as alternatives to circumvent these disadvantages associated with liquid catalysts. A wide variety of solid acid catalysts have been shown to catalyze aromatic alkylation in either the vapor or liquid phase. Some of these catalysts include oxides [15, 16], phosphates [17, 18], mixed metal oxides [19, 20], hydrotalcites [21–23] and zeolites [24–26]. However, zeolites have been the most widely adopted solid catalysts for industrial alkylation processes. As of 2002, approximately 24% of the aromatic

alkylations in industry are catalyzed by $\text{AlCl}_3\text{-HCl}$, 40% by zeolite catalysts in the gas phase and 36% by zeolite catalysts in the liquid phase [27].

The prevalent use of zeolites to replace liquid catalysts in industry can be attributed to the ease with which the structural and acidic properties of the zeolites can be tailored for alkylation reactions [28]. Zeolites are crystalline aluminosilicates that contain micropores in their framework. Due to their high crystallinity, they have only a narrow range of pore sizes and their pore topologies can be categorized by their largest pore size: 14+ member rings (extra-large), 12 member ring (large), 10 member ring (medium) or 8 member ring (small) pores. The various topologies and small diameters of these pores (2 – ~ 10 Å) allow zeolites to be shape selective towards certain products in alkylation reactions. This ability for increased selectivity is especially important for alkylation reactions where selectivity is often low due to various products formed from alkylation side reactions such as dealkylation, transalkylation, disproportionation and isomerization.

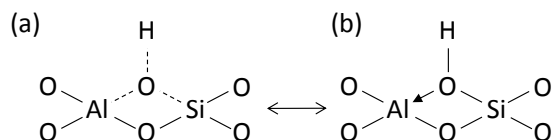


Figure 1.9 Brønsted acid structure in zeolites, resonance hybrid of (a) bridging hydroxyl and (b) terminal silanol with Al Lewis acid-base interaction [29]

Zeolites also have a net negative charge associated with the tetrahedrally-coordinated framework aluminum [30]. This net negative charge is often balanced by the presence of extra-framework cations like Na^+ and K^+ when synthesized, but these cations can be exchanged with protons to generate acid sites in the zeolite. The Brønsted acid

structure of zeolites is described as a resonance structure between a bridging hydroxyl and a terminal silanol with aluminium lewis acid-base interaction (Figure 1.9). These acid sites can vary depending on the Si/Al ratio of the zeolites, degree of ion-exchange and the presence of extra-framework aluminum. Consequently, the pore topology and acidity of the zeolite can be optimized to make zeolites highly active and selective alkylation catalysts.

Several articles in literature have described the use of various zeolites as catalysts for alkylation. In general, studies have concentrated on large pore zeolites such as HY (FAU), H β (BEA), HMOR (MOR), HZSM-5 (MFI), HZSM-11 (MEL), HZSM-12 (MTW), HMCM-22 and their rare earth (La, Cs, Ga) exchanged forms [31–33]. These studies focused on the effects of varying acid concentration and acid strength by Si/Al changes during synthesis [34, 35] or post-synthesis [36–38] using different zeolites, with particular emphasis on the reactant conversions and product distributions. When pore sizes were varied, it was generally observed that larger pores formed more di-alkylated products than medium pores and had higher reactant conversions [39–41]. The exchange of rare earth metals into zeolites resulted in increased total acidity, increased reactant conversions and higher activity [42–44]. Decreasing Si/Al ratios in zeolites typically correlates to an increase in acid concentration and decrease in acid strength. Different methods can be employed to change the Si/Al ratio but it is most commonly changed by varying Si/Al ratios during synthesis or by hydrothermal treatment where the zeolite is steamed at high temperatures. Generally, changes in Si/Al ratios greatly affected the reactant conversion. However, a specific trend between Si/Al and conversion rates could

not be discerned, even after accounting for the method employed to change the Si/Al ratio [38, 45–50].

Studies have demonstrated that Lewis solid acids (e.g. supported metal halides) and Brønsted solid acids (e.g. Amberlyst-15) have the ability to catalyze alkylation reactions [51]. Consequently, both the Brønsted and Lewis acid sites found in zeolites should be able to catalyze alkylation reactions but the literature suggests that the Brønsted acid sites are the catalytic sites in zeolites for alkylation. The adsorption of alkylation reactants with the bridging hydroxyl groups that act as Brønsted acid sites has been proposed [52] and studied via IR [53, 54], NMR [55, 56] and computer simulations [57–59]. More recently, various methods have been developed to alter the physical characteristics of the zeolites in order to obtain higher selectivity. In particular, zeolites with smaller particle sizes [60], varying degrees of crystallinities [61] and additional mesopores [62] have been synthesized to improve the performance of zeolites as alkylation catalysts.

The vast literature on alkylation reactions with zeolites has been primarily focused on the production of compounds like ethylbenzene and cumene, which have been of industrial interest. As such, there is little literature on zeolite catalysis of the alkylation of phenol with propylene. As stated before, this particular type of alkylation could be of increasing interest as industry seeks to integrate biofuels with current fuels from crude oil. From literature on alkylation, it is clear that there are several ways of optimizing zeolites for the reaction of interest. In particular, zeolite pore size, total acid concentration and acid strength are shown to greatly affect product selectivity and reactant conversions. Consequently, the focus is on identifying zeolites with the pore size that will enable it to

selectively catalyze the production of *o*-isopropylphenol, and optimizing the acid concentration and strength of zeolite to achieve higher target product selectivity.

1.4 Objectives, Hypotheses, and Specific Aims

The objective of this project is to produce phenolic monomers from the depolymerization and hydrodeoxygenation of switchgrass lignin that can then be alkylated to give species with either enhanced fuel characteristics or renewable chemicals. The first part of this thesis focuses on the conversion of switchgrass lignin to liquid products using Pt/C and formic acid. The second and the third parts focus on zeolite catalyzed production of *o*-isopropylphenol, a species that may cause less catalyst deactivation in subsequent hydrogenation steps based on the previous work done in our group. In particular, the work focuses on identifying zeolites with appropriate pore sizes and acid properties that will enable the coupling of high selectivity for *o*-isopropylphenol, high conversion of phenol and minimal coking in the alkylation of phenol with propylene.

Specific Aim 1: Study the efficacy of Pt/C and formic acid for the depolymerization and hydrodeoxygenation of switchgrass lignin

Hypothesis: The in situ production of hydrogen from formic acid and presence of Pt/C, a common hydrogenation catalyst, can provide conditions to enhance the simultaneous depolymerization and hydrodeoxygenation of switchgrass lignin in a one-step, batch process.

Approach: The products obtained from switchgrass lignin in the presence of Pt/C and/or formic acid are thoroughly characterized and studied to determine the effects of these reaction components. Some model compound studies were also initiated to understand the specific reactions that may occur under these reaction conditions.

Significance: Currently, several steps are required to depolymerize and hydrodeoxygenate lignin into liquid products that have characteristics suitable for use as fuel. A one step process will help reduce the number of reactions required and aid understanding the effects of various reaction components on the further development of technologies to convert lignin to liquid fuels.

Specific Aim 2: Optimize the zeolite pore size to maximize the selectivity of mono-alkylated, ortho-substituted isopropylphenol.

Hypothesis: Zeolite pore sizes can be tuned to maximize the selectivity of mono-alkylated, ortho-substituted isopropylphenol, 2-isopropylphenol. As larger pore zeolites will be more selective towards ortho-substituted products and di-alkylated products, and smaller pore zeolites will yield more para-substituted products and mono-alkylated products, whereas a medium pore size will allow the maximizing of the selectivity towards *o*-isopropylphenol.

Approach: Nine zeolites with a range of pore sizes bounded by 8, 10 and 12 member rings and bulk Si/Al molar ratios between 10 and 17 were

selected. Consequently, these zeolites will have different pore sizes but are expected to have similar acidic properties. The pore volume, pore size distribution and surface area of the zeolites were characterized. These zeolites were then tested in the vapor phase alkylation of phenol with propylene and their selectivity for mono-alkylated 2-isopropylphenol was determined.

Significance: Several side reactions such as transalkylation, isomerization and disproportionation occur together with alkylation, causing a wide variety of products to be formed in addition to the desired product. The zeolite pore topology can be optimized to obtain high selectivity for 2-isopropylphenol.

Specific Aim 3: Optimize zeolite Brønsted acid strength to maximize conversion of phenol while minimizing coking.

Hypothesis: The strength of Brønsted acid sites can be tuned to maximize the conversion of phenol as well the selectivity for 2-isopropylphenol. The strength of the acid site may influence the orientation of the adsorbed phenol molecule, the activity of side reactions and the subsequent products formed. Additionally, stronger Brønsted acid sites are expected to catalyze coking faster than weak and medium strength Brønsted acid sites. Hence, there may be an optimal acid strength at which high selectivity for 2-isopropylphenol can be obtained with reasonable catalyst deactivation.

Approach: Zeolite acid strength can be varied by isomorphously substituting the Al atom for other atoms that form metallosilicate structures. Here, Al-, Ga-, Zn-, and B-BEAs are synthesized to yield a set of zeolites that have varying acid strengths but similar pore topologies. The zeolite acid properties such as total amount of acid sites and percentage of strong acid sites were then characterized. The zeolites were tested in the vapor phase alkylation reaction and the conversion of phenol and rate of catalyst deactivation was determined.

Significance: To be industrially viable, the zeolite needs to have high conversion rates to maximize the production of 2-isopropylphenol and maintain its activity for long periods of time to reduce the catalyst regeneration frequency. Optimizing the zeolite acidity will thus increase the feasibility of its use in industry.

1.5 References

- [1] *Annual Energy Outlook 2013 with projections to 2040*; 2013.
- [2] Holladay, J. E.; Bozell, J. J.; White, J. F.; Johnson, D. Top Value-Added Chemicals from Biomass Volume II—Results of Screening for Potential Candidates from Biorefinery Lignin **2007**, 1–87.
- [3] Davis, S. C.; Parton, W. J.; Grosso, S. J. Del; Keough, C.; Marx, E.; Adler, P. R.; DeLucia, E. H. *Frontiers in Ecology and the Environment* **2012**, *10*, 69–74.
- [4] Boerjan, W.; Ralph, J.; Baucher, M. *Annual Review of Plant Biology* **2003**, *54*, 519–546.
- [5] Brunow, G.; Kilpeläinen, I.; Sipilä, J.; Syrjänen, K.; Karhunen, P.; Setälä, H.; Rummakko, P. Oxidative Coupling of Phenols and the Biosynthesis of Lignin. In

- Lignin and Lignan Biosynthesis*; American Chemical Society, 1998; Vol. 697, pp. 10–131.
- [6] Hu, G.; Cateto, C.; Pu, Y.; Samuel, R.; Ragauskas, A. J. *Energy & Fuels* **2012**, *26*, 740–745.
- [7] Azadi, P.; Inderwildi, O. R.; Farnood, R.; King, D. a. *Renewable and Sustainable Energy Reviews* **2013**, *21*, 506–523.
- [8] Kleinert, M.; Barth, T. *Energy & Fuels* **2008**, *22*, 1371–1379.
- [9] Zakzeski, J.; Bruijninx, P. C. A.; Jongerius, A. L.; Weckhuysen, B. M. *Chemical Reviews* **2010**, *110*, 3552–3599.
- [10] Pandey, M. P.; Kim, C. S. *Chemical Engineering & Technology* **2011**, *34*, 29–41.
- [11] Jacobson, K.; Maheria, K. C.; Kumar Dalai, A. *Renewable and Sustainable Energy Reviews* **2013**, *23*, 91–106.
- [12] Friedel, C.; Crafts, J. M. *Bulletin de la Societe Chimique de France* **1877**, *27*, 530.
- [13] Degnan Jr., T. F.; Smith, C. M.; Venkat, C. R. *Applied Catalysis A: General* **2001**, *221*, 283–294.
- [14] Marcilly, C. Alkylation of Aromatics by Olefins. In *Acido-Basic Catalysis*; Editions Technip: France, 2006; Vol. 2, pp. 515–535.
- [15] Rao, P. R. H. P.; Ueyama, K.; Matsukata, M. *Applied Catalysis A, General* **1998**, *166*, 97–103.
- [16] Sato, S.; Koizumi, K.; Nozaki, F. *Applied Catalysis a-General* **1995**, *133*, L7–L10.
- [17] Nozaki, F.; Kimura, I. *Bulletin of the Chemical Society of Japan* **1977**, *50*, 614–619.
- [18] Zhu, X. M.; Li, X. M.; Jia, M. J.; Liu, G.; Zhang, W. X.; Jiang, D. Z. *Applied Catalysis a-General* **2005**, *282*, 155–161.
- [19] Wang, Y. L.; Yang, P. P.; Liu, G.; Xu, L.; Jia, M. J.; Zhang, W. X.; Jiang, D. H. *Catalysis Communications* **2008**, *9*, 2044–2047.
- [20] Crocella, V.; Cerrato, G.; Magnacca, G.; Morterra, C.; Cavani, F.; Cocchi, S.; Passeri, S.; Scagliarini, D.; Flego, C.; Perego, C. *Journal of Catalysis* **2010**, *270*, 125–135.
- [21] Velu, S.; Swamy, C. S. *Applied Catalysis a-General* **1994**, *119*, 241–252.

- [22] Velu, S.; Swamy, C. S. *Applied Catalysis a-General* **1997**, *162*, 81–91.
- [23] Padmasri, A. H.; Venugopal, A.; Kumari, V. D.; Rao, K. S. R.; Rao, P. K. *Journal of Molecular Catalysis a-Chemical* **2002**, *188*, 255–265.
- [24] Balsama, S.; Beltrame, P.; Beltrame, P. L.; Carniti, P.; Forni, L.; Zuretti, G. *Applied Catalysis* **1984**, *13*, 161–170.
- [25] Marczewski, M.; Perot, G.; Guisnet, M. Alkylation of Aromatics II. Alkylation of Phenol with Methanol on Various Zeolites. In *Studies in Surface Science and Catalysis*; M. Guisnet, J. B. C. B. D. D. C. M.; Pérot, G., Eds.; Elsevier, 1988; Vol. Volume 41, pp. 273–282.
- [26] Waghlikar, S.; Mayadevi, S.; Sivasanker, S. *Applied Catalysis A: General* **2006**, *309*, 106–114.
- [27] Perego, C.; Ingallina, P. *Catalysis Today* **2002**, *73*, 3–22.
- [28] Weitkamp, J. *Solid State Ionics* **2000**, *131*, 175–188.
- [29] Corma, A. *Current Opinion in Solid State & Materials Science* **1997**, *2*, 63–75.
- [30] Burton, A. *Nat Mater* **2003**, *2*, 438–440.
- [31] Guzman, A.; Zuazo, I.; Feller, A.; Olindo, R.; Sievers, C.; Lercher, J. A. *Microporous and Mesoporous Materials* **2005**, *83*, 309–318.
- [32] Thomas, B.; Sugunan, S. *Indian Journal of Chemical Technology* **2005**, *12*, 676–688.
- [33] Zhao, Z. K.; Qiao, W. H.; Wang, G. R.; Li, Z. S.; Cheng, L. *Journal of Molecular Catalysis a-Chemical* **2006**, *250*, 50–56.
- [34] Bhattacharyya, K. G.; Talukdar, A. K.; Das, P.; Sivasanker, S. *Journal of Molecular Catalysis A: Chemical* **2003**, *197*, 255–262.
- [35] Kumar, G. S.; Saravanamurugan, S.; Hartmann, M.; Palanichamy, M.; Murugesan, V. *Journal of Molecular Catalysis a-Chemical* **2007**, *272*, 38–44.
- [36] Corma, A.; Martinez, A.; Martinez, C. *Applied Catalysis A: General* **1996**, *134*, 169–182.
- [37] Hornacek, M.; Hudec, P.; Nociar, A.; Smieskova, A.; Jakubik, T. *Chemical Papers* **2010**, *64*, 469–474.

- [38] Anand, R.; Maheswari, R.; Gore, K. U.; Tope, B. B. *Journal of Molecular Catalysis a-Chemical* **2003**, *193*, 251–257.
- [39] Sad, M. E.; Padró, C. L.; Apesteguía, C. R. *Applied Catalysis A: General* **2008**, *342*, 40–48.
- [40] Sad, M. E.; Padró, C. L.; Apesteguía, C. R. *Catalysis Today* **2008**, *133-135*, 720–728.
- [41] Klerk, A. De; Nel, R. J. J. *Ind. Eng. Chem. Res.* **2007**, 7066–7072.
- [42] Barman, S.; Pradhan, N. C.; Basu, J. K. *Catalysis Letters* **2006**, *111*, 67–73.
- [43] Gauthier, C.; Chiche, B.; Finiels, A.; Geneste, P. *Journal of Molecular Catalysis* **1989**, *50*, 219–229.
- [44] Parikh, P. A.; Subrahmanyam, N.; Bhat, Y. S.; Halgeri, A. B. *Applied Catalysis A: General* **1992**, *90*, 1–10.
- [45] Zhang, K.; Huang, C.; Zhang, H.; Xiang, S.; Liu, S.; Xu, D.; Li, H. *Applied Catalysis A: General* **1998**, *166*, 89–95.
- [46] Miyamoto, Y.; Katada, N.; Niwa, M. *Microporous and Mesoporous Materials* **2000**, *40*, 271–281.
- [47] Wang, B.; Lee, C. W.; Cai, T. X.; Park, S. E. *Catalysis Letters* **2001**, *76*, 219–224.
- [48] Sebastian, C. P.; Pai, S.; Sharanappa, N.; Satyanarayana, C. V. V *Journal of Molecular Catalysis A: Chemical* **2004**, *223*, 305–311.
- [49] Pai, S.; Gupta, U.; Chilukuri, S. *Journal of Molecular Catalysis A: Chemical* **2007**, *265*, 109–116.
- [50] Dumitriu, E.; Hulea, V. *Journal of Catalysis* **2003**, *218*, 249–257.
- [51] Modrogan, E.; Valkenberg, M. H.; Hoelderich, W. F. *Journal of Catalysis* **2009**, *261*, 177–187.
- [52] Nandhini, K. U.; Arabindoo, B.; Palanichamy, M.; Murugesan, V. *Journal of Molecular Catalysis A: Chemical* **2006**, *243*, 183–193.
- [53] Kondo, J. N.; Domen, K. *Journal of Molecular Catalysis a-Chemical* **2003**, *199*, 27–38.
- [54] Boronat, M.; Corma, A. *Applied Catalysis A: General* **2008**, *336*, 2–10.

- [55] Siffert, S.; Gaillard, L.; Su, B. L. *Journal of Molecular Catalysis A: Chemical* **2000**, *153*, 267–279.
- [56] Beutel, T.; Peltre, M. J.; Su, B. L. *Colloids and Surfaces A: Physicochemical and Engineering Aspects* **2001**, *187-188*, 319–325.
- [57] Zalazar, M. F.; Duarte, D. J. R.; Peruchena, N. M. *The Journal of Physical Chemistry A* **2009**, *113*, 13797–13807.
- [58] Namuangruk, S.; Pantu, P.; Limtrakul, J. *Journal of Catalysis* **2004**, *225*, 523–530.
- [59] Rigby, A. M.; Frash, M. V. *Journal of Molecular Catalysis A: Chemical* **1997**, *126*, 61–72.
- [60] Sakthivel, A.; Iida, A.; Komura, K.; Sugi, Y.; Chary, K. V. R. *Microporous and Mesoporous Materials* **2009**, *119*, 322–330.
- [61] Kasture, M. W.; Niphadkar, P. S.; Sharanappa, N.; Mirajkar, S. P.; Bokade, V. V.; Joshi, P. N. *Journal of Catalysis* **2004**, *227*, 375–383.
- [62] Xu, L.; Wu, S.; Guan, J.; Wang, H.; Ma, Y.; Song, K.; Xu, H.; Xing, H.; Xu, C.; Wang, Z.; Kan, Q. *Catalysis Communications* **2008**, *9*, 1272–1276.

CHAPTER 2

Depolymerization and Hydrodeoxygenation of Switchgrass Lignin

This chapter is largely reproduced from “Depolymerization and Hydrodeoxygenation of Switchgrass Lignin with Formic Acid” by Weiyin Xu, Stephen J. Miller, Pradeep, K. Agrawal, and Christopher W. Jones, published in *ChemSusChem*, in 2012, volume 5, pages 667-675 [1].

2.1 Introduction

Typically, biorefineries hydrolyze cellulose and hemicellulose into monosaccharides that can be fermented into ethanol or converted into chemical intermediates like hydroxymethylfurfural [2–4] or other furan compounds [5, 6]. However, this only utilizes approximately two-thirds of the lignocellulosic biomass feed, as lignin makes up the remaining fraction of plant mass. Currently, lignin is most-often burned as a cheap fuel to produce steam and electricity in biorefineries. To improve the economics of biorefineries, one should consider ways to convert lignin into higher value products such as fuel additives or aromatic chemicals [7]. As mentioned in the previous section, this can help make the production of fuels and chemicals a more sustainable process. In this work, the conversion of lignin into soluble liquids, also known as “lignin-to-liquid oils,” is explored. The conversion process involves the simultaneous depolymerization and hydrodeoxygenation of lignin with the use of a typical hydrodeoxygenation catalyst, Pt/C and an in situ hydrogen source, formic acid.

Lignin is a poly-aromatic structure that is synthesized in plants through the random radical polymerization of *p*-hydroxyphenylpropane units [8]. Lignin is particularly resistant to chemical degradation as its primary functions are to provide structural support and protection against pathogens in plants. The formation of lignin allows it to achieve these characteristics through various combinations of aryl-ether-aryl and aryl-aryl bonds, a variety of methoxy, phenolic, carbonyl and hydroxyl functional groups, and a range of bond strengths and chemical. Subsequently, a wide variety of chemical treatments have been attempted to effectively break down the complex lignin into useful biofuels.

Lignin conversion methods can be differentiated between those that optimize for syngas or bio-oil production. Additionally, some lignin conversion methods focus only on depolymerization, which can be followed with a second upgrading step to stabilize the products [7] while others attempt to combine depolymerization and processing steps such as hydrodeoxygenation in a one step process.

Depolymerization methods include acid or base catalysed depolymerization, gasification, supercritical fluid conversion, pyrolysis and liquefaction [9, 10]. Bio-oils produced usually have high water and oxygen content, high viscosity, low pH values, and low heating values [11, 12]. These bio-oils are thus corrosive, reactive, and difficult to transport, and generally lack the characteristics of a good fuel. Subsequently, a further processing step is often required to upgrade the bio-oil and improve its fuel properties.

To circumvent the two step process, studies have been conducted to improve upon the depolymerization process with the addition of capping agents such as phenol [13, 14]

and boric acid [15] to obtain bio-oils with lower molecular weight and improved fuel characteristics. Alternatively, it has been demonstrated that depolymerization and upgrading can be combined into a one-step process with considerable success [16]. A Co/Mo catalyst supported on γ -alumina combined with phosphoric acid was reported to quench lignin hydrogenolysis products, preventing them from recondensing with the lignin, forming oil yields of up to 60% [17]. Additionally, the removal of volatile products like phenol increased product yields by preventing their recombination with other lignin products. A combination of 5% Ru/ γ -Al₂O₃ with 20 bar of H₂ and supercritical ethanol was recently found to partially convert organosolv lignin into bio-oils with higher heating values of 36.2 MJ/kg [18]. Barta et al. used supercritical methanol and copper supported on a porous metal oxide to simultaneously depolymerize and hydrogenate organosolv sawdust lignin to obtain bio-oils with decreased oxygen content [19]. Applying high temperatures and formic acid to lignin dissolved in an organic solvent also yielded depolymerized and hydrodeoxygenated lignin-to-liquid oils with O/C ratios significantly lower than the starting lignins [20].

This work was inspired by the success of employing formic acid in an organic solvent to depolymerize various lignins and obtain up to 89% decrease and 50% increase in O/C and H/C molar ratios respectively [20]. Additionally, formic acid is a readily available green reagent in a biorefinery, as it can be manufactured from the decomposition of monosaccharides obtained from the biomass [21] or the oxidation of lignin with dilute hydrogen peroxide [22]. In this work, a hydrodeoxygenation catalyst, Pt/C, was added to utilize the hydrogen generated from the *in situ* decomposition of

formic acid. In principle, the extent of hydrodeoxygenation is expected to increase with the catalyst, therefore decreasing the O/C molar ratios even further.

This contribution describes the effect of increasing reaction times, and presence of formic acid and Pt/C on the product distributions obtained from switchgrass lignin.

2.2 Experimental Methods

2.2.1 Reaction Procedure

All reactions were performed in a batch reactor made with a 7.125-in length of 0.5-in O.D x 0.083-in thickness 316/316L stainless steel tubing capped at both ends. All reactor parts were obtained from Swagelok and a schematic of the reactor is shown in Figure 2.1. No significant metal corrosion or metal leaching [23] was observed in all of the reactions (see section 2.3.3).

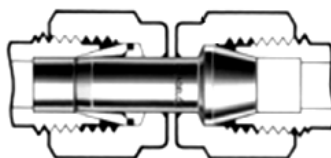


Figure 2.1 Schematic drawing of batch reactor

At the start of the reaction, 250 mg of switchgrass lignin, 25 mg of 20 wt% Pt/C catalyst (Alfa-Aesar), 1 g of formic acid (GR ACS, 98%, EMD Chemicals) and 5 g of ethanol (200 proof, anhydrous, $\geq 99.5\%$, Sigma-Aldrich) were loaded into the reactor. The reactor was then sealed and shaken for 1 minute to mix the reactants before it was

inserted into a sand bath that had been preheated overnight at 350 °C. After 1, 4, 8 or 20 hours, the reactor is removed from the sand bath, immersed in an ice bath for 20 minutes to quench the reaction and then removed from the ice bath to allow it to reach room temperature. The reactor is then carefully opened with wrenches to prevent any liquids from gushing out and the weight loss from the gas products was quantified using a mass balance. The solution was then filtered to remove any solid residues and the weight of any solids was measured. The Pt/C catalyst was characterized by the manufacturer to have Pt loading of 19.8% Pt and a Pt metal area of 124m²/g. The same procedure was followed for the model compound studies with the switchgrass lignin replaced with the model compound.

2.2.2 GC-FID/MS Analysis

Each sample was injected neat into a Shimadzu GC-2010 system for product identification via GC-MS and quantitative analysis via GC-FID. The oven temperature was held at 50°C for 2 min, heated to 300°C at a ramp of 10°C/min and held at the final temperature for 2 min. The columns used with the flame ionization detector (FID) and mass spectrometer (MS) detector were SHR5 (15m x 0.25mm x 0.25 μm) and SHR5XLB (30m x 0.25mm x 0.25 μm) respectively. The split ratios of 1 and 35 were used for the GC-FID and GC-MS analysis respectively. The mass spectrometer was set to scan the m/z range from 45 to 500. Known amounts of pure compounds were injected into the GC-MS for identity verification and the GC-FID to produce a calibration curve for quantification purposes. The yield of each individual compound was determined using the GC-FID and calculated using equation (2-1).

$$\text{Yield}(\text{weight}\%) = \frac{\text{Weight of compound}}{\text{Weight of lignin loaded}} \times 100\% \quad (\text{Equation 2-1})$$

2.2.3 Elemental Analysis

The C, H, O molar percentages were quantitatively determined via elemental analysis. The liquid product samples were concentrated by distillation at 135°C. GC-MS/FID of the distillate confirmed that there was no loss of products to the distillate. Concentrated liquid product samples were analyzed after drying at 79°C for 1 hour to remove any remaining ethanol. All elemental analysis was carried out by Columbia Analytical Services, Tucson, AZ. The carbon and hydrogen analyses were conducted by coupling combustion with thermal conductivity and infrared detection, while the amount of oxygen was determined by coupling pyrolysis and infrared detection.

2.2.4 Gel Permeation Chromatography

The molecular weight distribution of the lignin and products was measured using a Polymer Laboratories PL-GPC 50 Plus with an AM Gel guard column (5µm) and three Mesopore columns (300 x 7.5 mm). The concentrated samples were dissolved in tetrahydrofuran (THF) to obtain sample concentrations of approximately 20 mg/ml. The samples were subsequently filtered with a 0.2 µm nylon membrane to remove any particulate matter to prevent the plugging of columns. The temperature of the oven was 30 °C and a sample injection volume of 100 µL was used. A THF eluent flowrate was 0.8 ml/min.

2.2.5 Simulated Distillation using Thermogravimetric analysis

The weight loss of the concentrated samples (~10 mg) over a range of temperatures was determined via thermogravimetric analysis (TGA). The analysis was carried out with 60 ml/min of flowing nitrogen. The temperature program starts at 22 °C and employs a 5 °C/min ramp up to the final temperature of 800 °C while holding for 15 min at each temperature 200 °C, 250 °C, 300 °C, 350 °C and 400°C . At the end of the run, oxygen was introduced for 30 min at 800 °C to combust any material remaining in the pan. A baseline correction file consisting of a blank run using an empty pan under identical analytical conditions was applied in the evaluation of all the TGA profiles.

2.2.6 ¹H and ¹³C NMR

The concentrated samples were dissolved in d₆-DMSO (D, 99.96% + 0.03% v/v TMS, Cambridge Isotope Laboratories, Inc.) at approximate concentrations of 15 mg/ml. All NMR experiments were conducted with a Bruker DMX 400 MHz instrument with 5 mm broadband probehead. For the ¹³C NMR analysis of switchgrass lignin, 9 mg of chromium (III) acetylacetonate dissolved in 1 ml of d₆-DMSO was used as a solvent. Chromium (III) acetylacetonate was used as a relaxant to ensure that the carbon atoms will be fully relaxed when pulse delay times of 12s were used. Optimal pulse delays were determined based on systematic studies of various delay times. Additionally, an inverse-gated decoupling sequence was used to screen out the Nuclear Overhauser Effect (NOE), and more than 10,000 scans were used to obtain quantitative ¹³C spectra.

2.3 Results and Discussion

Several experiments were conducted to determine the effects of reaction time and the changes in the products obtained with varying the reaction conditions, specifically the presence/absence of formic acid and 20 wt% Pt/C catalyst. The reaction conditions used are shown in Table 2.1. In repeated reactions the product distributions were found to be moderately reproducible within 10% of the average values. The formic acid underwent complete decomposition under all reaction conditions and therefore did not interfere with the analysis of the liquid reaction products. The complete decomposition of formic acid was verified by the absence of formic acid in the HPLC analysis of the product solution. This corresponds with previous research which reported that formic acid thermally decomposed at reaction conditions of 350 – 400°C in an ethanol solvent even without a Pt/C catalyst [24]. The formic acid is expected to mainly decompose into hydrogen and carbon dioxide yielding a dihydrogen to atomic oxygen ratio in the lignin of 5.0. No solid products were recovered after all of the experiments except in A-20 where 4 wt% of solids were formed.

Some of the liquid products obtained from the depolymerization and hydrodeoxygenation of lignin were identified using the fragmentation patterns obtained via GC-MS. Subsequently, the products were verified by injecting the GC-MS with the authentic compounds. A total of seven compounds were identified and tracked throughout the reactions – phenol, *p*-cresol, guaiacol, *p*-methylguaiacol, *p*-ethylguaiacol, *p*-propylguaiacol, and homovanillyl alcohol. It should be noted that these are not the only low molecular weight products, but rather some of the most prominent of such products (Figure 2.2). These phenolic type products are in accordance with the expected products

from lignin depolymerization and are similar to those found in other reactions involving lignin [25, 26]. The majority of these identified compounds are guaiacol type compounds that are the products of depolymerization, obtained from the cleavage of bonds between the *p*-hydroxyphenylpropane units.

An example of a GC-MS spectrum obtained with reaction condition D-4 is shown in Figure 2.2 with the identified compounds labelled with their respective peak numbers. Further attempts were made to identify other low molecular weight compounds via HPLC, LC-MS and MALDI-TOF, but the identification was hindered by the difficulties in isolating the individual compounds chromatographically.

Table 2.1 Experimental reaction conditions for the depolymerization and hydrodeoxygenation of switchgrass lignin. All reactions were conducted at 350°C and with autogeneous pressure in a batch microreactor.

Condition	Reaction Time (h)	Formic acid	Pt/C catalyst
A-20	20	No	No
B-20	20	Yes	No
C-20	20	No	Yes
D-1	1	Yes	Yes
D-4	4	Yes	Yes
D-8	8	Yes	Yes
D-20	20	Yes	Yes

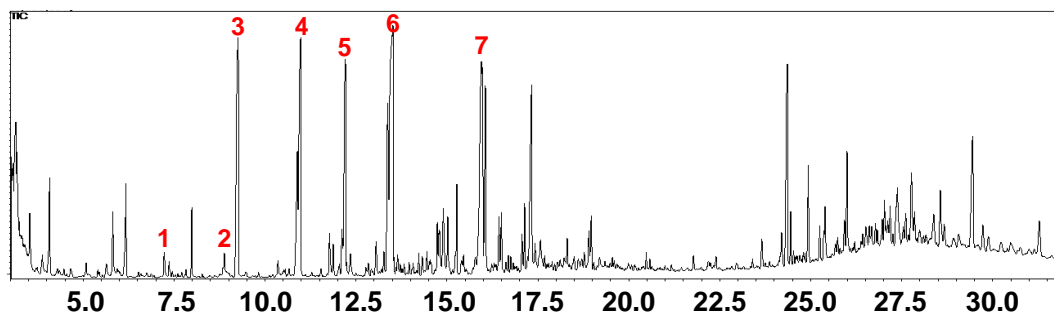


Figure 2.2 Example of a GC-MS spectrum of extracted liquid products obtained from reaction condition D-4 (Identified and quantified products: (1) phenol, (2) *p*-cresol, (3), guaiacol, (4) *p*-methylguaiacol, (5) *p*-ethylguaiacol, (6) *p*-propylguaiacol, (7) homovanillyl alcohol)

Signature peaks in the ^{13}C NMR spectrum of switchgrass lignin indicate the presence of *p*-hydroxyphenyl (H-unit, $\delta = 159.9$ ppm), guaiacyl (G-unit, $\delta = 125.1$ ppm) and syringyl (S-unit, $\delta = 104.1$ ppm) units in the starting material, as shown in Figure 2.3a. Other major peaks were also identified from the spectrum and their chemical assignments have been documented in Table 2.2).

The relative abundance of these units was estimated via the integrations of $\delta = 158 - 162$ ppm (H), $\delta = 113 - 110$ ppm (G) and half of the integration of $\delta = 103 - 109$ ppm (S). The estimated ratio of S:G:H was determined from the spectrum to be 38:28:34 with a G:S ratio of 0.74, similar to the compositions of other switchgrass lignin reported in literature [27].

Additionally, the organosolv switchgrass lignin has H/C and O/C molar ratios of 1.15 and 0.33 as determined by elemental analysis. Ethanol organosolv switchgrass lignin has been reported to have a wide range of molecular weights depending on the severity of the organosolv process as the organosolv treatment can initiate different degrees of degradation of the macromolecular structure of lignin [28]. Nonetheless, the organosolv switchgrass lignin had molecular weight averages consistent with similarly extracted switchgrass lignin with a weight average molecular weight (M_w) of 4807 and a number average molecular weight (M_n) of 2977 [29].

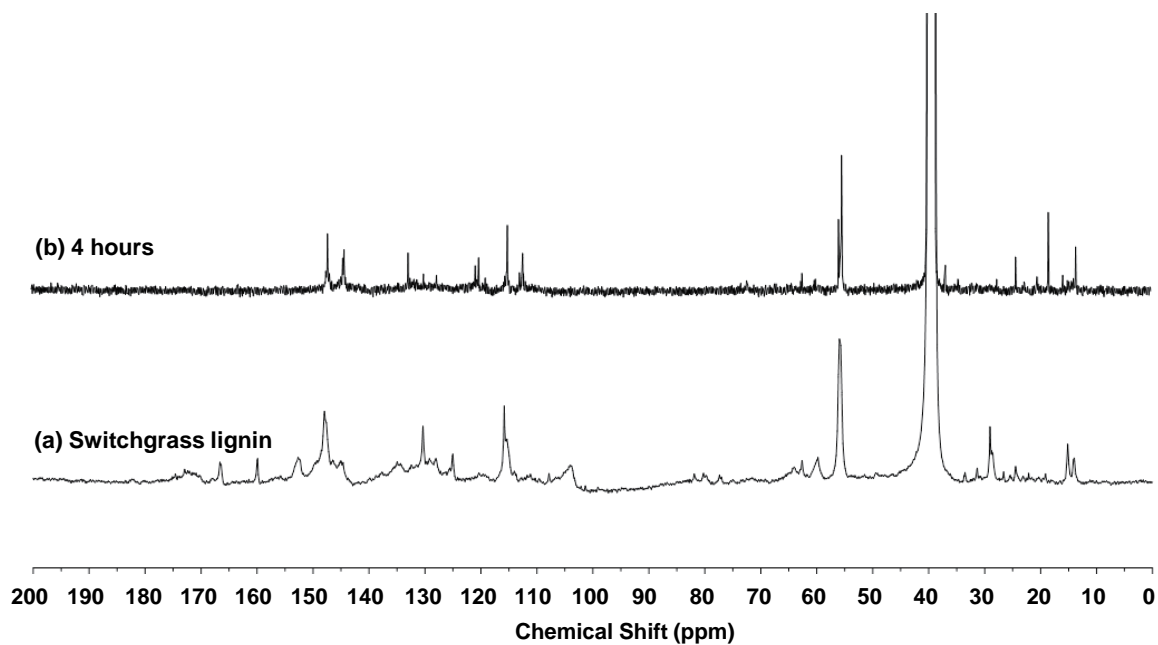


Figure 2.3 Quantitative ^{13}C NMR of the (a) switchgrass lignin feedstock and (b) liquid products from switchgrass lignin depolymerization and hydrodeoxygenation under reaction condition D-4

Table 2.2 Chemical assignments for major peaks in ^{13}C NMR spectra of switchgrass lignin feedstock [29]

Chemical Shift (ppm)	Assignments
166.7	C=O in conjugated COOR
159.9	C ₄ in H unit
152.7	C ₃ /C ₄ in G units, C ₃ /C ₅ in S units
148.0	C ₃ /C ₄ in G units, C ₃ /C ₅ in S units
130.4	C ₁ in G, S, and H units, C ₄ in S, C ₂ /C ₆ in H
125.1	C ₆ in G units
115.9	C ₅ in G, C ₃ /C ₅ in H
111.4	C ₂ in G
104.1	C ₂ /C ₆ in S units
62.7	C _γ in β-5 and β-O-4 with C _α =O in G and S units
59.8	C _γ in β-O-4 without C _α =O
56.0	Methoxyl
29.1	Aliphatic
15.2	Aliphatic

After the reaction under condition D-4, the products do not display the signature peaks for G, H and S units found in the starting lignin, indicating that the lignin has been broken down into other products (Figure 2.3b). No peaks were observed in the 78-90 ppm region due to the absence of C β in β -O-4, C α in β -5 and β - β linkages, which were broken under the reaction conditions, giving evidence for the depolymerization of lignin. The chemical shifts and chemical assignments for the major peaks found in the spectra are given in Table 2.2 and Table 2.3. Integrating within the regions associated with the different chemical environments (shown in parenthesis in Table 2.3), it was determined that 21.9% of the carbons are attributed to methoxyl carbon groups that are attached to the aromatic ring while 8.8% of the carbons are aliphatic in nature. Integrating within aromatic carbon regions, it was calculated that 26.1%, 24.0% and 15.2% of the carbons are aromatic carbons associated with a side group O, C and H respectively. The molar ratio of O/C determined using this integration is 0.26, very similar to the 0.23 ratio determined via elemental analysis. Consequently, most of the oxygen present in the product mixture is attached to the aromatic ring. This conjecture is further supported by the lack of carbon peaks that are characteristic of carbonyl, carboxylic and aldehyde groups in the product ^{13}C spectrum (Figure 2.3b). After a reaction time of 4 hours, approximately 2 out of 6 aromatic carbon atoms are attached to an oxygen group. These oxygen containing side groups are likely a hydroxyl group and a methoxy group, as the total yield of *identified* guaiacol type compounds is a significant 21% after 4 hours (Figure 2.8).

Table 2.3 Chemical assignments for main peaks in ^{13}C NMR spectra of liquid products from switchgrass lignin depolymerization and hydrodeoxygenation reaction under reaction condition D-4

Chemical Shift (ppm)	Assignments
145.3, 148.3	Aromatic C-side group O bond ($\delta = 166.5 - 142.0$)
133.9	Aromatic C-side group C bond ($\delta = 142.0 - 125.0$)
116.2, 121.3	Aromatic C- side group H bond ($\delta = 125.0 - 95.8$)
56.4, 57.0, 113.4	Aromatic methoxyl C ($\delta = 60.8 - 55.2$)
14.6 - 25.34	General aliphatic ($\delta = 55.2 - 0.0$)

2.3.1 Effects of Formic Acid and Catalyst

To better understand the effects of the formic acid and/or Pt/C catalyst on the products, the presence of these compounds was varied at reaction times of 4 and 20 hours. As the differences in products formed in the 20 hour reactions are more apparent, this section mainly focuses on the 20 hour reaction experiments with the exception of the discussion on elemental analysis.

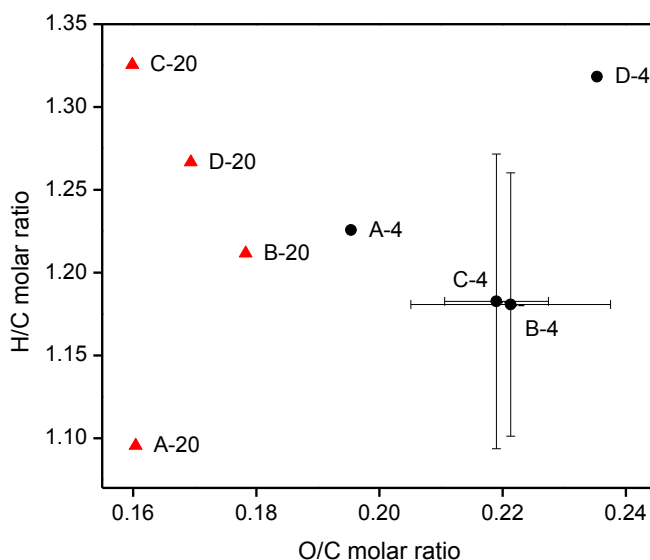


Figure 2.4 Change in H/C and O/C molar ratio of bulk liquid products obtained from switchgrass lignin depolymerization and hydrodeoxygenation with varying conditions – A-4, B-4, C-4 and D-4 (●), and A-20, B-20, C-20 and D-20 (▲)

In general, the product compositions showed that the presence of either formic acid and/or Pt/C catalyst yielded higher H/C molar ratio at 20h and significantly lower O/C molar ratios at 4h (Figure 2.4). Comparing between experiments B, C and D at the same reaction time of 4h or 20h, only small differences are observed but these differences are difficult to ascertain given the deviations found in the elemental analysis results derived from four repeated runs of experimental conditions B-4 and C-4. With increasing reaction time, experiment A had lower H/C and O/C molar ratios. However, since elemental analysis was performed only on the bulk liquid products, the H/C and O/C molar ratios of A-20 (the only experiment where solid lignin-derived products remained) could be affected by the formation of solid products that could be attributed to the repolymerization of lignin fragments monomers after the long reaction time [30]. The most significant trend is that experiments B, C and D all achieved higher H/C and lower O/C molar ratios with increasing reaction time. The change in reaction time yielded more significant changes in molar ratios than the variation of formic acid and Pt/C catalyst.

Thermogravimetric analysis (TGA) under inert conditions was used to analyse the starting lignin and the bulk thermal properties of the liquid products. For the products, the mass loss distribution under the flow of nitrogen is assumed to be due to the vaporization of individual components evolving at various temperatures, thus simulating a boiling point distribution of the liquid products. At higher temperatures, thermal decomposition of and reactions between individual components cannot be discounted but mass losses below the reaction temperature can be reliably attributed to only the vaporization of compounds, as any reactions that occur at or below the reaction temperature would have likely already occurred during the course of the reaction. Subsequently, this form of

analysis can be applied to approximate the distribution of bulk thermal properties of the product mixture and to compare the thermal properties of the mixtures obtained.

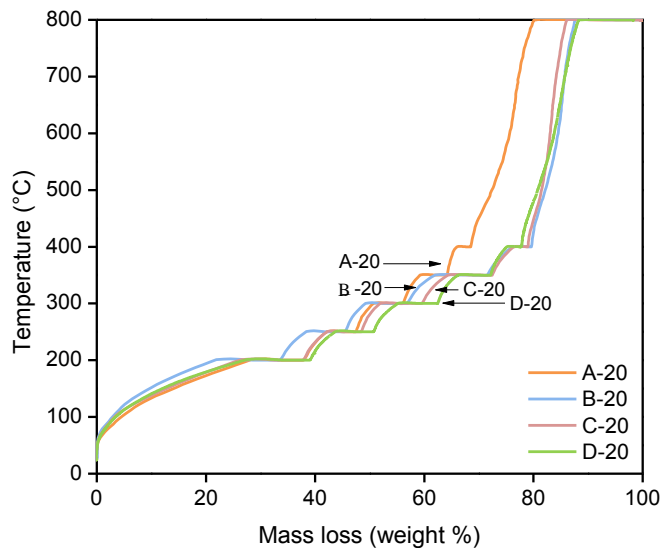


Figure 2.5 Thermogravimetric analysis of switchgrass lignin feedstock and bulk liquid products obtained from switchgrass lignin with varying presence of Pt/C and formic acid (conditions A-20, B-20, C-20 and D-20)

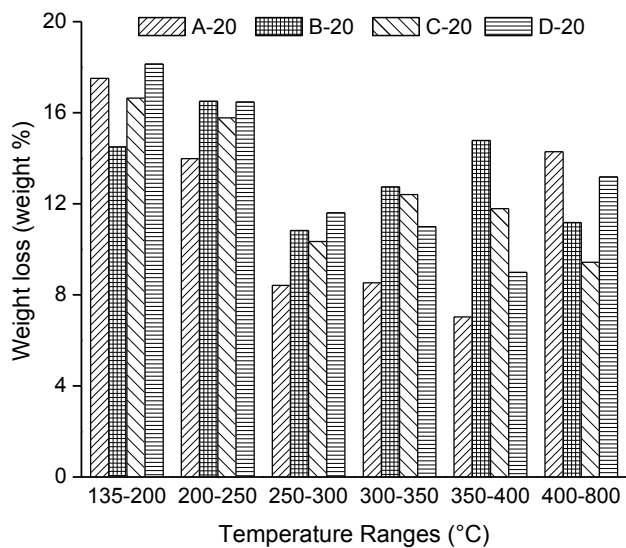


Figure 2.6 Mass loss distribution of bulk liquid products obtained from switchgrass lignin with varying presence of Pt/C and formic acid (conditions A-20, B-20, C-20 and D-20) between 135°C and 800°C of thermogravimetric analysis

The simulated distillation curves for these experiments showed that the amount of char at 800°C was the same for D-20 and B-20 at 12.3% while it was 14.4% for C-20 and 20.3% for A-20 (Figure 2.5). The largest difference between samples was observed in the 350 – 800°C range, where the fraction of products formed that vaporized in this combined range decreases with conditions B-20 > D-20 > A-20 > C-20 (Figure 2.6). Reported experiments with organosolv lignin, tetralin hydrogen donor and Ni catalyst showed that in the presence Ni, the lignin conversion remained approximately the same but the amount of gaseous products increased [31]. Similarly, with the presence of both catalyst and formic acid, an increase in lower molecular weight products was observed in the 135 – 300°C range. Consequently, the presence of both formic acid and Pt/C catalyst (condition D) yielded the highest fraction of lower molecular weight compounds and yielded one of the lowest amounts of char.

The molecular weight distribution curves of the products all yielded bimodal distributions with similar peak molecular weights (Figure 2.7) but D-20 had the lowest molecular weight peaks at 216 and 397 Da. The use of Pt/C catalyst (C-20) instead of formic acid (B-20) yielded a higher 2nd peak indicating an increase in fraction of products with molecular weights between 300 and 650 Da. The use of both formic acid and catalyst (D-20) yielded the highest fraction of products with molecular weight between 150 and 300 Da (highest 1st peak) as well as the lowest fraction of products with molecular weight above 650 Da. This corresponds well with the simulated distillation curve data that similarly showed that the combined use of both formic acid and catalyst (D-20) was the most effective in breaking down the lignin into liquid products, with the highest fraction of lower molecular weight compounds.

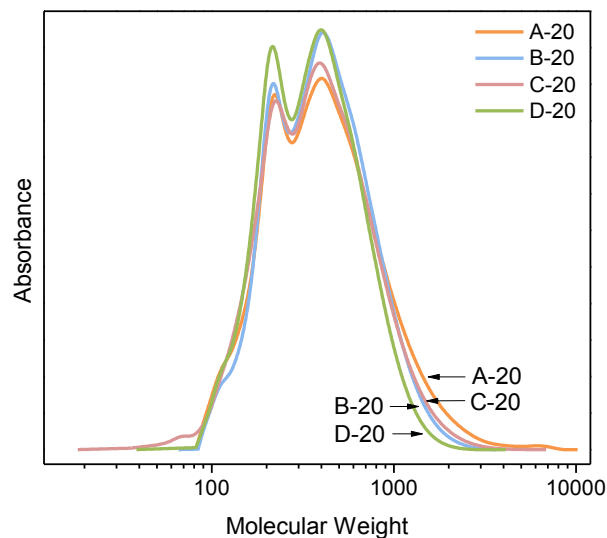


Figure 2.7 Molecular weight distribution of bulk liquid products from switchgrass lignin obtained with reaction conditions A-20, B-20, C-20, and D-20

2.3.2 Effects of Reaction Time

The elemental analysis results from the previous discussion highlighted the importance of reaction time on the O/C and H/C molar ratios. Thus, further experiments were conducted with varying reaction times 1h, 4h, and 8h to study the effect of reaction time on the products formed with the use of both formic acid and catalyst.

Analysis of the identified products (Figure 2.2) showed that the total yield of the identified products achieved a maximum between 4 and 8 hours of reaction. The largest observed yield was 21 wt% after 4 hours of reaction time and this decreased to 10 wt% after 20 hours, as shown in Figure 2.8. The subsequent decrease in yield of identified products is likely due to the consumption of these products in secondary reactions such as hydrodeoxygenation to unidentified products, repolymerization to form dimers or larger species, or recondensation with the lignin [13–15]. The latter is the least likely scenario,

as the molecular weight distribution of the products from increasing reaction times shows a decreasing trend of molecular weights, which is contrary to the increased percentage of higher molecular weight compounds expected to form via recondensation reactions.

In the literature, a wide range of guaiacol derivative yields are obtained using various conversion processes. Hydrogenolysis of organocell lignin using Pd/C catalyst in an H₂ pressurized batch reactor at 380 °C yielded a maximum of 2.13% guaiacol derivatives [32]. The use of supercritical water on alkaline lignin gave a maximum phenolic content derived from guaiacol derivatives of 35% while pyrolysis of softwood dioxane lignins had a maximum guaiacol derivative yield of 7.7% [33]. Subsequently, our yield of 7 – 21 wt% of quantified molecular products is within the range reported in the literature.

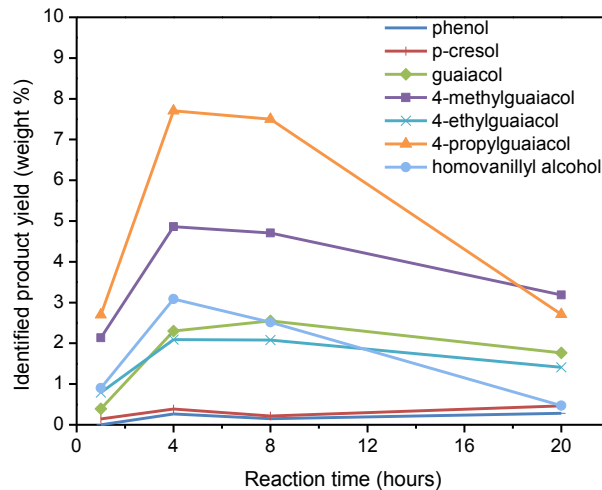


Figure 2.8 Change in individual yields of identified products with increasing reaction time. Identified products are p-cresol (-), phenol (|), guaiacol (♦), 4-methylguaiacol (■), 4-propylguaiacol (×), 4-ethylguaiacol (▲), and homovanillyl alcohol (●)

The yields of the individual identified compounds range from 0–8 wt% as shown in Figure 2.8. The trend in amount of products formed vs. reaction time remains approximately the same for all compounds, with a maximum yield achieved between 4 and 8 hours of reaction. After 4 hours, *p*-propylguaiacol is the dominant quantified product followed by *p*-methylguaiacol, homovanillyl alcohol, guaiacol and *p*-ethylguaiacol. Other compounds such as phenol and *p*-cresol were also produced, but only in trace amounts (< 0.5 wt%) and the yields of these products remain approximately constant as the reaction time increases. A possible mechanism for the formation of the guaiacol derivatives is the cleavage of the aryl-ether bonds with the abstraction of hydrogen to form the phenolic hydroxyl group [9]. Subsequent derivatives could be produced by the cleavage of C-C bonds of the alkyl side chains. Phenol and *p*-cresol are likely formed by the hydrodeoxygenation of guaiacol and its derivatives to remove methoxy side chains.

The H/C and O/C molar ratios obtained via elemental analysis provide a measure of the extent of hydrodeoxygenation and a means of comparing the liquid products with other possible bio-oils or biofuel mixtures in a Van Krevelan plot. The change in H/C and O/C molar ratios with time is shown in Figure 2.9. Overall, the H/C molar ratios showed very little change with increasing reaction time. The O/C molar ratio decreased very sharply after just 1 hour of reaction and continued to decrease at a slower rate between 1 and 20 hours. After 20 hours of reaction, the H/C molar ratio increased only by about 10%. In contrast, the O/C molar ratio decreased nearly 50%. This much larger decrease in O/C molar ratio than the increase in H/C molar ratio would be consistent with a mechanism of dehydration followed by hydrogenation of aromatic side chain alcohols

[19] or the loss of alcohol groups via thermal degradation of C-C bonds in the side chain [34].

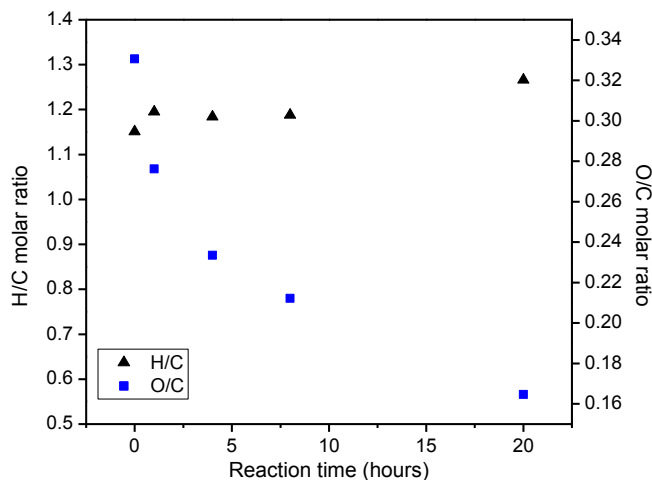


Figure 2.9 Change in H/C (▲) and O/C (■) molar ratios of bulk liquid products obtained from switchgrass lignin depolymerization and hydrodeoxygenation with increasing reaction time

Thermogravimetric analysis (TGA) was used to obtain simulated distillation curves of the bulk liquid products. The TGA profile of the starting switchgrass lignin (Figure 2.10) has been included to provide a characterization of the starting reactant and a basis for comparing how the reaction has improved the thermal properties of the lignin by breaking it down into smaller, lower boiling components. Under such TGA conditions, the lignin undergoes pyrolysis during which several reactions can occur, such as thermal bond cleavage, radical formation, repolymerization [35]. The mass loss obtained with the lignin samples is generally associated with the thermal degradation of lignin bonds to form various products such as gases (e.g. CO, CO₂, CH₄, C₂H₆) and tar that volatilizes [36]. Up to 20 wt% of the mass loss from pyrolyzing lignin has been reported to be from the production of light gases [25]. Lignin is expected to have a maximum decomposition

rate between 625 and 725K [37], and this can be observed in Figure 2.10, where the maximum loss of 21.5 wt% occurred within the 350°C to 450°C range. At 800°C, 58 wt% of the initial lignin sample has been lost and 42 wt% remains as char.

Generally, the TGA curves of the reaction products shift further to the right for samples with increasing reaction time, indicating that a larger fraction of the products vaporizes at lower temperatures with increasing reaction time. The shapes of the curves are very similar for the 1h, 4h and 8h reactions, but the 20h reaction curve is notably different. The 20h curve bisects the 8h curve at 350°C, as it has two distinct distributions of products – those that vaporize under 350°C and those that vaporize between 350°C to 800°C. Considering the weight losses within the different temperature ranges, the 20h reaction has the largest mass losses in the 135-200°C, 200-250°C and 250-300°C regions (Figure 2.10 and Figure 2.11). By 800 °C, the 20 h sample, D-20, achieves the highest total mass loss compared to D-1, D-4 and D-8.

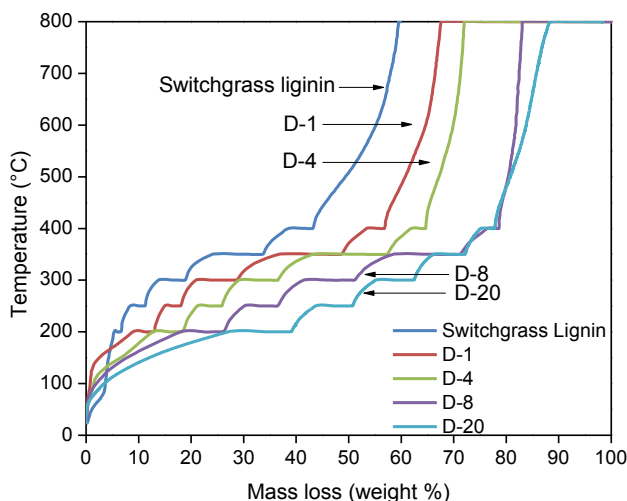


Figure 2.10 Thermogravimetric analysis of switchgrass lignin feedstock and bulk liquid products obtained from switchgrass lignin under reaction conditions D-1, D-4, D-8 and D-20

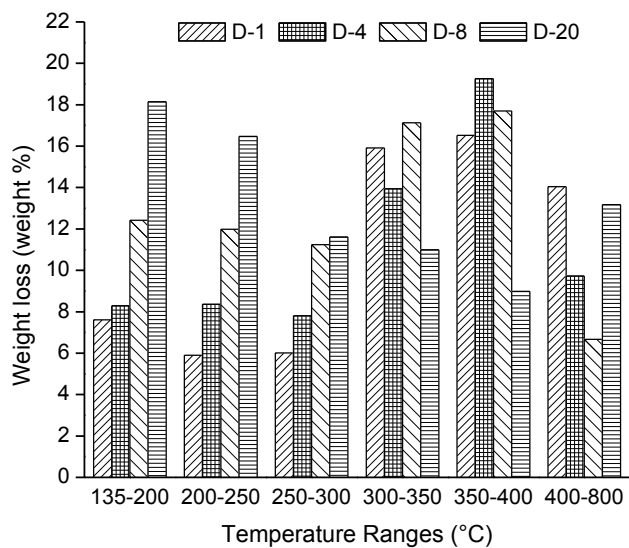


Figure 2.11 Mass loss distribution of bulk liquid products obtained from switchgrass lignin with Pt/C and formic acid at different reaction times (conditions D-1, D-4, D-8 and D-20) between 135°C and 800°C of thermogravimetric analysis

It is apparent that as reaction time increases, a larger fraction of the product volatilizes at a lower temperature range. In particular, the maximum mass loss from 135 – 300°C is by the D-20 sample, 300 - 350°C is by the D-8 sample and 350 - 400°C is by the D-4 sample. This indicates that as reaction time increases, a larger fraction of the products is likely of a lower molecular weight. This change in boiling point distribution with reaction time could be a key variable in modifying the products to make additives for different types of fuels. Jet fuels and diesel fuels have boiling point ranges of 150 – 250°C and 190 – 370°C respectively [38]. Subsequently, the D-20 conditions could potentially produce the highest fraction of products that might be suitable fuel blending components for a jet fuels while D-8 conditions would produce the largest fraction of possible fuel additives for diesel.

Lignin that is not depolymerized could manifest as char that is leftover at 800°C. Subsequently, less char might indicate a higher conversion of lignin into other products and the final amount of mass loss achieved at 800 °C could be analysed to determine the amount of char leftover. Figure 2.10 shows more mass loss is achieved by 800°C as the reaction time of the sample increases. The percentage of char remaining is 32.6%, 28.1%, 16.9% and 12.3% for samples with reaction conditions D-1, D-4, D-8 and D-20 respectively. An increase in the reaction time is thus shown to decrease the amount of char in the product mixture. Hence, to decrease the amount of char formation and increase fractions of lower boiling point products, a longer reaction time should be used.

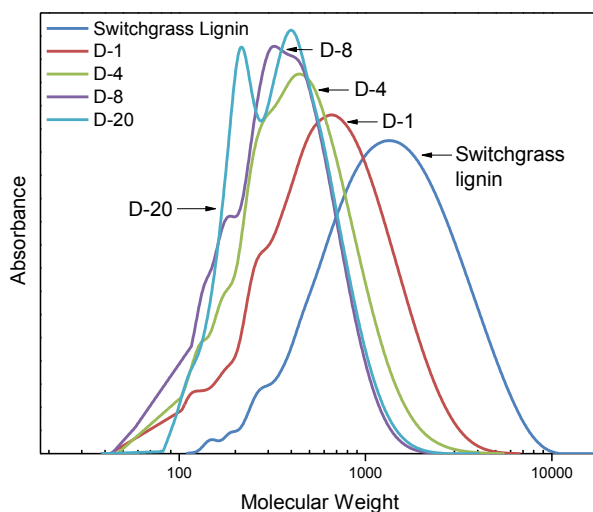


Figure 2.12 Molecular weight distribution of bulk liquid products from switchgrass lignin obtained with reaction conditions D-1, D-4, D-8 and D-20

The molecular weight distribution of the liquid products markedly changed with increasing reaction time (Figure 2.12), and the calculated average molecular weights are shown in Table 2.4. The initial rate of decrease in weighted average molecular weight,

M_w , is relatively high up to 8 hours, after which, the rate of decrease is slower. After 1h, the M_w , decreases by 56% compared to that of the starting switchgrass lignin and after 20h, an 82% decrease in M_w is observed. With increasing reaction time, the overlap between the product weight distributions and switchgrass lignin distribution decreases, indicating that more of the lignin depolymerizes into lower molecular weight fragments, in accordance with the TGA char results.

Table 2.4 Molecular weight averages of switchgrass lignin and bulk liquid products of switchgrass lignin from different reaction conditions (poly(styrene) weight equivalents)

Sample / Condition	M_n	M_w	Polydispersity index
Switchgrass lignin	946	1755	1.85
A-20	324	533	bimodal
B-20	324	469	bimodal
C-20	299	469	bimodal
D-20	297	419	bimodal
D-1	407	775	1.90
D-4	313	512	1.64
D-8	257	396	1.54

The peak molecular weight of D-1 is 659, D-4 is 442, D-8 is 325 and D-20 has peaks at 216 and 397. Similar to the simulated distillation results, the 20 hour reaction produced a product with a molecular weight distribution that is significantly different from those obtained at lower reaction times. Furthermore, the GPC results establish that the 20h sample has a bimodal molecular weight distribution. This corresponds with the two maximum weight losses of the D-20 product which had larger weight losses than D-8 up to 300 °C and between 350 – 800 °C. Hence, results from the simulated distillation using TGA give a good estimate of the extent of depolymerization and possible distribution of molecular weights that are verified by the GPC results.

Consequently, reaction time is a variable that can be used to vary the characteristics of the product mixture. The depolymerization of switchgrass was observed at all times above 1h and the extent of depolymerization increases with reaction time as verified by the simulated distillation and molecular weight distribution data. The extent of hydrodeoxygenation also increases with reaction time and a maximum of 50% of the oxygen is removed after 20 hours. A closer examination of the products using ^{13}C NMR reveals the loss of β -O-4 bonds associated with depolymerization and a lack of carbonyl, carboxylic acid and aldehyde functional groups in the product solution. A reaction time of 4 hours allows for the maximization of the identified guaiacol derivative products. Lastly, phenol and p-cresol remain minor products with combined yields of less than 1 wt% after 20 hours of reaction.

To further understand the reactions that lignin and its subsequent fragments undergo, some experiments with model compounds were carried out. 2-Phenylethyl phenyl ether was used to model aromatic β -O-4 bonds in lignin while phenol and guaiacol represented the fragments that were identified. These experiments showed that under reaction condition D-4, β -O-4 bonds are broken, phenolic units can be ethylated by the ethanol solvent and the methoxy group of guaiacol can be removed. These experiments and results are further discussed in Sections 2.3.4-2.3.6.

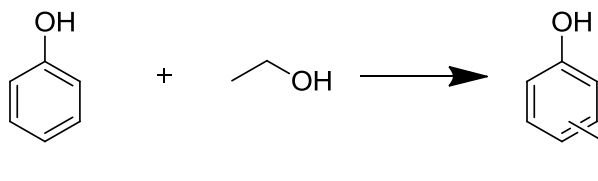
2.3.3 Effects of Reactor Corrosion

Stainless steel can be corroded by strong bases and acids; leaching metals into solutions [23]. Previous studies reported 70 ppm Fe in solution that was leached from a

stainless steel reactor when sodium hydroxide and lactic acid was used [39]. Additionally, sodium hydroxide alone was also able to leach up to 7 ppm of Fe from a Hastelloy-C reactor [40]. Similarly, corrosion was observed in these reactions when formic acid was used, even though formic acid is expected to decompose very quickly under the reaction conditions. Inductively coupled plasma (ICP) analysis revealed that approximately 3.4 ppm of Fe, 0.8ppm of Ni, and less than 0.02 ppm of Cr is in the ethanol solution after a blank reaction run in a brand new reactor using conditions D-4 (omitting the lignin). The formic acid solution is also expected to contribute some trace metals and ICP analysis of the formic acid showed that it contributes 0.05 ppm of Fe, 0.009 ppm of Ni and less than 0.005 ppm of Cr. The metals found in the blank solution are therefore more than that expected from just the formic acid solution alone. Thus, metals did leach from the reactor but the amount leached is still substantially less than the 5 mg of Pt that was added.

A blank run was also conducted on a reactor that has been used for one reaction under condition D-4. ICP analysis of this ethanol solution showed comparable amounts of metals as was found in the blank run in a brand new reactor. This means that the amount of metals leached remains approximately constant regardless of the number of times the reactor is used. Hence, even though metals are leached from the reactor, any effects of leached metals on the reactions are expected to be minor and can furthermore be expected to be approximately constant between runs.

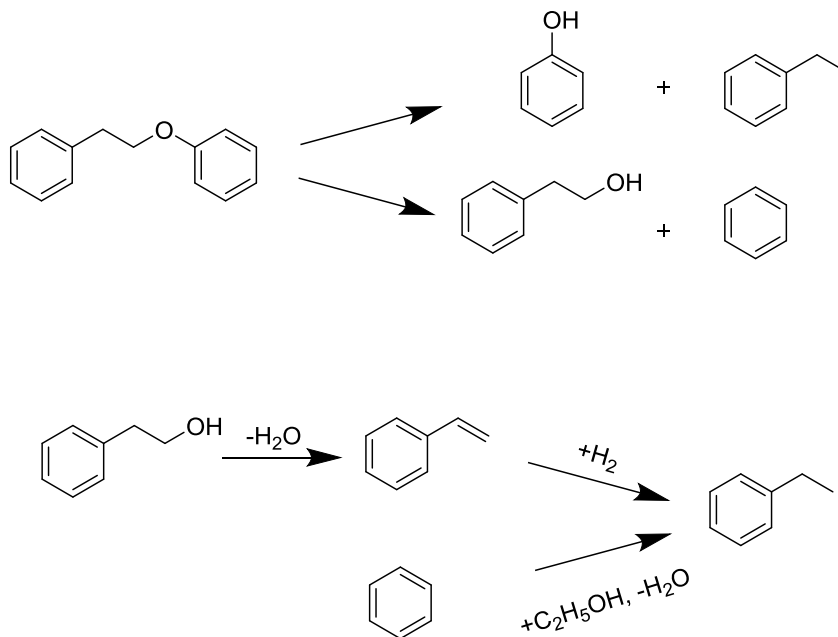
2.3.4 Model Compound Studies with Phenol



Scheme 2.1 Proposed reaction to alkylate phenol to p-ethylphenol in the presence of formic acid, ethanol and a Pt/C catalyst at 350°C

In addition to being a solvent for the reaction, ethanol could also be incorporated into the aromatic rings, increasing the H/C molar ratio of the products. Exploring this hypothesis, phenol, the simplest model compound for a demethoxylated lignin monomer, was applied in a reaction under condition A-4 where 250 mg of phenol was loaded into the reactor. Analysis of the product mixture showed that 9.6 mol% of phenol was converted into ethylphenols, demonstrating that the ethanol not only acts as a solvent but also reacts with aromatics to form alkylated compounds (Scheme 2.1). This also suggests that other phenolic products could be similarly alkylated to give improved H/C molar ratios. Ethylated phenols were also reported in literature when lignin base-catalyzed depolymerization was conducted in ethanol [41]. Using a KOH/ethanol mixture at 290 °C, 20% phenol was converted to 2- and 4-ethyl phenols. Subsequently, even though alkylation with ethanol is possible, only a small fraction of the phenolic compounds are expected to be alkylated.

2.3.5 Model Compound Studies with 2-Phenylethyl Phenyl Ether



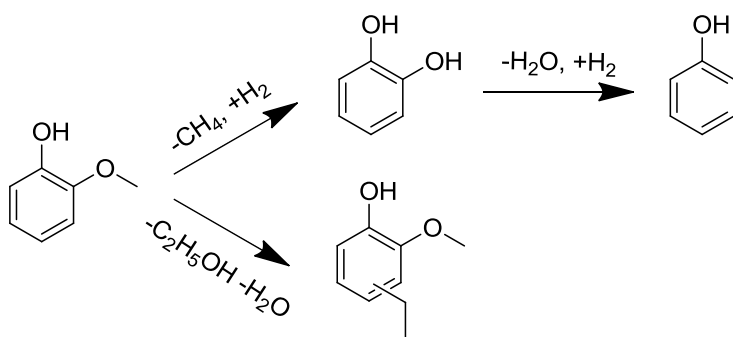
Scheme 2.2 Proposed reaction for the cleavage of the β-O-4 linkage of 2-phenylethyl phenyl ether to form phenol, styrene, 2-phenylethyl alcohol, benzene and ethylbenzene in the presence of formic acid, ethanol and a Pt/C catalyst at 350°C

The effect of reaction condition (D-4) on the β-O-4 linkages in lignin was simulated by the reaction of 2-phenylethyl phenyl ether (PPE) to verify that lignin bonds such as β-O-4 bonds can be broken under such condition. The main products formed were benzene, phenol, ethylbenzene and 2-phenylethyl alcohol. β-O-4 linkages of PPE broke to form 6.9 mol% phenol and 5.6 mol% 2-phenylethyl alcohol. A large amount of ethylbenzene was also produced. The larger amount of phenol than 2-phenylethyl alcohol produced is consistent with the expectation that the β-O-4 linkage is more likely to break at the β-O end rather than the O-4 end, since the former has a lower bond energy of 58 kJ/mol [42]. In the previous phenol model compound studies, it was demonstrated that alkylation reactions with ethanol were possible under our reaction conditions. Similarly,

benzene may be alkylated to form ethylbenzene. The dehydration of 2-phenylethyl alcohol could also form styrene and contribute to the production of ethylbenzene (Scheme 2.2).

Previous bond cleavage studies with PPE under strongly reducing reaction conditions using hydrogen donor solvents like tetralin and/or hydrogen to pressurize the reactors yielded phenol and ethylbenzene as the dominant products with conversions of approximately 80 mol% after 1-2 hours [43, 44]. When a metal such as iron was introduced into the reducing reaction environment, these remained the predominant products but the conversion of PPE decreased by half [45]. Under supercritical water conditions, PPE was found to form phenethyl alcohol via hydrolysis in addition to phenol and styrene via pyrolysis. Furthermore, styrene was also found to undergo secondary reactions to produce ethylbenzene, toluene, benzene and other minor products [46].

2.3.6 Model Compound Studies with Guaiacol



Scheme 2.3 Proposed hydrodeoxygenation reactions of guaiacol in an ethanol solvent with formic acid and Pt/C at 350°C

In the absence of Pt/C and formic acid, 0.33% and 0.29% of the guaiacol are converted into catechol and 4-ethylguaiacol respectively (Scheme 2.3). Trace amounts of phenol are also observed. With Pt/C and formic acid, an increase in the formation of these products is observed, with 5.52%, 1.25% and 0.48% of the guaiacol being converted into catechol, phenol and 4-ethylguaiacol respectively. The removal of the methoxy group could proceed either via demethylation or demethoxylation to yield methane or methanol respectively [47, 48]. In Scheme 2.3, guaiacol is shown to demethylate to form the observed catechol, which is subsequently converted to phenol. Alternatively, phenol could also be directly formed from the demethoxylation of guaiacol. However, the analysis of the gas products was not carried out for these reactions to establish the specific pathway of phenol formation. The extent of hydrodeoxygenation clearly increases with the addition of Pt/C and formic acid. Similar results have been reported in the literature when a hydrogen donor, tetralin, was used to quench free radicals while suppressing the hydrodeoxygenation [49].

2.4 Conclusions

In all cases, switchgrass lignin was successfully depolymerized and hydrodeoxygenated to yield phenolic monomers with improved H/C and O/C molar ratios via treatment in ethanol at 350 °C. No solid products were recovered from all reactions except A-20. The presence of formic acid and/or catalyst was found to inhibit the formation of solid products. Further, the combined presence of both formic acid and Pt/C catalyst yielded the highest fraction of lower molecular weight liquid products and the least amount of char formed during thermogravimetric analysis.

Elemental analysis demonstrated the importance of reaction time on the H/C and O/C molar ratios of the products as reaction time was varied between 1 and 20 hours. Additionally, our product mixture was found to fall within the same range of H/C and O/C as other lignin to liquid (LtL) oils reported in literature as shown in Figure 2.13. Maximum total yields of the identified molecular compounds were obtained between 4 and 8 hours of reaction, while the highest H/C and lowest O/C molar ratios were obtained after 20 hours of reaction with formic acid as the hydrogen source and 20 wt% Pt/C as catalyst. Consequently, reaction time can be varied to tailor the properties of the products obtained from lignin.

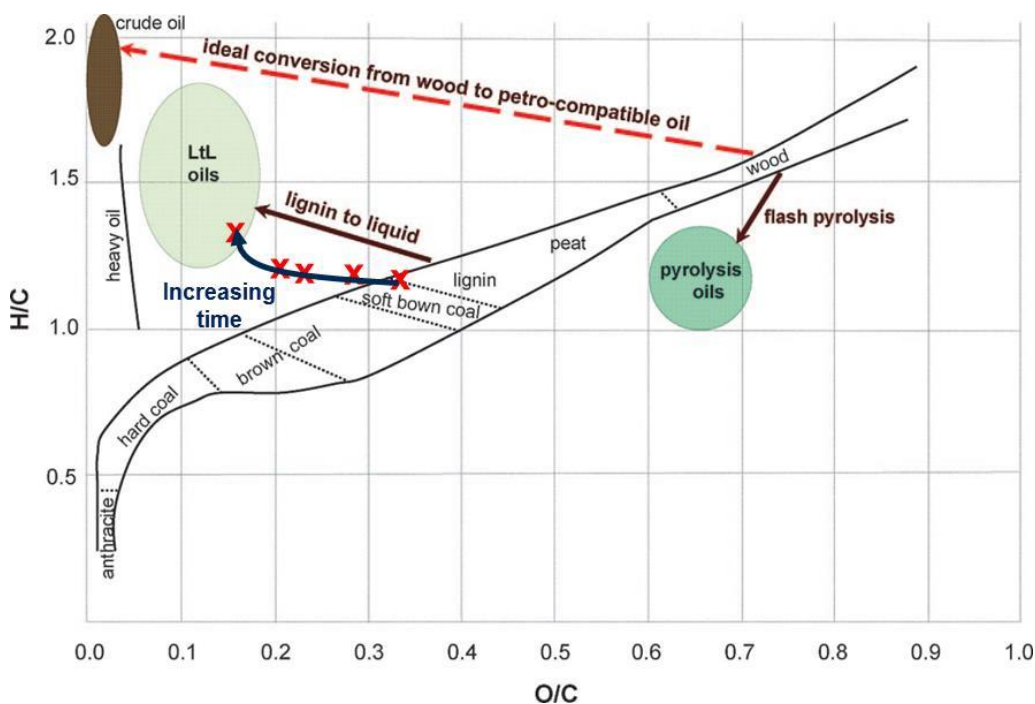


Figure 2.13 Comparing lignin oil properties on Van Krevelan diagram

2.5 References

- [1] Xu, W.; Miller, S. J.; Agrawal, P. K.; Jones, C. W. *ChemSusChem* **2012**, *5*, 667–75.
- [2] Sievers, C.; Musin, I.; Marzioletti, T.; Valenzuela Olarte, M. B.; Agrawal, P. K.; Jones, C. W. *ChemSusChem* **2009**, *2*, 665–671.
- [3] Crisci, A. J.; Tucker, M. H.; Lee, M.-Y.; Jang, S. G.; Dumesic, J. A.; Scott, S. L. *ACS Catalysis* **2011**, *1*, 719–728.
- [4] Nikolla, E.; Román-Leshkov, Y.; Moliner, M.; Davis, M. E. *ACS Catalysis* **2011**, *1*, 408–410.
- [5] Medlin, J. W. *ACS Catalysis* **2011**, 1284–1297.
- [6] Choudhary, V.; Pinar, A. B.; Sandler, S. I.; Vlachos, D. G.; Lobo, R. F. *ACS Catalysis* **2011**, *1*, 1724–1728.
- [7] Zakzeski, J.; Bruijninx, P. C. A.; Jongerius, A. L.; Weckhuysen, B. M. *Chemical Reviews* **2010**, *110*, 3552–3599.
- [8] Boerjan, W.; Ralph, J.; Baucher, M. *Annual Review of Plant Biology* **2003**, *54*, 519–546.
- [9] Amen-Chen, C.; Pakdel, H.; Roy, C. *Bioresource Technology* **2001**, *79*, 277–299.
- [10] Elliott, D. C.; Beckman, D.; Bridgwater, A. V.; Diebold, J. P.; Gevert, S. B.; Solantausta, Y. *Energy & Fuels* **1991**, *5*, 399–410.
- [11] Zhang, Q.; Chang, J.; Wang, T.; Xu, Y. *Energy Conversion and Management* **2007**, *48*, 87–92.
- [12] Mortensen, P. M.; Grunwaldt, J. D.; Jensen, P. A.; Knudsen, K. G.; Jensen, A. D. *Applied Catalysis A: General* **2011**, *407*, 1–19.
- [13] Okuda, K.; Umetsu, M.; Takami, S.; Adschiri, T. *Fuel Processing Technology* **2004**, *85*, 803–813.
- [14] Fang, Z.; Sato, T.; Smith Jr, R. L.; Inomata, H.; Arai, K.; Kozinski, J. A. *Bioresource Technology* **2008**, *99*, 3424–3430.
- [15] Roberts, V. M.; Stein, V.; Reiner, T.; Lemonidou, A.; Li, X.; Lercher, J. A. *Chemistry – A European Journal* **2011**, *17*, 5939–5948.

- [16] Pandey, M. P.; Kim, C. S. *Chemical Engineering & Technology* **2011**, *34*, 29–41.
- [17] Ratcliff, M.; Johnson, D.; Posey, F.; Chum, H. *Applied Biochemistry and Biotechnology* **1988**, *17*, 151–160.
- [18] Patil, P. T.; Armbruster, U.; Richter, M.; Martin, A. *Energy & Fuels* **2011**, *25*, 4713–4722.
- [19] Barta, K.; Matson, T. D.; Fettig, M. L.; Scott, S. L.; Iretskii, A. V; Ford, P. C. *Green Chemistry* **2010**, *12*, 1640–1647.
- [20] Kleinert, M.; Barth, T. *Energy & Fuels* **2008**, *22*, 1371–1379.
- [21] Kabyemela, B. M.; Adschiri, T.; Malaluan, R. M.; Arai, K. *Industrial & Engineering Chemistry Research* **1999**, *38*, 2888–2895.
- [22] Hasegawa, I.; Inoue, Y.; Muranaka, Y.; Yasukawa, T.; Mae, K. *Energy & Fuels* **2011**, *25*, 791–796.
- [23] Di Mondo, D.; Ashok, D.; Waldie, F.; Schrier, N.; Morrison, M.; Schlaf, M. *ACS Catalysis* **2011**, *1*, 355–364.
- [24] Kleinert, M.; Gasson, J. R.; Barth, T. *Journal of Analytical and Applied Pyrolysis* **2009**, *85*, 108–117.
- [25] Mullen, C. A.; Boateng, A. A. *Fuel Processing Technology* **2010**, *91*, 1446–1458.
- [26] Thring, R. W.; Chornet, E.; Overend, R. P. *Journal of Chromatography A* **1989**, *467*, 441–446.
- [27] Yan, J.; Hu, Z.; Pu, Y.; Charles Brummer, E.; Ragauskas, A. J. *Biomass and Bioenergy* **2010**, *34*, 48–53.
- [28] El Hage, R.; Brosse, N.; Sannigrahi, P.; Ragauskas, A. *Polymer Degradation and Stability* **2010**, *95*, 997–1003.
- [29] Samuel, R.; Pu, Y.; Raman, B.; Ragauskas, A. *Applied Biochemistry and Biotechnology* **2010**, *162*, 62–74.
- [30] Saisu, M.; Sato, T.; Watanabe, M.; Adschiri, T. *Energy & Fuels* **2003**, *17*, 3124–3130.
- [31] Thring, R. W.; Breau, J. *Fuel* **1996**, *75*, 795–800.
- [32] Meier, D.; Ante, R.; Faix, O. *Bioresource Technology* **1992**, *40*, 171–177.

- [33] Kuroda, K.-I.; Inoue, Y.; Sakai, K. *Journal of Analytical and Applied Pyrolysis* **1990**, *18*, 59–69.
- [34] Brebu, M.; Vasile, C. *Cellulose Chemistry and Technology* **2010**, *44*, 353–363.
- [35] Mohan, D.; Pittman, C. U.; Steele, P. H.; Pittman, C. U. *Energy & Fuels* **2006**, *20*, 848–889.
- [36] Ferdous, D.; Dalai, A. K.; Bej, S. K.; Thring, R. W. *Energy & Fuels* **2002**, *16*, 1405–1412.
- [37] Demirbas, A. *Energy Conversion and Management* **2000**, *41*, 633–646.
- [38] Cookson, D. J.; Iliopoulos, P.; Smith, B. E. *Fuel* **1995**, *74*, 70–78.
- [39] Ramírez-López, C. A.; Ochoa-Gómez, J. R.; Fernández-Santos, M.; Gómez-Jiménez-Aberasturi, O.; Alonso-Vicario, A.; Torrecilla-Soria, J. J.; Ramirez-Lopez, C. A.; Ochoa-Gomez, J. R.; Fernandez-Santos, M.; Gomez-Jimenez-Aberasturi, O. *Industrial & Engineering Chemistry Research* **2010**, *49*, 6270–6278.
- [40] Roy, D.; Subramaniam, B.; Chaudhari, R. V. *ACS Catalysis* **2011**, *1*, 548–551.
- [41] Miller, J. E.; Evans, L.; Littlewolf, A.; Trudell, D. E. *Fuel* **1999**, *78*, 1363–1366.
- [42] Faravelli, T.; Frassoldati, A.; Migliavacca, G.; Ranzi, E. *Biomass and Bioenergy* **2010**, *34*, 290–301.
- [43] Britt, P. F.; Buchanan III, A. C.; Malcolm, E. A.; Buchanan, A. C. *Journal of Organic Chemistry* **2008**, *60*, 6523–6536.
- [44] Korobkov, V. Y.; Grigorieva, E. N.; Bykov, V. I.; Senko, O. V.; Kalechitz, I. V. *Fuel* **1988**, *67*, 657–662.
- [45] Cassidy, P. J.; Jackson, W. R.; Larkins, F. P. *Fuel* **1983**, *62*, 1404–1411.
- [46] Townsend, S. H.; Abraham, M. A.; Huppert, G. L.; Klein, M. T.; Paspek, S. C. *Industrial & Engineering Chemistry Research* **1988**, *27*, 143–149.
- [47] Centeno, A.; Laurent, E.; Delmon, B. *Journal of Catalysis* **1995**, *154*, 288–298.
- [48] Edward, F. *Applied Catalysis A: General* **2000**, *199*, 147–190.
- [49] Vuori, A. I.; Bredenberg, J. B. *Industrial & Engineering Chemistry Research* **1987**, *26*, 359–365.

CHAPTER 3

Zeolite Topology Effects in the Alkylation of Phenol with Propylene

This chapter is largely reproduced from “Zeolite Topology Effects in the Alkylation of Phenol with Propylene” by Weiyin Xu, Stephen J. Miller, Pradeep, K. Agrawal, and Christopher W. Jones, published in *Applied Catalysis A: General*, in 2013, volume 459, pages 114-120 [1].

3.1 Introduction

Interest in renewable raw materials has driven research in the processing of lignocellulosic biomass into chemicals and fuels [2–4]. In many cases, zeolites have been used effectively as catalysts for a variety of conversions of biomass-derived substrates [5–11]. At present, bio-oils derived from lignin via fast pyrolysis are very corrosive, highly viscous and have low heating value [12, 13], requiring upgrading before they can be used as a fuel. These qualities of bio-oils can be improved by increasing the H/C molar ratio and decreasing the O/C molar ratio of the mixture, and some success has been reported using hydrodeoxygenation processes [1, 14]. However, phenolic compounds are often still found in the final bio-oil composition due to the difficulties in completely removing oxygen from the bio-oil. An alternative way to further improve bio-oils is to enhance their H/C ratios via alkylation [15, 16]. Alkylated phenols may serve as useful chemicals, or they may be subsequently subjected to hydrogenation treatments to reduce the oxygen content and produce fuels, as described above. In this work, we evaluate alkylation of phenol, a model compound representing species in bio-oils, with propylene,

catalyzed by a variety of zeolites. A specific focus is placed on understanding the role of zeolite topology in controlling the 2-/4-distribution in the alkylated products, with an emphasis placed on obtaining the 2-alkylated products, in contrast to typical zeolite processes that focus on generating 4-substituted products. In past work, we have found that some 2-monoalkylated phenols can be hydrogenated with less catalyst deactivation than 4-substituted analogues [17].

Zeolites are commonly employed commercially for alkylation reactions as they are non-corrosive, have tunable acidic properties and can be easily recycled, unlike traditional liquid catalysts (e.g. aluminum chloride and solid phosphoric acid) [18]. More specifically, zeolites have been widely studied for the production of industrially important chemicals via reactions that are conceptually similar to the reactions studied here, such as the alkylation of benzene to form ethylbenzene and cumene [19], and of phenols to form cresols [20, 21]. Generally, these studies have focused on maximizing conversion while minimizing the accompanying deactivation to obtain high productivity. Reactions involving phenol to produce cresols have an additional focus on increasing C-alkylation over O-alkylation to increase selectivity for the target product and past studies generally agree that stronger acid catalysts favor C-alkylation while more basic catalysts favor O-alkylation.

The open literature on the isopropylation of phenol is very limited [22–25]. Wei et al. optimized the conditions for the alkylation of phenol with isopropanol over MCM-49 to obtain high conversion and high selectivity to isopropylphenols [22]. Savidha and co-authors reported the vapor phase alkylation of phenol with isopropylacetate catalyzed by Zn-Al-MCM-41, Fe-Al-MCM-41 and Al-MCM-41 [23, 24]. They observed that

substituting Al with Fe and Zn resulted in higher conversions and an increase in selectivity towards 4-IPP, via an increase in the strength of the Brønsted acid sites. Wang et al. studied the vapor phase alkylation of phenol with propylene using HZSM5 while varying the Si/Al ratio and introducing Cs⁺ sites via ion-exchange [25]. Similar to the studies of alkylation of phenol with methanol, more O-alkylation was observed at lower temperatures while C-alkylation dominated at temperatures higher than 250°C. Cs⁺ was introduced to perturb the acid strength distribution of zeolite and the authors found that moderate strength acid sites favored 4-isopropylphenol formation while weak acid sites favored 2-isopropylphenol.

In this work, the reaction pathway in the zeolite catalyzed alkylation of phenol with propylene at 350°C is established and the impact of pore size on product selectivity is elucidated. Much like in the case of n-hexane hydroisomerization, m-xylene isomerization and related reactions of aromatic compounds, phenol alkylation selectivity can give useful insights into the structure of zeolites whose crystal structures are currently unknown [26–30].

3.2 Experimental Methods

3.2.1 Materials

All zeolites and other silicate catalysts materials used have bulk Si/Al ratios between 10 and 17 to yield comparable acid properties among the zeolite samples. Both commercial zeolites as well as zeolites provided by Chevron were used for these studies. Commercial zeolites HFAU (CBV 720), NH₄BEA (CP814E), NH₄MOR (CBV 21A) and

NH₄MFI (CBV 3024E) were obtained from Zeolyst International. Zeolites TNU-9, ZSM-11, MTT and SSZ-13 were obtained in proton form from Chevron, while SSZ-25 was obtained in the as-synthesized form. The description of the framework type, pore size and pore dimensions of these zeolites has been summarized in Table 3.1 below, together with their measured silicon to aluminum ratios. SSZ-25 was calcined at 540°C for 4 hours and then heated to 600°C for an additional 4 hours in flowing air with a temperature ramp of 1°C/min. The calcined zeolite was then ion-exchanged three times in a 1M NH₄NO₃ solution at 80°C for 12 hours using a solid to liquid weight ratio of 1:5. All ammonium form catalysts were activated at 500°C for 4 hours to yield their final acidic forms. The proton forms of the zeolites were pelletized binder free, crushed and sieved to yield particles of size 0.178 – 0.354mm (US mesh -45/+80). This particle size was determined experimentally to be free of (non-zeolitic) intraparticle diffusion limitations and possibly film mass transfer effects as increasing and decreasing the particle size by 60% did not yield significant differences in the conversion (Table 3.2).

Table 3.1 Summary of zeolites used in this study

Zeolite (Type)	Si/Al _{bulk}	Si/Al _{framework} ^a	Pore Structure (Å) / Pore Dimensionality
Y (FAU)	14.9	16	7.4 (12) / 3D
BEA (BEA)	12.5	22	7.6 x 6.4 (12), 5.5 x 5.5 (12) / 3D
MOR (MOR)	10	11	7.0 x 6.5 (12), 5.7 x 2.6 (8) / 3D
ZSM-5 (MFI)	15	16	5.1 x 5.5 (10), 5.3 x 5.6 (10) / 3D
TNU-9 (TUN)	12-14	15	5.1 x 5.5 A (10), 5.4 x 5.5 (10), 5.6 x 5.5 (10) / 3D
ZSM-11 (MEL)	15.7	16	5.3 x 5.4 (10) / 3D
SSZ-25 (MWW)	~16	22	4.0 x 5.5 (10), 4.1 x 5.1 (10) / 2D
MTT (MTT)	16.6	20	4.5 x 5.2 (10) / 1D
SSZ-13 (CHA)	13-15	15	3.8 x 3.8 (8) / 3D

^a Determined by the quantification of extraframework aluminum (EFAL) via ²⁷Al NMR

Table 3.2 Investigating the effects of intraparticle diffusion limitations on alkylation reaction. Reaction conditions: T = 350°C, Pressure = 1 atm, Catalyst = HY, Catalyst loading = 20mg, Phenol concentration = 0.9mol%, Phenol to propylene molar ratio = 1

Zeolite	Particle Size (mm)	D_{avg}/D_0	Conversion, X %
Y - D_{small}	0.149 – 0.177 (0.163)	$0.6D_0$	4.8
Y - D_0	0.177 – 0.355 (0.266)	D_0	6.3
Y - D_{large}	0.355 – 0.500 (0.4275)	$1.6D_0$	5.5

In addition to the zeolites, an acidic mesoporous material, Al-SBA-15, was synthesized via a co-condensation method. A mixture of 4g of Pluronic P123 in 100ml of 0.2M HCl was stirred for 1 hour at room temperature. Then, 1.8g of aluminium (III) isopropoxide was added to the mixture and stirred for 30mins. Finally, 9.0g of tetraethyl orthosilicate (TEOS) was added to the mixture. The final mixture was first stirred for 1 day at 40°C and then aged at 110°C for 2 days under static conditions. The precipitated material was filtered, dried and calcined at 550°C for 10 hours in air.

Zeolites Y and MTT were also subjected to a tetraethyl orthosilicate (TEOS) treatment to poison external surface acid sites using the following procedure. The zeolite was added to a 5% TEOS in hexane solution with a solid to liquid ratio of 0.2 and stirred for 15h. The treated zeolite was recovered by filtration and rinsed with hexane. Finally, the treated zeolite was dried in air and calcined.

3.2.2 Materials Characterization

The crystallinity of all the zeolites was verified with X-ray diffraction (XRD) and porosity analysis. The powder XRD experiments were performed using a PAnalytical X'pert Pro diffractometer with a Cu K α source, a diffracted beam collimeter and a

proportional detector. Scans were obtained using a step size of 0.05° between two theta angles of 5° and 50° . The micropore volumes of the zeolites were estimated from their nitrogen physisorption isotherms obtained on a Micromeritics Tristar II at 77K using approximately 100mg of sample. Subsequently, the micropore volumes were calculated using the quantity of nitrogen adsorbed at a relative pressure of 0.3 [31]. The pore size distribution of mesoporous Al-SBA-15 was calculated by applying the BdB-FHH (Frenkel–Halsey–Hill-modified Broekhoff–de Boer) method on its nitrogen adsorption isotherm [32].

The Brønsted acid site densities were determined using the temperature-programmed desorption (TPD) of isopropylamine [33]. In these experiments, 100 mg of zeolite was activated at 400°C for 1 hour using a temperature ramp of $5^\circ\text{C}/\text{min}$ in 100ml/min of nitrogen to remove adsorbed water, and then the samples was cooled back down to 30°C . Next, 100 μL of isopropylamine was introduced into the nitrogen stream and the nitrogen flow continued over the catalyst for an hour to allow for the removal of physisorbed isopropylamine. Finally, the temperature-programmed desorption was conducted by increasing the temperature at a rate of $10^\circ\text{C}/\text{min}$ and measuring the amount of propylene released from the decomposition of isopropylamine using a Pfeiffer Vacuum Omnistar mass spectrometer.

The amount of extraframework aluminum (EFAL) was estimated from the integration of the ^{27}Al solid-state nuclear magnetic resonance (NMR) spectra of the material. The NMR experiments were carried out on a Bruker AV3-400 spectrometer at a resonance frequency of 104.3MHz. The samples were fully hydrated with deionized water and packed into a 4mm MAS rotor which was spun at 10 kHz during the data

acquisition. The spectra were obtained at room temperature and the ^{27}Al chemical shifts were referenced to aqueous $\text{Al}(\text{NO}_3)_3$ at 0 ppm.

The zeolite Brønsted to Lewis acid site ratio was determined from infra-red measurements conducted on a Thermo Scientific Nicolet 8700 FT-IR spectrometer with samples pressed into self-supported wafers of size 9 – 12 mg/cm^2 , loaded into a high vacuum transmission FT-IR cell. The spectrometer was equipped with a MCTA detector and spectra were obtained at 128 scans per spectrum with a resolution of 4cm^{-1} . The samples were activated at 400°C for 1 hour in vacuum ($< 10^{-6}\text{mbar}$) prior to obtaining the background spectra at 150°C . Pyridine was introduced at 0.1 mbar for 30 mins at 150°C , after which physisorbed pyridine was removed by exposing the sample to vacuum for 1 hour before taking the difference spectra. The peaks at 1545 cm^{-1} and 1455 cm^{-1} represent the interaction between pyridine and the Brønsted and Lewis acid sites, respectively. Molar extinction coefficients of $1.67\text{cm}/\mu\text{mol}$ and $2.22\text{cm}/\mu\text{mol}$ were used for the Brønsted and Lewis acid sites respectively [34].

Zeolite bulk compositions were provided by Galbraith Laboratories via elemental analysis. Metal contents were analyzed using inductively coupled plasma optical emission spectrometry (ICP-OES) and organic content was determined by combustion.

3.2.3 Catalytic Testing

Catalytic alkylation experiments were carried out in a vertical packed bed reactor at 350°C and atmospheric pressure. Phenol was transferred into a heated syringe and pumped into the reactor using a Harvard Apparatus Pump 11 Elite. The flow rates of the propylene and helium gases were controlled with individual Brooks mass flow controllers

via a Labview interface. Catalyst mass ranged from 20–400 mg, depending on the activity of the catalyst, and SiC (250 – 400 mesh, Sigma-Aldrich) was mixed with the catalyst to achieve a total catalyst bed volume of 1cm³ for all experimental runs. All catalysts were activated at 400 °C for 1 hour in Helium (with 2% Nitrogen, as an internal standard) and then cooled to the reaction temperature of 350°C. In a typical experiment, phenol was introduced over the catalyst bed for 1 hour until the baseline stabilized. Thereafter, the reaction was started when propylene was introduced. Further experiments showed that the length of time phenol was introduced over the catalyst bed prior to the introduction of propylene did not affect the catalyst activity. The amounts of reactants and products were measured using an on-line Shimadzu GC2010 gas chromatograph (GC) equipped with a Vici six port valve, a Rxi-5ms column associated with a flame ionization detector (FID) and a RT-Q-Plot column associated with a thermal conductivity detector (TCD). All weight hourly space velocities were calculated with respect to the aromatic feed. Conversions, X, were calculated based on the molar flowrate of products formed, F_{products} , and molar flowrate of phenol feed, $F_{\text{phenol feed}}$ as shown in Equation 3-1 below.

$$\text{Conversion, } X \% = \frac{F_{\text{products}}}{F_{\text{phenol feed}}} \times 100\% \quad [\text{Equation 3-1}]$$

A normalized deactivation rate, r_d , was used to calculate the loss of catalyst activity with time based on the change in conversion with time, dX/dt , and initial conversion, $X_{t=0}$, as shown in Equation 3-2 below. Since the quantity of products formed is expected to contribute to the catalyst deactivation, all deactivation rates were normalized with the initial conversion of the experimental run.

$$\text{Normalized deactivation rate, } r_D = \frac{dX/dt}{X_{t=0}} \times 100\% \quad [\text{Equation 3-2}]$$

The chemicals used in the experiments were phenol (99%, Sigma-Aldrich), 2-isopropylphenol (98%, Sigma-Aldrich), 3-isopropylphenol (97%, Sigma-Aldrich), 4-isopropylphenol (98%, Sigma-Aldrich), isopropylphenyl ether (95%, Ace Synthesis), and propylene (2% in helium, Airgas).

3.3 Results and Discussion

3.3.1 Characterization of Zeolites

The physical characteristics of the zeolites used are shown in Table 3.3. The micropore volumes of all the zeolites are in the range of 0.106 – 0.379 cc N₂/g, which is typical for zeolites and generally similar to their expected micropore volumes obtained via simulation [35, 36]. Generally, the acid properties of the 9 zeolites are similar due to the relatively narrow range of framework Si/Al ratios used, falling between 11 and 22 (Table 3.1). The Brønsted acid concentrations are between 27 and 821 μmol/g, and Brønsted and Lewis acid site ratios fall between 1 and 4, with an outlier at 53.4 (Table 3.4).

Table 3.3 Micropore volume and external surface area characterization of zeolites

Zeolite (Type)	V _{micropore} (cc N ₂ /g)	Crystal Size	Agglomeration Size
Y (FAU)	0.324	0.5 – 0.7µm	1 – 2µm
BEA (BEA)	0.256	0.2 – 0.3µm	2 – 4µm
MOR (MOR)	0.194	1 – 2µm	0.5 – 3µm
ZSM-5 (MFI)	0.169	0.2 – 0.3µm	1 – 2µm
TNU-9 (TUN)	0.200	0.5 – 1µm	7 – 28µm
ZSM-11 (MEL)	0.166	0.1 – 0.2µm	-
SSZ-25 (MWW)	0.183	0.4 – 0.6µm	1 – 3 µm
MTT (MTT)	0.106	0.1 – 0.3µm	-
SSZ-13 (CHA)	0.379	0.1 – 0.2µm	1 – 2µm

Table 3.4 Characterization of zeolite acid sites via ²⁷Al MAS NMR, isopropylamine temperature programmed desorption and pyridine FT-IR

Zeolite (Type)	Framework Si/Al(µmol/g) ^a	Brønsted Acidity (µmol/g) ^b	B/L ratio at 150°C ^c
Y (FAU)	922	444 ± 21	3.0
BEA (BEA)	681	772	1.1
MOR (MOR)	1308	821	4.1
ZSM-5 (MFI)	922	692	2.7
TNU-9 (TUN)	980	623	2.4
ZSM-11 (MEL)	922	577	>50
SSZ-25 (MWW)	681	546	1.6
MTT (MTT)	746	267	2.8
SSZ-13 (CHA)	980	27	3.4

^a Determined by the quantification of extraframework aluminum (EFAL) via ²⁷Al NMR and yH⁺(xSiO₂.yAlO₂) formula

^b Quantified by the temperature programmed desorption of isopropylamine

^c Measured via Pyridine FT-IR

The framework Si/Al ratios of the zeolites were estimated by adjusting the bulk Si/Al ratio with the fraction of framework aluminum species estimated from the ²⁷Al MAS NMR spectra. The broad resonances around 50-60 ppm in the ²⁷Al MAS NMR spectra correspond to tetrahedrally coordinated species characteristic of aluminum that is incorporated in the framework of the zeolite [37]. Extraframework Al species manifest as pentahedrally and octahedrally coordinated species that have peaks at 30 ppm and 0 ppm respectively. The spectra show that while most of the zeolites contain some octahedral

aluminum, none showed any pentahedral aluminum species. However, these species may exist in the dry samples, but hydration of the samples before NMR should convert these species into octahedrally coordinated species.

Infrared measurements of the Brønsted and Lewis acid site ratios were conducted with pyridine as the probe molecule. The Brønsted to Lewis acid ratios derived from FT-IR spectra of the pyridine loaded samples were found to be lower than the ones calculated using ^{27}Al NMR, which is expected based on previous literature reports [38]. However, the Brønsted to Lewis acid ratio trends obtained via both methods were generally similar (Figure 3.1).

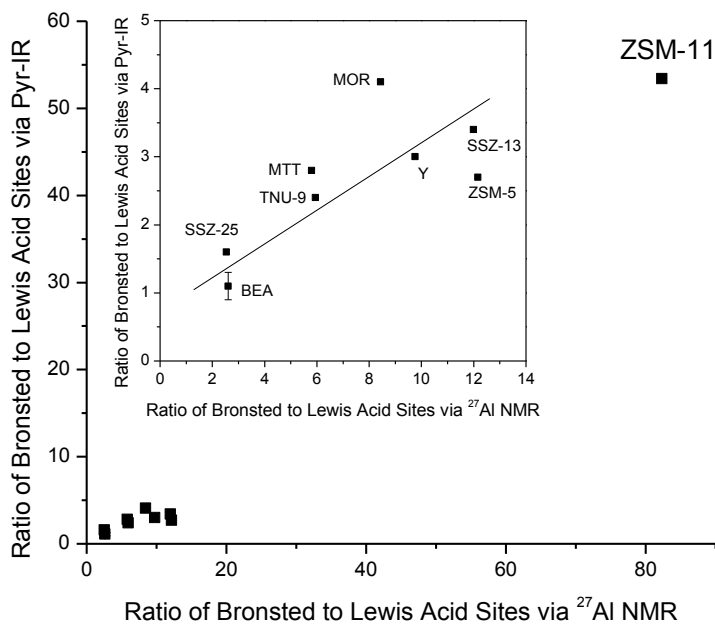


Figure 3.1 Relationship between Brønsted to Lewis acid site ratio calculated via pyridine FT-IR and ^{27}Al NMR.

The concentration of Brønsted acid sites obtained via isopropylamine TPD were comparable to the concentrations calculated based on the weight percent of Al in the zeolites obtained via elemental analysis, as corrected by the Brønsted to Lewis acid ratios obtained with pyridine FT-IR. All of the zeolites have a mix of Brønsted and Lewis acid site except ZSM-11 which appears to have predominantly Brønsted acid sites. Furthermore, the trend of the concentrations generally agreed with the calculated framework Si/Al ratios, with zeolites with higher Si/Al ratios having a correspondingly smaller concentration of Brønsted acid sites. Isopropylamine has been shown to be unable to fit into 8-member ring channels such as those found in FER and MOR [39, 40]. Consequently, the acid concentration shown for MOR only represents the acid sites in its 12-member ring channels and the small acid concentration of SSZ-13 represents only the external surface acid sites. However, isopropylamine is expected to be able to access all the acid sites of the other zeolites employed and their Brønsted acid site concentrations are expected to accurately represent the total Brønsted acid site concentrations.

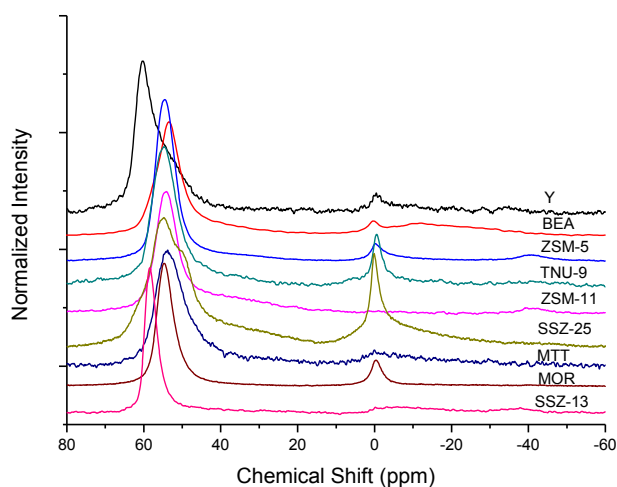


Figure 3.2 ^{27}Al NMR spectra of fully hydrated zeolites in proton form

3.3.2 Alkylation Reaction Pathway

During a typical alkylation reaction involving phenol and propylene at phenol conversions between 2% and 10%, 2-isopropylphenol and 4-isopropylphenol are detected as the main products, making up approximately 95% of the products, with di-alkylated species making up the remainder. Based on literature reports on phenol methylation with methanol, other reactions such as O-alkylation, isomerization and de-alkylation reactions can occur simultaneously [41–43]. Thus, to establish the dominant reaction pathways that occur under atmospheric pressure at 350°C, the expected alkylation products - 2-isopropylphenol, 3-isopropylphenol, 4-isopropylphenol, and isopropyl phenyl ether- were reacted at a fixed WHSV over the HY zeolite and the products formed were assessed via online GC. The results of these runs are tabulated in Table 3.5. A summary of the primary reaction pathways based on this set of reactions is provided in Figure 3.3.

Table 3.5 Assessing the reaction pathway via conversion of reactants, products and possible intermediate species. Reaction conditions: T = 350°C, Pressure = 1 atm, Catalyst = HY, Catalyst loading = 20mg, Aromatic reactant concentration = 0.8 –0.9 mol%

Feed	WHSV (h ⁻¹)	X ₀ %	Selectivity (t = 0 min)				2-IPP/4-IPP ratio
			Phenol	IPPE	2-IPP	Others	
IPPE	13.9	100	89.5	-	8.3	0.1	2.1
2-IPP	15.2	40.5	75.4	0	-	2.2	22.4
3-IPP	14.9	0.6	-	-	-	-	-
4-IPP	14.9	1.8	-	-	-	-	-

were at 100% conversion, with approximately four times more 2-isopropylphenol formed than 4-isopropylphenol. Since the ratio of 2-isopropylphenol over 4-isopropylphenol in this case is higher than the 1.73 ratio obtained via direct alkylation of phenol with propylene, the 2-isopropylphenol is likely formed not only via the alkylation of the phenol product but also through the direct isomerization of isopropylphenyl ether.

All of the products were expected to undergo de-alkylation reactions. It was thus surprising to find that only 2-isopropylphenol was de-alkylated under our reaction conditions. De-alkylation reactions are expected to be catalyzed by highly acidic catalysts. The literature reports 2 different adsorption modes of phenol on acid surfaces – (i) a vertical orientation of phenol with only the hydroxyl group interacting with the surface [43, 44] and (ii) an orientation of phenol with the aromatic ring more parallel to the surface on stronger acid sites, with not only the hydroxyl group but also the ring interacting at the same time [45, 46]. For the de-alkylation of isopropylphenols, it is conceivable that the alkyl group needs to be relatively close to the phenolic oxygen for de-alkylation to occur. Subsequently, the observed de-alkylation reactions would be easier with 2-isopropylphenol than 3-isopropylphenol and 4-isopropylphenol, in the absence of stronger acid sites or appropriately paired acid sites.

3.3.3 Effects of Zeolite Pore Topology

To determine the effects of pore topology on the product selectivity, all 9 zeolites were compared at the same initial conversion of approximately 5%. The conversion and product selectivity data obtained from a typical reaction run are shown in Figure 3.4.

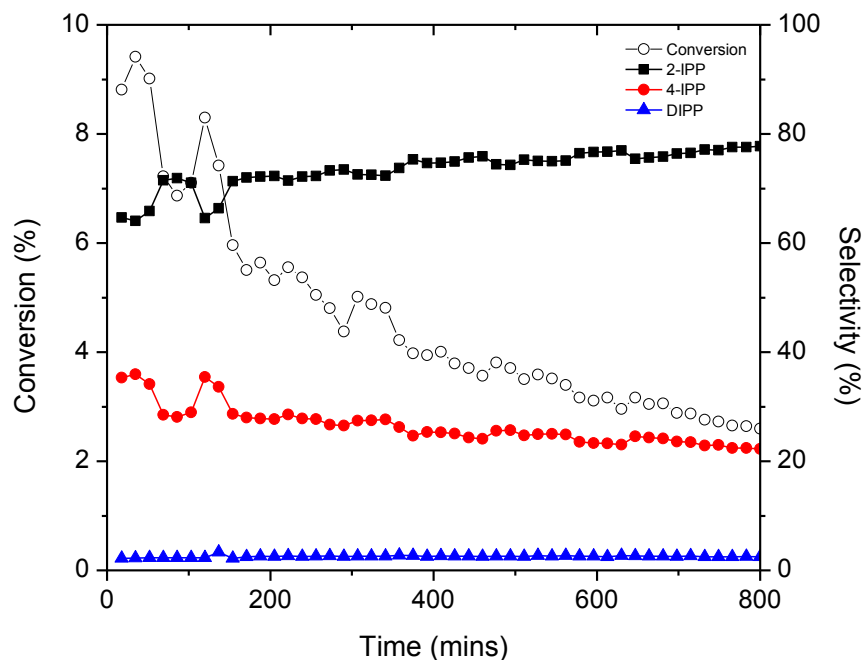


Figure 3.4 Example of reactivity data obtained with increasing time on stream - conversion of phenol (○), 2-isopropylphenol selectivity (■), 4-isopropylphenol selectivity (●) and di-isopropylphenols selectivity (▲). Catalyst = HBEA, T = 350°C, Pressure = 1 atm, WHSV = 8.0 h⁻¹, Phenol concentration = 1.4 mol%, Phenol to propylene ratio = 1.4

As shown in the figure, some fluctuations that may affect the accuracy of the data are observed in the first 200 mins of the run. To address this, all reactions were run for 12 hours to allow the catalyst to stabilize and data after 400mins of reaction were extrapolated to time zero to estimate initial rates and selectivities. The reaction conversion and product selectivities obtained from the 9 zeolites are given in Table 3.6.

Most of the zeolites evaluated had similar conversions ranging from 3.9 – 6.3%. The exception was SSZ-13, which had very low activity and only gave an initial conversion of 1.6% even when a WHSV of 1.3 h⁻¹ was used. All of the zeolites had

similar normalized rates of deactivation, with conversions decreasing by 3-5 % per hour. Deactivation could be caused by either the inability to access active sites due to pore blockage or by the formation of the coke on the acid site itself, preventing further reaction. If deactivation is mainly caused by pore blockage, the deactivation rate would be expected to increase with $1D > 2D > 3D$ pores. However, no correlation between the normalized deactivation rate and dimensionality of the pores was observed. Instead, the similarities in the normalized rates of deactivation regardless of the dimensionality of the pores or whether the reaction occurred mostly within the pores (Y, BEA, MOR, ZSM-5, TNU-9, ZSM-11, see below) or on the external surface of the zeolite crystal (SSZ-25, MTT, SSZ-13), indicates that active site deactivation is the more likely mechanism for loss of activity.

Table 3.6 Product selectivities of different zeolites at a similar initial phenol conversion of 5%. Reaction conditions: T = 350°C, Pressure = 1 atm, WHSV = 0.8 - 16.1 h⁻¹, Phenol concentration = 1.4 mol%, Phenol to propylene ratio = 1.4

Zeolite	$X_{(t=0)}$	$-r_{\text{phenol}}^{\text{phenol}}(t=0)$ (mol h ⁻¹ gcat ⁻¹)	r_D (% h ⁻¹)	$N_{2\text{-IPP}}/N_{4\text{-IPP}}(t=0)$
Y (FAU)	6.30	0.0107	3.94	1.73
BEA (BEA)	5.67	0.0048	4.16	2.23
MOR (MOR)	3.85	0.0009	4.68	1.51
ZSM-5 (MFI)	4.42	0.0012	3.12	0.10
TNU-9 (TUN)	4.98	0.0020	3.61	0.22
ZSM-11 (MEL)	6.33	0.0054	3.92	0.06
SSZ-25 (MWW)	5.16	0.0044	3.76	2.48
MTT (MTT)	5.74	0.0049	4.69	2.79
SSZ-13 (CHA)	1.60	0.0002	2.96	2.41
Al-SBA-15	4.56	0.0052	3.94	3.26

An initial hypothesis was that within the same family of zeolites with similar acid strengths, with increasing pore size, the reaction would become less selective towards 4-isopropylphenol and more selective towards 2-isopropylphenol. Additionally, it was

hypothesized that there would be a maximum pore size that maximizes selectivity for 2-isopropylphenol, as still larger pore sizes would favor further conversion of the isopropylphenols to form di-isopropylphenols. The trends observed from the experiments suggest that the reaction occurs in the pores and supports our initial hypothesis that reactions occurred within the pores of the zeolites (Y, BEA, MOR, ZSM-5, TNU-9 and ZSM-11). In Figure 3.5, a plot of the 2-isopropylphenol to 4-isopropylphenol ratio versus the average dimension of the largest pore in the zeolite shows a maximum as the average of the largest pore dimension increases from 5.4 Å to 7.4 Å. Furthermore, in Figure 3.6, there is a clear increase in the selectivity of di-isopropylphenols as the average largest pore dimension increases between 5.4 Å and 7.4 Å. Given the o-, p- directing properties of the hydroxyl group, 2,4-diisopropylphenol and 2,6-diisopropylphenol were the expected dialkylated compounds and were observed in very small concentrations. Qualitatively, the selectivity for 2,6-diisopropylphenol, the kinetically smaller diisopropylphenol, decreased in the following manner: TNU9 \approx ZSM11 > ZSM5 > Y \approx BEA > MOR. Consequently, the experimental results support the initial hypothesis and it was determined that zeolite BEA yielded the highest selectivity for 2-isopropylphenols for reactions occurring primarily in the pores.

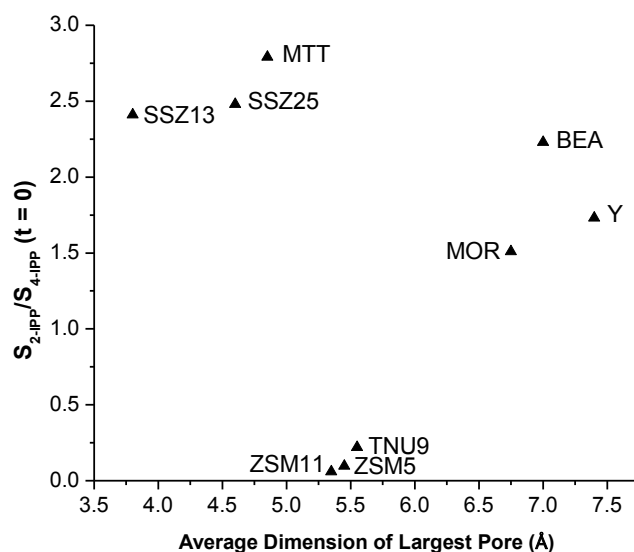


Figure 3.5 Relationship between 2-IPP and 4-IPP molar ratios and the average dimension of the largest zeolite pore. These runs were all conducted with approximately the same conversions (see Table 3.6).

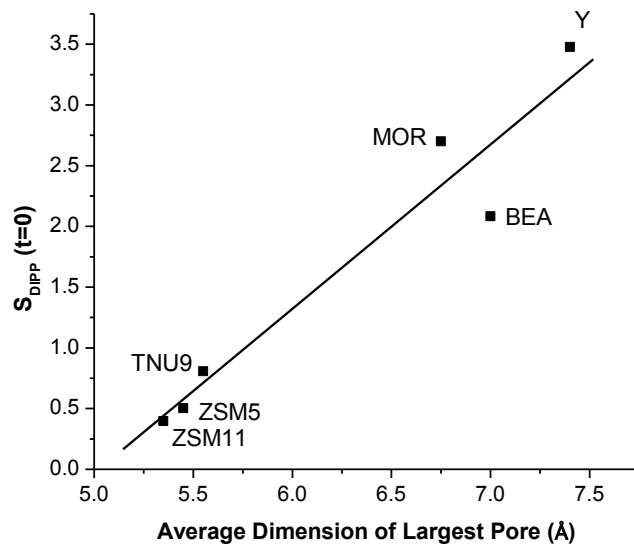


Figure 3.6 Relationship between selectivity of di-isopropylphenols and the average dimension of the largest zeolite pore. These runs were all conducted with approximately the same conversions and data can be found in Table 3.6.

It is interesting to note that the ratio of 2-isopropylphenols to 4-isopropylphenols was higher for zeolites with pore sizes less than 4.8 Å. At such small pore sizes, phenol, which has a molecular diameter of ca. 6.2 Å, is likely unable to enter the micropores and react on internal acid sites within the zeolites [47]. Subsequently, the ratio represents the intrinsic selectivity of the acid sites, without being masked by pore diffusion or steric effects. This notion suggests that other catalysts with unconstrained pores would give similar elevated ratios of 2-isopropylphenol to 4-isopropylphenol. To this end, a mesoporous material with Brønsted acid sites, Al-SBA-15, was synthesized, characterized (Figure 3.7) and used to catalyze this reaction.

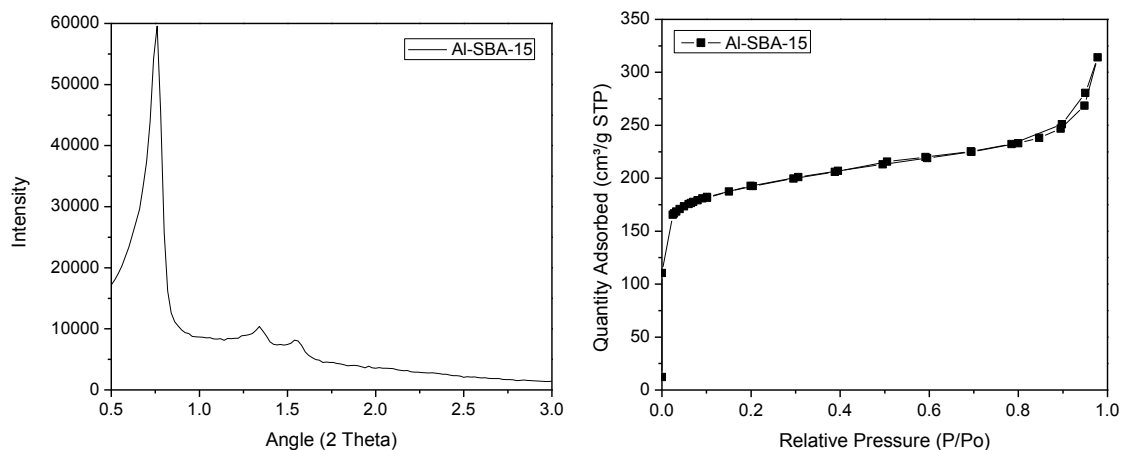


Figure 3.7 X-ray diffraction (XRD) and nitrogen physisorption characterization of Al-SBA-15 (Si/Al = 26.6)

Over this catalyst, phenol alkylation with propylene is not expected to be limited by the pore size of catalyst as it has an average pore diameter of 70 Å [48]. Thus, the 2-isopropylphenol to 4-isopropylphenol ratio obtained with Al-SBA-15 is expected to be representative of ratio obtained when the reactions are not restricted by the pore size. At

4.6% initial conversion, the 2-isopropylphenol to 4-isopropylphenol ratio obtained on Al-SBA-15 was 3.26. Like MTT, SSZ-25 and SSZ-13, this ratio is higher than that found with other zeolites where the reaction occurs in the pore and selectivity is expected to be influenced by the pore size, providing evidence that the external zeolite surface sites are responsible for the high ratio obtained.

Table 3.7 Investigating the effects of surface acid sites on catalytic activity. Characteristics of catalysts before and after TEOS treatment. Reaction conditions: T = 350°C, Pressure = 1 atm, Catalyst loading normalized by aluminum content, phenol concentration = 1.4 mol%, Phenol to propylene ratio = 1.4

Zeolite	Si/Al _{bulk}	V _{micropore} (cc N ₂ /g)	Brønsted Acidity (μmol/g)	WHSV (h ⁻¹)	X ₀ %
HY	14.9	0.324	439	16.1	6.3
HY-TEOS	16.9	0.270	399	14.6	5.8
MTT	16.6	0.106	267	8.1	5.8
MTT-TEOS	18.8	0.091	111	7.5	0.7

To further probe whether the external surface acid sites were responsible for the high 2-isopropylphenol selectivities over MTT, SSZ-25 and SSZ-13, an alternative set of experiments was undertaken involving the passivation of surface acid sites by treating the zeolites with tetraethyl orthosilicate (TEOS) [49, 50]. The characterization and reaction results of Y and MTT catalysts (before and after silanization treatments) are summarized in Table 3.7. Experiments with zeolite Y served as control experiments that show that acidity decreased by 9% and conversion decreased by 8% after the TEOS treatment. Thus, significant conversion still occurred over the silane-treated Y zeolite, demonstrating that much of the reaction occurs within the zeolite pores over this large pore zeolite. In contrast, the acidity of MTT decreased by 58% and conversion decreased by 88% after the TEOS treatment. This large decrease in conversion after the TEOS

treatment further supports the hypothesis that surface acid sites are largely responsible for the activity of MTT and the product selectivity. This suggests that the high 2-isopropylphenol to 4-isopropylphenol ratio over zeolites with pores of similar size also occur primarily or exclusively over the zeolite external surface.

3.4 Conclusions

The reaction pathways for the alkylation of phenol with propylene catalyzed by zeolites at 350°C and the effects of pore size on product selectivity have been elucidated. The reaction pathway studies showed that 2-isopropylphenol and 4-isopropylphenol are the main products of the alkylation reactions and no O-alkylation was observed. Secondary reactions involving possible alkylation products were also evaluated and the de-alkylation of 2-isopropylphenol and isopropylphenyl ether was found to be feasible under the conditions used, while 3-isopropylphenol and 4-isopropylphenol did not participate in secondary reactions. Maximum 2-isopropylphenol to 4-isopropylphenol ratios were obtained when reactions occurred on the surface of the zeolites while maximum 4-isopropylphenol selectivity was obtained from 10-member ring zeolites with an average largest pore dimension between 5.25Å and 5.75Å. With 2-isopropylphenol a useful product that could be hydrogenated to propylcyclohexane with good catalyst stability, catalysts that maximize this product may prove useful for molecular weight enhancement for biofuel production from lignin-derived feeds [17].

At low reactant concentrations, when side reactions are minimized and crystal sizes are comparable, phenol isopropylation product selectivity can be used to estimate

pore topology. Medium pore zeolites (10-member rings) will yield more mono-alkylated 4-isopropylphenol, while large pore zeolites (12-member rings) will yield more mono-alkylated 2-isopropylphenol, with the amount of di-alkylated products increasing with pore size. Subsequently, this reaction could be employed as a test reaction as the selectivity of the products is sensitive to the zeolite pore size for pore sizes $> \sim 5.25 \text{ \AA}$.

3.5 References

- [1] Xu, W.; Miller, S. J.; Agrawal, P. K.; Jones, C. W. *Applied Catalysis A: General* **2013**, *459*, 114–120.
- [2] Zakzeski, J.; Bruijninx, P. C. A.; Jongerius, A. L.; Weckhuysen, B. M. *Chemical Reviews* **2010**, *110*, 3552–3599.
- [3] Binder, J. B.; Raines, R. T. *Journal of the American Chemical Society* **2009**, *131*, 1979–85.
- [4] Sun, Y.; Cheng, J. *Bioresource technology* **2002**, *83*, 1–11.
- [5] Williams, C. L.; Chang, C.; Do, P.; Nikbin, N.; Caratzoulas, S.; Vlachos, D. G.; Lobo, R. F.; Fan, W.; Dauenhauer, P. J. *ACS Catalysis* **2012**, *2*, 935–939.
- [6] Holm, M. S.; Saravanamurugan, S.; Taarning, E. *Science* **2010**, *328*, 602–5.
- [7] Moliner, M.; Román-Leshkov, Y.; Davis, M. E. *Proceedings of the National Academy of Sciences of the United States of America* **2010**, *107*, 6164–8.
- [8] Corma, A.; Huber, G. W.; Sauvanaud, L.; O’connor, P. *Journal of Catalysis* **2008**, *257*, 163–171.
- [9] Corma, A.; Huber, G. W.; Sauvanaud, L.; Oconnor, P. *Journal of Catalysis* **2007**, *247*, 307–327.
- [10] Choudhary, V.; Pinar, A. B.; Sandler, S. I.; Vlachos, D. G.; Lobo, R. F. *ACS Catalysis* **2011**, *1*, 1724–1728.
- [11] Neumann, G. T.; Hicks, J. C. *ACS Catalysis* **2012**, *2*, 642–646.

- [12] Mohan, D.; Pittman, C. U.; Steele, P. H.; Pittman, C. U. *Energy & Fuels* **2006**, *20*, 848–889.
- [13] Czernik, S.; Bridgwater, A. V *Energy & Fuels* **2004**, *18*, 590–598.
- [14] Kleinert, M.; Gasson, J. R.; Barth, T. *Journal of Analytical and Applied Pyrolysis* **2009**, *85*, 108–117.
- [15] Nie, J.-Q.; Chen, H.-W.; Song, Q.-H.; Liao, B.; Guo, Q.-X. *Energy & Fuels* **2010**, *24*, 5722–5726.
- [16] Zhang, Z.; Wang, Q.; Tripathi, P.; Pittman Jr, C. U. *Green Chemistry* **2011**, *13*, 940.
- [17] D. Y. Hong, P. K. Agrawal, C. W. Jones, unpublished work (**2009**).
- [18] Tsai, T.; Liu, S.; Wang, I. *Applied Catalysis A: General* **1999**, *181*, 355–398.
- [19] Degnan Jr., T. F.; Smith, C. M.; Venkat, C. R. *Applied Catalysis A: General* **2001**, *221*, 283–294.
- [20] Bregolato, M.; Bolis, V.; Busco, C.; Ugliengo, P.; Bordiga, S.; Cavani, F.; Ballarini, N.; Maselli, L.; Passeri, S.; Rossetti, I. *Journal of Catalysis* **2007**, *245*, 285–300.
- [21] Sad, M. E.; Padró, C. L.; Apesteguía, C. R. *Applied Catalysis A: General* **2008**, *342*, 40–48.
- [22] Wei, L.; Shang, Y.; Yang, P. *Reaction Kinetics and Catalysis Letters* **2008**, *93*, 265–271.
- [23] Savidha, R.; Pandurangan, A.; Palaichamy, M.; Murugesan, V. *Catalysis Letters* **2003**, *91*, 49–61.
- [24] Savidha, R.; Pandurangan, a *Applied Catalysis A: General* **2004**, *262*, 1–11.
- [25] Wang, B.; Wee, C.; Cai, T.; Park, S. *Catalysis Letters* **2001**, *76*, 219–224.
- [26] Min, H.-K.; Cha, S. H.; Hong, S. B. *ACS Catalysis* **2012**, *2*, 971–981.
- [27] Čejka, J.; Wichterlová, B. *Catalysis Reviews* **2002**, *44*, 375–421.
- [28] Corma, A.; Corell, C.; Llopis, F.; Martinez, A.; Perez-Pariente, J. *Applied Catalysis A: General* **1994**, *115*, 121–134.
- [29] Jones, C. W.; Zones, S. I.; Davis, M. E. **1999**, *181*.

- [30] Chen, C. Y.; Ouyang, X.; Zones, S. I.; Banach, S. a.; Elomari, S. a.; Davis, T. M.; Ojo, a. F. *Microporous and Mesoporous Materials* **2012**, *164*, 71–81.
- [31] De Boer, J. H.; Lippens, B. C. *Journal of Catalysis* **1965**, *4*, 319–323.
- [32] Lukens, W. W.; Schmidt-winkel, P.; Zhao, D.; Feng, J.; Stucky, G. D. *Langmuir* **1999**, *15*, 5403–5409.
- [33] Parrillo, D. J.; Adamo, a. T.; Kokotailo, G. T.; Gorte, R. J. *Applied Catalysis* **1990**, *67*, 107–118.
- [34] Selli, E.; Forni, L. *Microporous and Mesoporous Materials* **1999**, *31*, 129–140.
- [35] Roque-malherbe, R. *Microporous and Mesoporous Materials* **2000**, *41*, 227–240.
- [36] Jiri Cejka, Avelino Corma, S. Z. Modeling of Transport and Accessibility in Zeolites. In *Zeolites and Catalysis: Synthesis, Reactions and Applications, Volume 1*; 2010; p. 345.
- [37] Smith, M. E. *Applied Magnetic Resonance* **1993**, *4*, 1–64.
- [38] Kiricsi, I.; Flego, C.; Pazzuconi, G.; Parker, W. O. J.; Millini, R.; Perego, C.; Bellussi, G. *The Journal of Physical Chemistry* **1994**, *98*, 4627–4634.
- [39] Palkhiwala, A. G.; Gorte, R. J. *Catalysis Letters* **1999**, *57*, 19–23.
- [40] Tromp, M.; Van Bokhoven, J. a.; Garriga Oostenbrink, M. T.; Bitter, J. H.; De Jong, K. P.; Koningsberger, D. C. *Journal of Catalysis* **2000**, *190*, 209–214.
- [41] Balsama, S.; Beltrame, P.; Beltrame, P. L.; Carniti, P.; Forni, L.; Zuretti, G. *Applied Catalysis* **1984**, *13*, 161–170.
- [42] Marczewski, M.; Bodibo, J.-P.; Perot, G.; Guisnet, M. *Journal of Molecular Catalysis* **1989**, *50*, 211–218.
- [43] Santacesaria, E.; Grasso, D.; Gelosa, D.; Carra, S. *Applied Catalysis* **1990**, *64*, 83–99.
- [44] Klemm, L. H.; Klopfenstein, C. E. *Journal of Organic Chemistry* **1970**, *35*, 1069–1075.
- [45] Beutel, T.; Peltre, M.-J.; Su, B.-L. *Colloids and Surfaces A: Physicochemical and Engineering Aspects* **2001**, 319–325.
- [46] Reddy, K. R.; Ramesh, K.; Seela, K. K.; Rao, V. V.; Chary, K. V. R. *Catalysis Communications* **2003**, *4*, 112–117.

- [47] Hsieh, C.-T.; Teng, H. *Carbon* **2000**, 38, 863–869.
- [48] Kruk, M.; Cao, L. *Langmuir* **2007**, 23, 7247–54.
- [49] O'Connor, C. T.; Möller, K. P.; Manstein, H. *Cattech* **2001**, 5, 172–182.
- [50] Andy, P.; Lee, G.; Gonzalez, H.; Jones, C. W.; Davis, M. E. *Journal of Catalysis* **2000**, 192, 215–223.

CHAPTER 4

Zeolite Acid Strength Effects in the Alkylation of Phenol with Propylene

4.1 Introduction

Zeolites are widely applied in the petroleum and petrochemical industry for selective heterogeneous acid catalysis as they are stable at elevated temperatures and have molecular pore sizes that give them shape selective properties. Zeolites have been applied to reactions such as aromatic alkylation (e.g. alkylation of benzene with propylene to form cumene), xylene isomerization and toluene disproportionation [1, 2]. Zeolite acid properties can be varied by changing the silicon to aluminum (or other framework metal) ratio, the introduction of various cations through ion-exchange, by adjusting the extent of ion-exchange or through the incorporation of other metals in the framework [3]. Subsequently, zeolite acid density and acid strength can be varied to optimize for increased catalyst stability through reduced catalyst deactivations or for increased selectivity to specific target products via the inhibition of certain reaction pathways [4–6].

Several studies have reported the change in acid strength in zeolites via the isomorphous substitution of other metals into the framework, such as gallium, iron, gallium or boron, for silicon or aluminum. Both experimental characterization [7, 8] and computational calculations [9, 10] broadly suggest that these isomorphous substitutions result in decreases in Brønsted acid strength in the order of Al > Ga > Fe > B. The application of ZSM5 containing framework gallium, iron and boron for the production of

cymenes or xylenes via the alkylation of toluene with isopropanol or methanol respectively has been widely investigated [11–16]. Generally, the studies show that weaker acid sites show lower activity but are better able to suppress competitive reactions such as isomerization [12, 14, 16].

Zeolite BEA was first synthesized by Mobil Research and Development Laboratories as an aluminosilicate in the 1960s [17] and is known to have twelve member ring, three dimensional pore systems that have dimensions of 5.6Å by 5.6Å or 6.4Å by 7.6Å [18]. Since then, much progress has been made in the BEA synthesis procedures, allowing for other metals such as boron and gallium to be isomorphously inserted into the framework instead of aluminum [19]. More recently, in 1998, a synthesis procedure for ZnBEA, also known as CIT-6, was invented, allowing for zinc to be isomorphously inserted into the BEA framework [20]. Several papers have discussed the synthesis and characterization of ZnBEA [21–23] but little is known about its acidic properties and catalytic activity for alkylation and related reactions. Further, to our knowledge, only one other paper has applied a series of isomorphously substituted zeolite BEAs to an alkylation reaction, whereby it was reported that weaker acid sites prevented side reactions such as cracking and transalkylation in the alkylation of benzene with isopropanol while increasing the selectivity to cumene [24].

Here, the acidic properties of ZnBEA with AlBEA and GaBEA were compared and the use of ZnBEA or CIT-6 for the alkylation of phenol with propylene was explored. The effect of zeolite acid strength on the alkylation of phenol with propylene is also discussed.

4.2 Experimental Methods

4.2.1 Zeolite Synthesis

Chemical reagents used were sodium hydroxide (>98%, Sigma-Aldrich), tetraethylammonium hydroxide (TEAOH, 35 wt% aqueous solution, Alfa Aesar), sodium aluminate, gallium nitrate (99.9%, Sigma-Aldrich), lithium hydroxide monohydrate (98+%, Sigma-Aldrich), zinc acetate dehydrate (100%, J.T. Baker), nitric acid, ammonium nitrate. The composition of the synthesis mixtures in molar ratios are as follows.

AIBEA: 0.02 NaOH/0.53 TEAOH/0.04 Na₂O·Al₂O₃/SiO₂/10.60 H₂O

GaBEA: 0.12 NaOH/1.30 TEAOH/0.08 Ga(NO₃)₃/SiO₂/6.03 H₂O

ZnBEA: 0.05 LiOH/0.65 TEAOH/0.03 Zn(CH₃COO)₂·2H₂O/SiO₂/30.05 H₂O

Different silica sources were used for the zeolites synthesized - Cab-O-Sil M5 (Cabot corporation) was used for AIBEA, Tetraethyl orthosilicate (TEOS, 99.9%, Alfa Aesar) was used for GaBEA, Ludox AS-40 (40wt%, Sigma-Aldrich) was used for ZnBEA-3, and Ludox HS-40 (40wt%, Sigma-Aldrich) was used for ZnBEA-1 and ZnBEA-2.

For AIBEA synthesis, Cab-O-Sil M5 was added to TEAOH and stirred for 2h. Sodium aluminate and sodium hydroxide was then dissolved in water and added to the silica solution. The final mixture was stirred for 4h then loaded into Teflon-lined autoclaves. The autoclaves were rotated at 20rpm and heated at 150°C for 3 days to crystallize AIBEA.

For GaBEA synthesis, TEOS was added to TEAOH and stirred thoroughly. Gallium nitrate was then dissolved in some water and added to the silica solution. The final mixture is obtained by adding sodium hydroxide that had been dissolved in some water. The final mixture was stirred at 80°C in a slightly vented container until all evolved ethanol is removed then loaded into Teflon-lined autoclaves that are rotated at 20rpm and heated at 140°C for 9 days to crystallize GaBEA. GaBEAs with different Si/Ga ratios were obtained by varying the amount of gallium nitrate used in the synthesis.

For ZnBEA synthesis, the synthesis method found in another paper was closely followed [22].

After crystallization, all zeolites were washed thoroughly with water and were recovered by centrifugation. AIBEA, GaBEAs and ZnBEA-1 were dried at 120°C for 8h and then calcined at 550°C for 6h in flowing air. These zeolites were then ion-exchanged in a 1M NH₄NO₃ solution at 80°C for 12h. The ion-exchange was repeated 3 times. The zeolites were then washed and dried at 120°C for 8h then deammoniated at 500°C for 4h to yield their final protonated forms. The ZnBEA was dried overnight at 70°C but not calcined prior to treatment with the same ion-exchange procedure. After the ion-exchange, ZnBEA was washed and dried at 70°C for 12h, then deammoniated at 450°C for 4h. A temperature ramp of 1°C/min was used for all temperature programs.

4.2.2 Catalyst Characterization

The zeolites were characterized using N₂ physisorption, X-ray diffraction, pyridine Fourier transform infrared (FT-IR) spectroscopy, isopropylamine temperature

programmed desorption (TPD), ^{29}Si NMR, ^{27}Al NMR, and elemental analysis. These methods were described in a previous paper [25].

In addition to the aforementioned techniques, ^{71}Ga solid-state NMR was also utilized. All solid NMR measurements were conducted using a Bruker AV3-400 spectrometer operating in a magnetic field of 9.4 T. All samples were packed in a 4mm ZrO_2 rotor and spun at the magic angle at 13 kHz for ^{71}Ga NMR. ^{71}Ga NMR was conducted with a pulse length of 1.7 μs . Here, a concentrated aqueous solution of gallium nitrate was used for the calibration of the chemical shift (peak at 0 ppm).

4.2.3 Reaction Procedure

The gas phase alkylation of phenol with propylene was conducted in a vertical packed bed reactor at 350°C, 1 atm pressure and a phenol to propylene ratio of 1.4. The phenol was preheated and fed through a syringe pump (Harvard Apparatus Pump 11 Elite) while the propylene and helium diluents were fed via a mass flow controller (Brooks Instrument). All reactants and products were analyzed using an online gas chromatograph (GC) equipped with a thermal conductivity detector (TCD) and flame ionization detector (FID). The amount of catalyst and/or the flow rates were varied to obtain the desired initial conversion. The zeolites were pelletized and sieved to obtain a particle size of 0.178–0.354 mm and diluted with inert silicon carbide. Further details of the reaction and analysis procedure can be found elsewhere [25].

4.3 Results and Discussion

4.3.1 Characterization of Synthesized Zeolites

All zeolites were synthesized with the objective of obtaining similar crystal sizes and Si/M ratios, and were thoroughly characterized using a variety of methods to verify their physical and chemical properties. The X-ray diffraction patterns of all the synthesized zeolites in their proton forms had identical peaks that are characteristic of the *BEA topology (Figure 4.1). Both ZnBEA89 and ZnBEA91 had X-ray diffraction patterns that contained impurity peaks at $2\theta = 6.0^\circ$, 12.0° , 16.5° and 20.7° prior to attaining their final proton forms (Figure 4.2). The peak at $2\theta = 16.5^\circ$ has been attributed to the presence of the structure directing agent after synthesis [22] and was shown to disappear after repeated ion-exchange in an aqueous ammonium nitrate solution, as was also observed here. The remaining impurity peaks were observed to disappear after a heat treatment at 450°C for 4h in air and are speculated to be caused by the presence of zinc silicate species but their specific identities are unknown.

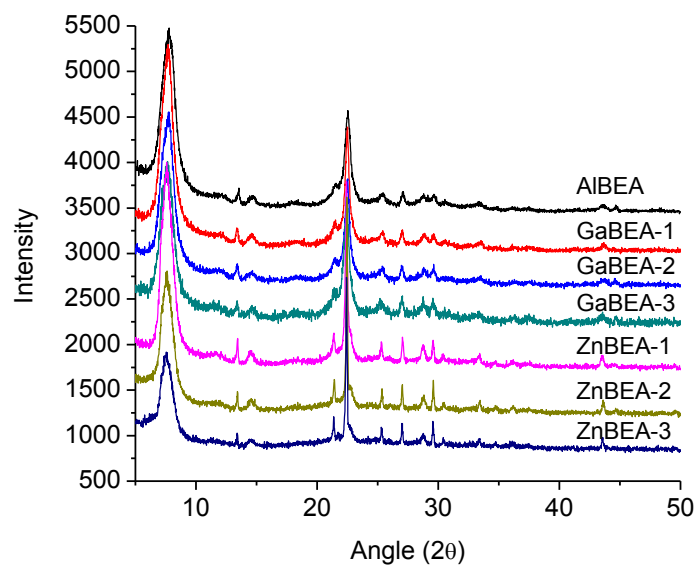


Figure 4.1 X-ray diffraction (XRD) patterns of synthesized zeolites

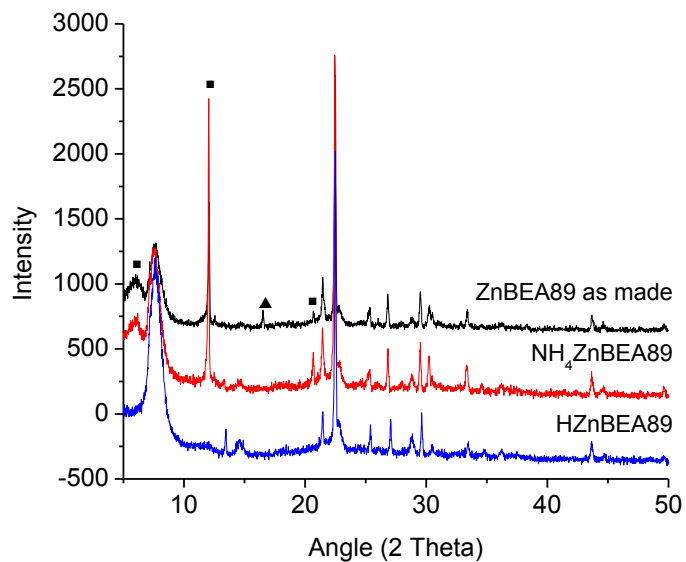


Figure 4.2 XRD pattern of ZnBEA89 as made, ZnBEA89 after ion-exchange ($\text{NH}_4\text{ZnBEA89}$) and ZnBEA89 after ion-exchange and deammoniation (HZnBEA89). Peaks due to impurities that disappear after ion-exchange step and the deammoniation step are indicated with \blacktriangle and \blacksquare respectively.

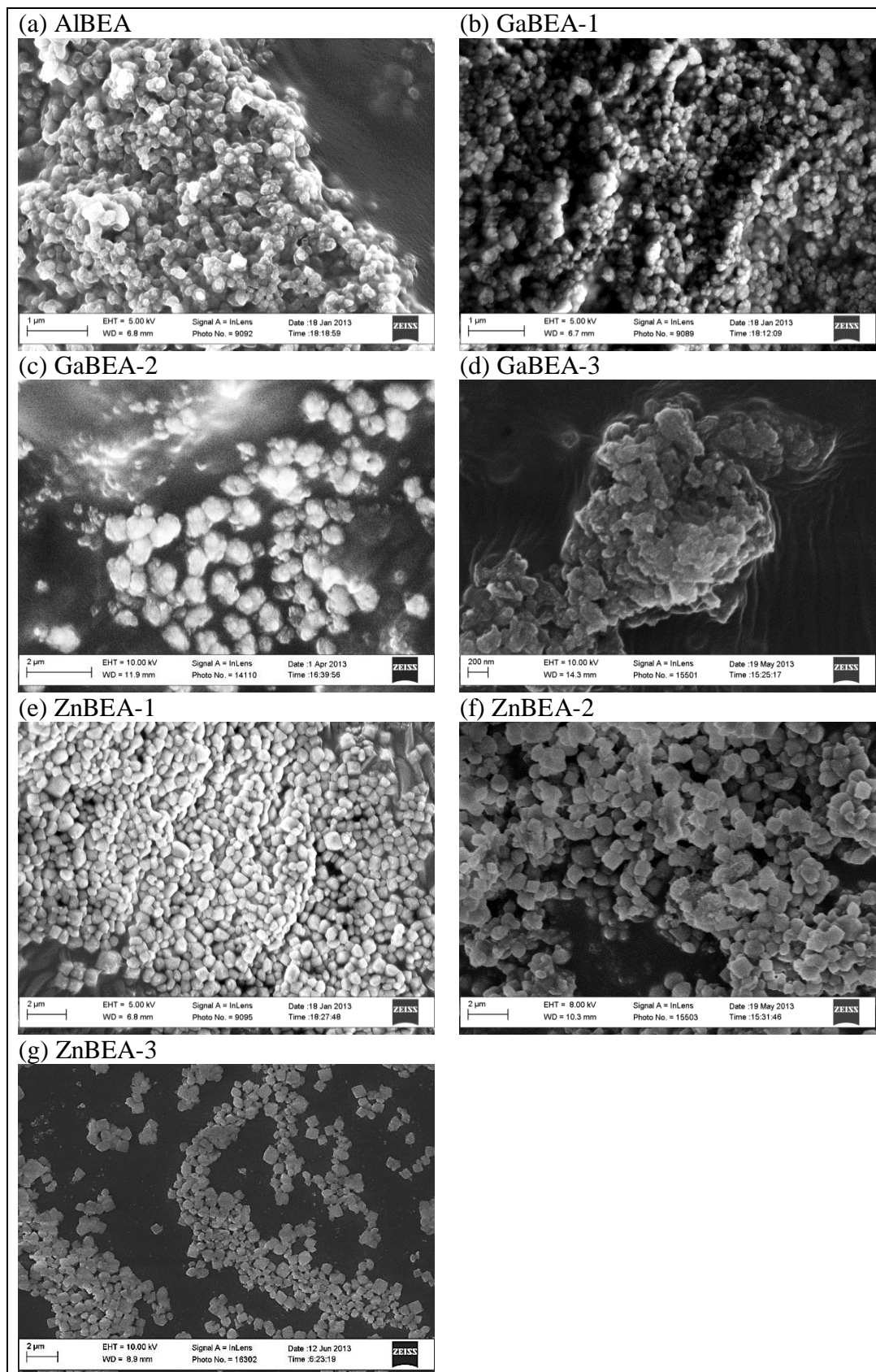


Figure 4.3 SEM images of synthesized zeolites

The crystal sizes of the synthesized zeolites were determined via scanning electron microscopy (Figure 4.3) and transmission electron microscopy. All zeolites synthesized had crystal sizes of 100–300 nm with the exception of the ZnBEAs which had a slightly larger crystal size range of 300–600 nm. Generally, all synthesized BEAs exhibited rounded morphologies. The ZnBEA crystals also had a rounded morphology but some pseudo-cubic shaped crystals were also observed [23].

Table 4.1 Characterization of zeolites - silicon to metal ratio, micropore volume, Brønsted to Lewis acid ratio at 350°C and Brønsted acid site concentration

Catalyst	Si/M ^a	V _{micro} (cc N ₂ /g)	B/L _{250°C} ^b	Brønsted acid site concentration ^c (μmol/g)
AlBEA	10.4	0.29	1.19	935
GaBEA-1	21.3	0.26	0.81	643
GaBEA-2	14.3	0.27	0.91	665
GaBEA-3	13.6	0.29	0.87	754
ZnBEA-1	10.0	0.22	0.10	75
ZnBEA-2	9.3	0.20	0.07	338
ZnBEA-3	7.3	0.17	0.08	247

^a Silicon to metal molar ratio (Si/M) where M = Al, Ga or Zn

^b Brønsted to lewis acid ratio at 350°C determined via pyridine FT-IR

^c Brønsted acid site concentration determined via isopropylamine temperature programmed desorption

The micropore volumes of the zeolites of AlBEA and GaBEAs were between 0.26–0.29 ccN₂/g, typical of BEA zeolites [26]. In contrast, ZnBEAs had slightly smaller micropore volumes of 0.17–0.22 ccN₂/g, which are similar to that of other ZnBEAs reported in literature [23]. The smaller pore volumes of ZnBEAs compared to the other BEAs could be caused by the higher amounts of extraframework species found in ZnBEAs than in the other BEAs, as indicated by their smaller Brønsted to Lewis acid ratios, which could cause partial blockage of access to micropores [27].

In addition to ensuring that the zeolites were of similar crystal sizes, all zeolites were also synthesized to have similar Si/M ratios so they would have similar acid site densities. Most of the zeolites had bulk Si/M ratios that ranged from 7.3 to 14.3 with the exception of GaBEA-1 which was synthesized with a slightly lower Si/M ratio so that the effects of higher acid site densities could be investigated. Based on pyridine FT-IR experiments, GaBEAs had lower Brønsted to Lewis acid ratios compared to AIBEA, indicating that the GaBEAs have more extraframework species. The Brønsted to Lewis acid ratios of GaBEA-1, GaBEA-2 and GaBEA-3 were relatively similar indicating similar distributions framework and extraframework gallium in these zeolites. The ZnBEAs have the lowest Brønsted to Lewis acid ratios, indicating that the least amount of zinc was incorporated into the BEA framework compared to the GaBEAs and AIBEA, even though they have similar overall Si/M ratios.

Isopropylamine temperature programmed desorption was used to calculate the concentration of Brønsted acid sites in the synthesized BEAs. AIBEA had the highest concentration of Brønsted acid sites at 935 $\mu\text{mol/g}$ which is not surprising as it has the lowest bulk Si/Al ratio. The GaBEAs have the next highest concentration of Brønsted acid sites ranging from 643 – 754 $\mu\text{mol/g}$. Both ZnBEA-2 and ZnBEA-3 have lower Brønsted acid site concentrations even though they have similar Si/M ratios as the rest of the zeolites which provides further evidence that less zinc is incorporated into the BEA framework. However, of all the zeolites, ZnBEA-1 has the lowest Brønsted acid site concentration of 75 $\mu\text{mol/g}$. Based on the elemental analysis of the ZnBEAs (Table 4.2), the ZnBEAs are expected to contain aluminum concentrations of approximately 20–40 $\mu\text{mol/g}$ of catalyst. This concentration of aluminum is very close to that of the

Brønsted acid site concentration of ZnBEA-1 and could indicate that framework aluminum sites could be the dominant source of the Brønsted acid sites in ZnBEA-1.

Table 4.2 Li/Zn and Si/Al ratios in ZnBEA zeolites

Catalyst	Na/Zn	Li/Zn	Si/Al
ZnBEA-1	0.11	0	> 500
ZnBEA-2	0	0.44	> 500
ZnBEA-3	0	1.05	> 500

Since less is known about ZnBEA, the Li/Zn and Si/Al ratios of ZnBEA were also analyzed to provide an indication of the efficacy of the ion-exchange as well as to determine if any trace amounts of aluminum in the silica source (Ludox HS-40 or Ludox AS-40) were incorporated into zeolite. The maximum cation to zinc ratio is expected to be 2 and elemental analysis showed that in the ZnBEA-1, about 89% of the cations were protons, 11% were sodium ions and only trace amounts of aluminum was found in the zeolite (Si/Al = > 500). On the other hand, neither ZnBEA-2 nor ZnBEA-3 contained sodium cations. Rather, the cations found in ZnBEA-2 were approximately 22% lithium ions and 78% protons, whereas those in ZnBEA-3 were approximately 53% lithium ions and 47% protons. This shows that empirically, more lithium remains in the pores when ZnBEA is synthesized with Ludox HS-40 consisting of a sodium stabilizing counterion (ZnBEA-2) than when it is synthesized with Ludox AS-40 which has an ammonium stabilizing anion. Regardless of the silica source, both ZnBEA-2 and ZnBEA-3 also contained trace amounts of aluminum, with silicon to aluminum ratios of > 500.

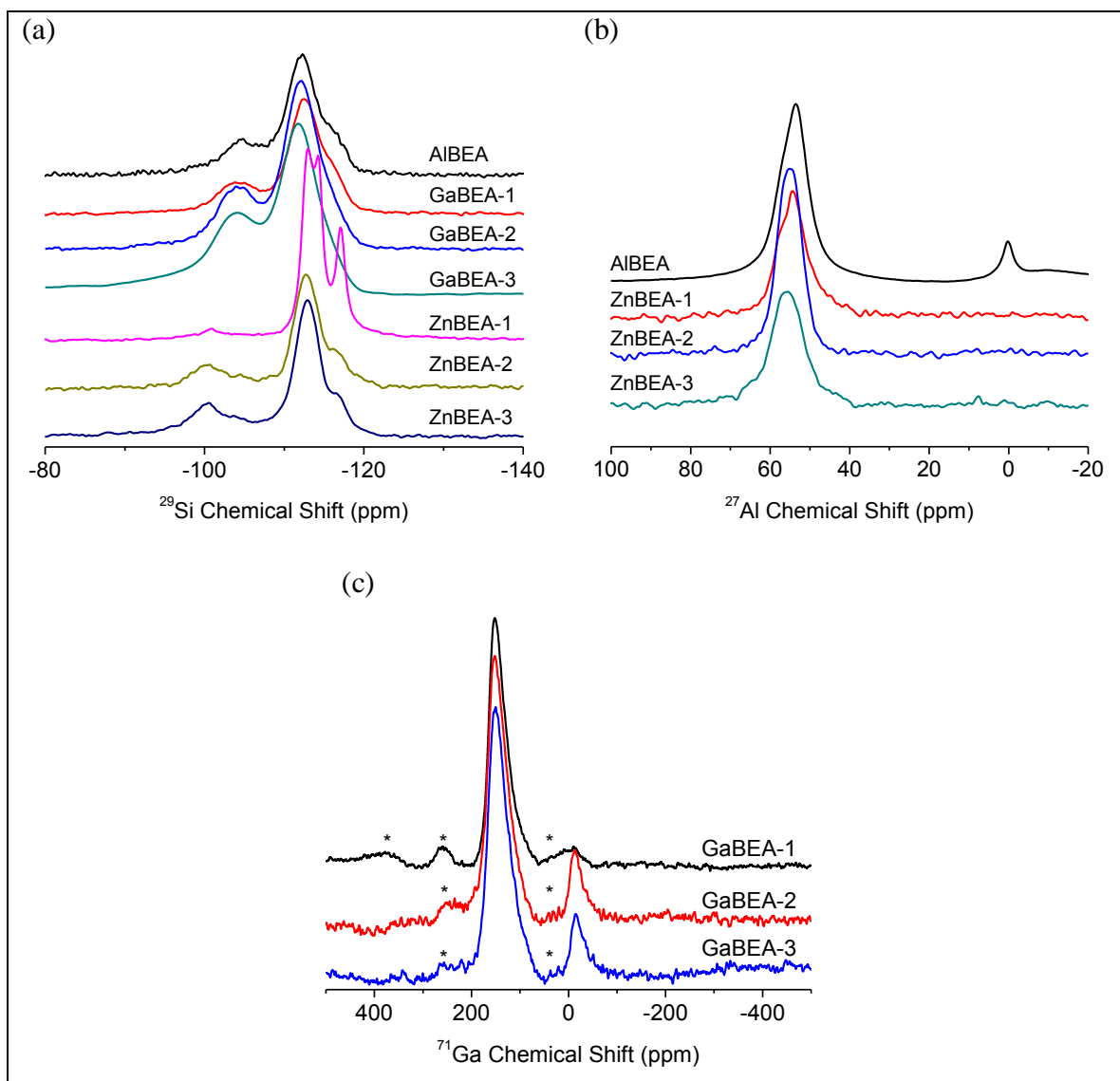


Figure 4.4 ^{29}Si NMR, ^{27}Al NMR and ^{71}Ga NMR spectra of synthesized zeolites

The ^{29}Si NMR spectra of the zeolites provide evidence for the integration of the metals in the framework. The Si(1Al) species and Si(0Al) species have characteristic chemical shifts in the -95 to -105 ppm and -100 to -115 ppm regions, respectively [28, 29]. The ^{29}Si NMR spectra of AIBEA and GaBEA zeolites exhibited peaks at -105 ppm and -112 ppm, indicating that aluminum and gallium were incorporated into the frameworks (Figure 4.4a). Their respective ^{27}Al and ^{71}Ga spectra provide further

evidence the presence of framework metals (Figure 4.4b and Figure 4.4c). The ^{27}Al NMR spectrum of AlBEA shows peaks at 54 ppm and 0 ppm that correspond to tetrahedral (framework) and octahedral (extraframework) aluminum, respectively [30]. Similar to ^{27}Al NMR spectra, ^{71}Ga NMR spectra of the GaBEAs exhibit characteristic tetrahedral gallium peaks at -156 ppm and octahedral gallium at 0 ppm [31]. GaBEA-2 and GaBEA-3 have larger peaks at 0 ppm, indicating that they have more extraframework gallium than GaBEA-3. The octahedral gallium peak in GaBEA-1 does not appear prominently in Figure 4.4c. This is due to overlap with the spinning side-band occurring for a spinning speed of 13 kHz at ~ 50 ppm. However, line shapes observed at 10 kHz and associated changes of the lineshapes when comparing data obtained at different spinning speeds provide clear evidence for the presence of this peak.

The ZnBEA-1 ^{29}Si NMR spectrum has peaks at -101 ppm, -113 ppm, -114 ppm and -117 ppm. The multiple peaks in the ^{29}Si NMR Q⁴ region are similar to those found in highly siliceous SiBEA and what was obtained previously when ZnBEA was extracted with acetic acid [22, 32]. Combined with the analysis that ZnBEA-1 has the lowest Brønsted acid site concentration, this suggests that the Zn in ZnBEA-1 was extracted when the as made ZnBEA was calcined at 550°C prior to or during the ion-exchange procedure, with only a small fraction of the Zn left in the framework, as indicated by the small peak at -101 ppm.

To retain zinc in the BEA framework, ZnBEA-2 and ZnBEA-3 were treated differently and ion-exchange was conducted on their as made forms, after which the samples were heated at 450°C to yield the final protonated form. ZnBEA-2 and ZnBEA-3 both have peaks at -100 ppm and -113 ppm in their ^{29}Si NMR spectra, with a shoulder at

-117 ppm. Previous research indicates that peaks at -98 ppm and -102 ppm are indicative of Si(1Zn) and Q³ sites respectively [21]. Thus, the presence of both of these species could be interpreted from the broad peak at -100 ppm found in the ²⁹Si NMR of the ZnBEA-2 and ZnBEA-3 zeolites. The Brønsted acid site concentrations of ZnBEA-2 and ZnBEA-3 discussed previously was found to be approximately 10 times larger than the analyzed concentration of aluminum in these zeolites, further attesting to the presence of framework zinc that contributes Brønsted acidity.

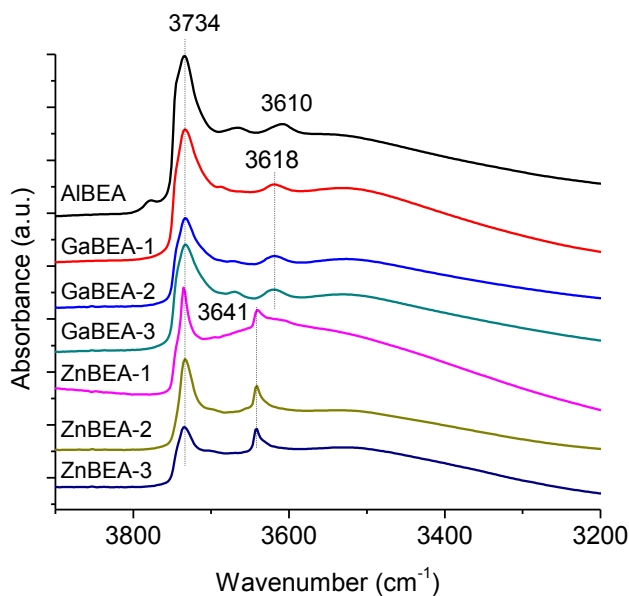


Figure 4.5 FT-IR spectra hydroxyl region of activated zeolites

The hydroxyl region of FT-IR spectra of the activated zeolites are shown in Figure 4.5. All BEA spectra exhibit a peak at 3734cm⁻¹ that has been attributed to terminal and internal SiOH groups [33]. The AIBEA had peaks at 3666 cm⁻¹ and 3610 cm⁻¹ that are associated with non-framework AlOH and Brønsted acid sites of bridging

hydroxyls [34]. In general, the bridging hydroxyl peak was observed to shift to higher wavenumbers as the zeolite metal was isomorphously substituted with gallium and zinc. This shift to higher wavenumbers indicates that the OH bond is more strongly attached to the framework metal [8, 35]. In GaBEAs, this bridging hydroxyl peak was at 3618cm^{-1} while in ZnBEAs the peak occurred at 3641cm^{-1} .

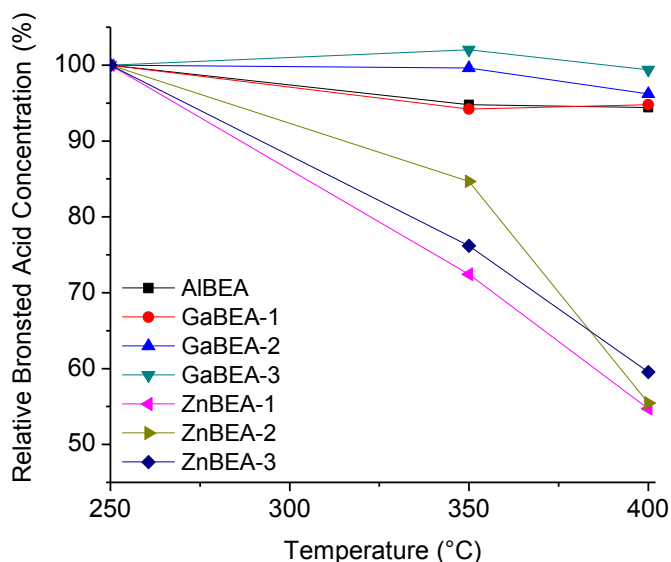


Figure 4.6 Change in number of Brønsted acid sites with increasing pyridine desorption temperature. Percentage of Brønsted acid sites remaining is relative to the number of Brønsted acid sites at 250°C.

The distribution of acid strengths can also be approximated with the amount of pyridine retained on the Brønsted acid sites at different desorption temperatures [36]. The stronger acid sites are expected to retain pyridine at higher temperatures, whereas the pyridine desorbs from the weaker acid sites. The amount of pyridine absorbed at 250°C is taken to represent the total amount of Brønsted acid sites present and subsequent acid site

concentrations were calculated relative to this total amount. The AlBEA and the GaBEAs seem to retain most (>95%) of their Brønsted acid sites even at 400°C while the ZnBEAs lose approximately 40% of their Brønsted acid sites at 400°C. This further provides evidence that ZnBEA has weaker acid strengths than AlBEA and GaBEA.

4.3.2 Catalytic Performance of Synthesized Zeolites

The acid strengths of the zeolites characterized by the wavenumber of the bridging hydroxyls indicated that the strength of the zeolites decreased in the manner AlBEA > GaBEA > ZnBEA while the pyridine temperature desorption indicates that the strength varied as AlBEA \approx GaBEA > ZnBEA. Comparing the $S_{2IPP/4IPP}$ of the different zeolites at similar conversions of approximately 3.7%, it is shown that the ratio increases from AlBEA < GaBEA < ZnBEA (Table 4.3 and Table 4.4). Specifically, the $S_{2IPP/4IPP}$ of AlBEA was 3.0 while that of the GaBEAs were approximately 3.7. The slightly different $S_{2IPP/4IPP}$ obtained with the GaBEAs were found to be insignificant given the standard $S_{2IPP/4IPP}$ errors of ± 0.15 , which were obtained by repeating the same experiment three times with GaBEA-3. Consequently, the differences in Si/Ga ratios and varying amounts of extraframework gallium in the GaBEAs did not seem to have any significant effect on the product selectivities obtained at the same conversion. The turnover frequencies, calculated based on the moles of phenol converted per mole of Brønsted acid site, for AlBEA and GaBEAs were relatively similar, spanning 4 – 11h⁻¹.

Table 4.3 Comparison of deactivation rates and selectivity of 2-IPP to selectivity of 4-IPP at $X_0 \approx 4\%$

Zeolite	X (%)	$-\frac{dX}{dt}$ (10^{-3} %/min)	$N_{2-IPP}/N_{4-IPP\ t=0}$	TOF (h^{-1})
AIBEA	3.81	2.2	3.0	6
GaBEA-1	3.95	1.8	3.6	11
GaBEA-2	3.56	2.4	3.7	3
GaBEA-3	4.15	2.6	3.8	4
GaBEA-3	3.08 ± 0.22	2.0 ± 0.2	3.2 ± 0.2	

At similar conversions, the ZnBEAs synthesized without calcination prior to the ion-exchange showed very different selectivities than GaBEA-3 at the same conversion. The $S_{2IPP/4IPP}$ of ZnBEA-1 that was synthesized with calcination prior to ion-exchange was 4.0 while ZnBEA-2 and ZnBEA-3 had a much higher $S_{2IPP/4IPP}$ of 27. Prior characterization indicated that the high temperature treatment removed most of the Zn species from the framework, but the ^{27}Al NMR spectroscopy showed the presence of framework aluminum species that could catalyze the alkylation reaction. Consequently, the lower $S_{2IPP/4IPP}$ obtained with ZnBEA-1 is likely because it is catalytically more similar to a high Si/Al AIBEA. Further, the turnover frequency calculated for ZnBEA-1 is relatively similar to that obtained with the synthesized AIBEA while the turnover frequencies for ZnBEA-2 and ZnBEA-3 are an order of magnitude smaller than the other zeolites indicating that the Brønsted acid resulting from framework zinc has much lower activity.

Previous studies have shown that the zeolite LiX is able to catalyze the alkylation of the aromatic ring of toluene with methanol to give xylenes [37] and xylene to give trimethylbenzenes [38]. However, since the ions in these zeolites are not 100% Li, residual Brønsted acid sites in these catalysts are likely responsible for the alkylation.

Here, ZnBEA-2 and ZnBEA-3 exhibited the same activity at the same weight hourly space velocity and showed similar $S_{2IPP/4IPP}$ even though they had different Li/Zn ratios, suggesting that in this case, lithium ions do not influence the reaction and affect the product selectivities.

Table 4.4 Comparison of deactivation rates and selectivity of 2-IPP to selectivity of 4-IPP at $X_0 \approx 2\%$

Zeolite	X (%)	$-\frac{dX}{dt}$ ($10^{-3}\%/min$)	$N_{2-IPP}/N_{4-IPP\ t=0}$	TOF (h^{-1})
GaBEA-3	1.82	0.6	5	4
ZnBEA-1	1.10	0.7	4	5
ZnBEA-2	1.84	0.6	27	0.3
ZnBEA-3	1.14	0.2	27	0.2

The effect of the presence of lithium cations in the zeolite on alkylation selectivity was further investigated with a lithium ion-exchange of GaBEA-2. However, additional experiments with LiGaBEA-2 showed little change in reactivity and product selectivity, indicating that the lithium ions are unlikely to influence the product selectivity obtained with the catalyst under these activated zeolites alkylation reaction conditions.

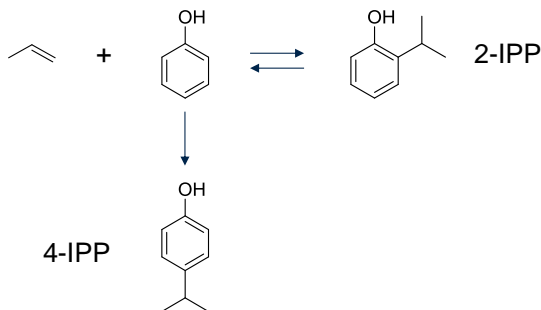


Figure 4.7 Schematic of dominant reactions occurring in the gas phase alkylation of phenol with propylene at $T = 350^\circ C$ and $P = 1\text{ atm}$ [25]

Previous research on the gas phase alkylation of phenol with propylene at the same reaction conditions indicated that the dominant reactions are the direct alkylation of

phenol with propylene to 2-isopropylphenol or 4-isopropylphenol, as well as the de-alkylation of 2-isopropylphenol to produce phenol and propylene, as shown in Figure 4.7 [25]. Since de-alkylation is known to be catalyzed by strong acid sites [39], the higher $S_{2IPP/4IPP}$ observed with zeolites with weaker acid strengths could be because 2-isopropylphenol is less likely to de-alkylate over these zeolites. To test this, 2-isopropylphenol was reacted over GaBEA-3 and ZnBEA-3 at the same molar ratio of 2-isopropylphenol to Brønsted acid sites (Figure 4.8). Over GaBEA-3, 2-isopropylphenol was observed to de-alkylate to form phenol and propylene while no conversion of 2-isopropylphenol was observed over ZnBEA-3. Consequently, this supports the hypothesis that the increase in selectivity for the 2-alkylated product when the acid strength was decreased is due to the suppression of the de-alkylation pathway.

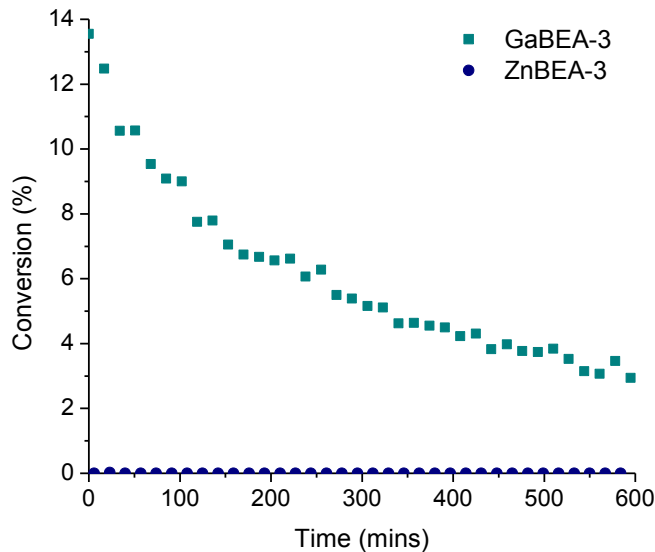


Figure 4.8 Plot of conversion of 2-isopropylphenol over time on stream catalyzed by GaBEA-3 (■) or ZnBEA-3 (●). T = 350°C, Pressure = 1 atm,

4.4 Conclusions

A series of isomorphously substituted BEAs was synthesized with similar crystal sizes and varying acid strengths. ZnBEA was shown to have weaker acid strength than AlBEA and GaBEA. ZnBEA was found to be much more selective for 2-isopropylphenol than AlBEA and GaBEA in the gas phase alkylation of phenol with propylene. With decreasing acid strength, more 2-isopropylphenol was observed and was attributed to the suppression of de-alkylation of 2-isopropylphenol.

It was demonstrated that ZnBEA can be used to catalyze gas phase alkylation of phenol with propylene but with much lower rates. However, since the framework zinc in ZnBEA is demonstrated to be thermally unstable, it will be difficult to recycle the ZnBEA catalyst by burning off any coke that accumulates.

4.5 References

- [1] Vermeiren, W.; Gilson, J.-P. *Topics in Catalysis* **2009**, *52*, 1131–1161.
- [2] Stöcker, M. *Microporous and Mesoporous Materials* **2005**, *82*, 257–292.
- [3] Weitkamp, J. *Solid State Ionics* **2000**, *131*, 175–188.
- [4] Sotelo, J. L.; Uguina, M. a.; Valverde, J. L.; Serrano, D. P. *Industrial & Engineering Chemistry Research* **1996**, *35*, 1300–1306.
- [5] García, L.; Giannetto, G.; Goldwasser, M. R.; Guisnet, M.; Magnoux, P. *Catalysis Letters* **1996**, *37*, 121–123.
- [6] Shamzhy, M. V.; Shvets, O. V.; Opanasenko, M. V.; Kurfiřtová, L.; Kubička, D.; Čejka, J. *ChemCatChem* **2013**, n/a–n/a.
- [7] Berndt, H.; Martin, A.; Kosslick, H.; Lucke, B. *Microporous Materials* **1994**, *2*, 197–204.

- [8] Chu, C. T.-W.; Chang, C. D. *Journal of Physical Chemistry* **1985**, *89*, 1569–1571.
- [9] Stave, M. S.; Nicholas, J. B. *Journal of Physical Chemistry* **1995**, *99*, 15046–15061.
- [10] Yuan, S. P.; Wang, J. G.; Li, Y. W.; Jiao, H. *The Journal of Physical Chemistry A* **2002**, *106*, 8167–8172.
- [11] Cejka, J.; Kapustin, G. A.; Wichterlov, B. **1994**, *108*, 187–204.
- [12] Cejka, J.; Kapustin, G. A.; Wichterlov, B. *Applied Catalysis A, General* **1994**, *108*, 187–204.
- [13] Čejka, J.; Vondrová, A.; Wichterlová, B.; Vorbeck, G.; Fricke, R. *Zeolites* **1994**, *14*, 147–153.
- [14] Parikh, P. A.; Subrahmanyam, N.; Bhat, Y. S.; Halgeri, A. B. *Applied Catalysis A: General* **1992**, *90*, 1–10.
- [15] Park, Y. K.; Park, K. Y.; Woo, S. I. *Catalysis Letters* **1994**, *26*, 169–180.
- [16] Derewiński, M.; Dźwigaj, S.; Haber, J.; Mostowicz, R.; Sulikowski, B. *Zeitschrift für Physikalische Chemie* **1991**, *171*, 53–73.
- [17] Wadlinger, R. L.; Kerr, G. T.; Rosinski, E. J. Catalytic composition of a crystalline zeolite **1967**.
- [18] Higgins, J. B.; LaPierre, R. B.; Schlenker, J. L.; Rohrman, A. C.; Wood, J. D.; Kerr, G. T.; Rohrbaugh, W. J. *Zeolites* **1988**, *8*, 446–452.
- [19] Reddy, K. S. N.; Eapen, M. J.; Joshi, P. N.; Mirajkar, S. P.; Shiralkar, V. P. *Journal of Inclusion Phenomena and Molecular Recognition in Chemistry* **1995**, *20*, 197–210.
- [20] Takewaki, T.; Davis, M. E. Molecular Sieve CIT-6 **2004**.
- [21] Takewaki, T.; Beck, L. W.; Davis, M. E. *Topics in catalysis* **1999**, *9*, 35–42.
- [22] Takewaki, T.; Beck, L. W.; Davis, M. E. *The Journal of Physical Chemistry B* **1999**, *103*, 2674–2679.
- [23] Serrano, D. P.; Van Grieken, R.; Davis, M. E.; Melero, J. a; Garcia, a; Morales, G. *Chemistry (Weinheim an der Bergstrasse, Germany)* **2002**, *8*, 5153–60.
- [24] Reddy, K. S. N.; Rao, B. S.; Shiralkar, V. P. *Applied Catalysis A: General* **1993**, *95*, 53–63.

- [25] Xu, W.; Miller, S. J.; Agrawal, P. K.; Jones, C. W. *Applied Catalysis A: General* **2013**, *459*, 114–120.
- [26] Cejka, J.; Corma, A.; Zones, S. I. No Title. In *Zeolites and Catalysis: Synthesis, Reactions and Applications, vol. 1*; Wiley-VCH, 2010; p. 345.
- [27] Marques, J. .; Gener, I.; Ayrault, P.; Bordado, J. .; Lopes, J. .; Ramôa Ribeiro, F.; Guisnet, M. *Microporous and Mesoporous Materials* **2003**, *60*, 251–262.
- [28] Ramdas, S.; Klinowski, J. *Nature* **1984**, *308*, 521–523.
- [29] Klinowski, J. *Annual Review of Materials Science* **1988**, *18*, 189–218.
- [30] Bourgeat-lami, E.; Massiani, P.; Renzo, F. Di; Espiau, P.; Fajula, F. *Applied Catalysis* **1991**, *72*, 139–152.
- [31] Genet, J.; Chao, K. J.; Sheu, S. P.; Feng, M. H. *Zeolites* **1997**, *18*, 18–24.
- [32] Cambor, M. A.; Corma, A.; Valencia, S. *Chemical Communications* **1996**, 2365–2366.
- [33] Hegde, S. G.; Kumar, R.; Bhat, R. N.; Ratnasamy, P. *Zeolites* **1989**, *9*, 231–237.
- [34] Baran, R.; Millot, Y.; Onfroy, T.; Krafft, J.-M.; Dzwigaj, S. *Microporous and Mesoporous Materials* **2012**, *163*, 122–130.
- [35] Cambor, M. A.; Perez-Pariente, J.; Fornes, V. *Zeolites* **1992**, *12*, 280–286.
- [36] Corma, A.; Gómez, V.; Martínez, A. *Applied Catalysis A: General* **1994**, *119*, 83–96.
- [37] Yashima, T.; Sato, K.; Hayasaka, T.; Hara, N. *Journal of Catalysis* **1972**, *26*, 303–312.
- [38] Yang, C.; Meng, Z. *Applied Catalysis* **1991**, *71*, 45–54.
- [39] Dehydration, I. M.; Dealkylation, C. **1986**, *141*, 132–141.

CHAPTER 5

Conclusions and Future Work

As mentioned in the introduction, lignin is a byproduct of the cellulosic ethanol production process and is currently treated as a low value waste product and burned as fuel. However, lignin could be more effectively utilized if it could be converted to more valuable chemicals or liquid transportation fuel. A schematic of how lignin could be converted to fuel is shown in Figure 5.1 below.

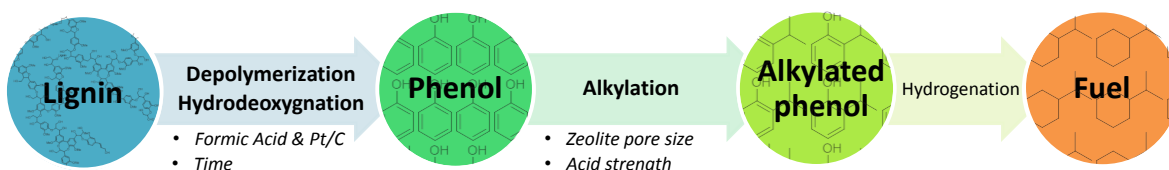


Figure 5.1 Hypothetical schematic for converting lignin to fuel

In chapter 2, a one pot depolymerization and hydrodeoxygenation process was investigated to convert switchgrass lignin into fuel using formic acid and platinum on carbon catalyst. Experiments showed that the use of both formic acid and the catalyst was crucial for decreasing the production of char and maximizing the liquid products, and reaction time was an important factor for obtaining lower molecular weight distributions. The process yielded liquid products with H/C and O/C ratios that were improved but not close to that of crude oil. Consequently, further processing steps are required to convert lignin to fuel.

Based on previous research conducted in the group, a phenol substituted at the ortho-position with a three carbon side chain exhibited significantly less catalyst deactivation during hydrogenation compared to other substituted phenols. Hence, 2-isopropylphenol could be a good feed for hydrogenation step and was selected to be the target product to be formed from the alkylation of phenol, a model compound for the monomers obtained from the depolymerization and hydrodeoxygenation of switchgrass lignin.

The zeolite catalyzed alkylation of phenol with propylene to produce 2-isopropylphenol was studied in chapter 3 and chapter 4. In chapter 3, the effect of pore topology on 2-isopropylphenol selectivity was investigated with nine different zeolite topologies. For reactions occurring in the pores, smaller pore sizes favored the production of 4-isopropylphenol while larger pore sizes favored the production of diisopropylphenols. *BEA was found to maximize 2-isopropylphenol selectivity by balancing the diffusion and steric limitations with secondary reactions producing di-alkylated products.

In chapter 4, the effect of zeolite acid strength on 2-isopropylphenol selectivity was examined using isomorphously substituted BEA. ZnBEA was determined to have weaker acid sites than GaBEA and AlBEA, and had the highest selectivity for 2-isopropylphenol. The weaker acid sites were thought to be selective for 2-isopropylphenol through the suppression of 2-isopropylphenol de-alkylation. Even though ZnBEA had higher selectivity than the other BEAs, it had much lower activity. Consequently, GaBEA would be the more practical catalyst to use, as it has slightly better selectivity for 2-isopropylphenol than AlBEA with higher activity than ZnBEA.

Furthermore, GaBEA is more thermally stable and will be better able to withstand the high temperatures required to burn off coke and recycle the catalyst.

This thesis work suggests that the aforementioned route of converting lignin to fuels could indeed be possible by depolymerizing and hydrodeoxygenating lignin with formic acid and Pt/C, and alkylating phenolic compounds found in the lignin oils with ZnBEA to obtain high selectivity for 2-isopropylphenol which could be hydrogenated with a Pt/HY catalyst. However, further work still needs to be done to apply this process practically.

First, the depolymerization and hydrodeoxygenation of lignin should be optimized to ideally produce a higher fraction of phenolic compounds instead of substituted guaiacols as it was shown to produce. Other heterogeneous hydrodeoxygenation catalysts such as Raney Ni, Pd/C, Rh/C or Ru/C could be applied in the reaction to determine if the reaction can be more successful at removing the methoxy group of guaiacols while simultaneously depolymerizing lignin. Since these catalysts can be relatively expensive, their recyclability should also be investigated to determine if they can maintain their activity over multiple runs.

Second, more experiments should be conducted to verify that the maximum trend observed in Chapter 3 as the graph could also be interpreted as monotonically increasing. To do so, extra-large pore zeolites (> 12 MR) such as UTD-1, SSZ-53 or SSZ-59 could be synthesized and applied to the alkylation reaction to provide more data points beyond that of Y zeolite to verify the existence of a downward N2-IPP/N4-IPP trend beyond Y.

Last, the ortho-alkylation of substituted phenols should be investigated using substituted mesoporous silica materials that have Brønsted acid sites. In this work, the alkylation of phenol was investigated. However, the identified compounds obtained from lignin were mainly substituted guaiacols. Additionally, even if there was a good hydrodeoxygenating catalyst that is able to remove the methoxy group, the resulting phenolic compounds are likely to still have up to 3 carbon alkyl side chains. To accommodate the ortho-alkylation of these longer compounds, larger pore substituted mesoporous materials similar to the AISBA-15 studied in Chapter 3 should be investigated.